RNAi Mouse Models of Breast Cancer Tumor Suppressor Genes

A thesis submitted to the faculty of the Watson School of Biological Sciences
In partial fulfillment of the requirement for the degree of Doctor of Philosophy

By
Saya Hayashi Ebbesen

Cold Spring Harbor, NY
2013

Signature page

Abstract

Breast cancer is a biologically and clinically heterogeneous disease that makes clinical management challenging. Cancer genomics can identify underlying candidate genetic lesions, but functional studies are required to dissect which changes impact disease progression, treatment efficacy, and development of resistance. The generation of experimental models that can faithfully reproduce the spectrum of human disease is therefore essential. RNA interference (RNAi) is a powerful tool that allows for systematic loss of function genetics in mammalian systems. This thesis presents two complementary approaches for the development of new mouse models of breast cancer based upon RNAi technology. The first experimental chapter describes efforts to build a 'mosaic' orthotopic transplantation model for the purpose of conducting an *in vivo* RNAi screen for novel tumor suppressor genes relevant to the human disease. A pilot screen led to the identification of *neurofibromin 1* (*NF1*) as having a putative tumor suppressor activity in breast cancer. The following chapter involves the development of a transgenic RNAi mouse model of human epidermal growth factor receptor 2 (HER2) positive breast cancer. This new multi-allelic inducible RNAi platform was subsequently used to investigate the efficiency of the tumor suppressor gene *PTEN* (*phosphatase and tensin homolog*) knockdown in driving disease acceleration and to assess its role in tumor maintenance. Taken together, this work extends the application of RNAi technology, and identifies new (*NF1*) and expands upon known (*PTEN*) molecular and genetic interactions underlying the progression and maintenance of HER2 positive breast cancer.

Table of Contents

List of Tables

List of Figures

List of Abbreviations

CAGs	CMV early enhancer element/chicken beta actin artificial promoter
CK	Cytokeratin
CMV	Cytomegalovirus promoter enhancer
Cre	Cre Recombinase
DCIS	Ductal carcinoma *in situ*
DOX	Doxycycline
EMT	Epithelial-mesenchymal transition
EGFR	Epidermal growth factor receptor
ER	Estrogen receptor
ErbB2	Mouse HER2/neu ortholog, epidermal growth factor receptor
ERBB2	v-erb-b2 erythroblastic leukemia viral oncogene homolog 2
ESC	Embryonic stem cell
FACS	Fluorescence activated cell sorting
GEMM	Genetically engineered mouse model
GEMM-ESCs	Rederived embryonic stems cells from GEMMs
GFP	Green fluorescent protein
HER2	Human epidermal growth factor receptor 2, encoded by *ERBB2* gene
H&E	Hematoxylin and eosin stain
IDC	Invasive ductal carcinoma
IRES	Internal ribosome entry site
LOH	Loss of heterozygosity
LSL	LoxP-STOP-LoxP cassette
Luci	Firefly luciferase
MEF	Mouse embryonic fibroblast
miR	microRNA
MaSCs	Mammary stem and progenitor cells
MLP	MSCV LTR miR30-shRNA Puro IRES GFP vector
MLS	MSCV LTR miR30-shRNA SV40 GFP vector
mKate2	Katushka fluorescent protein
MMTV	Mouse Mammary Tumor Virus Long Terminal Repeat

MOI	Multiplicity of infection
MRI	Magnetic resonance imaging
Neu	Rat ErbB2 homologue
NeuNT	Neu with activating mutation V664E
NF1	Neurofibromin 1
PR	Progesterone receptor
PTEN	Phosphatase and tensin homolog
R26	*ROSA26* locus
RIK	pCAGs-LSL-rtTA3-ires-mKate2 transgenic allele
RLuc	Renilla-Luciferase
RNAi	RNA interference
rtTA	Reverse tetracycline transactivator protein
RTK	Receptor tyrosine kinase
ROMA	Representational Oligonucleotide Microarray Analysis
shRNA	Short hairpin RNA
Tet	Tetracycline
TG-shRNA	TRE-GFP-miR30 transgenic allele
TRE	Tetracycline responsive element
TSG	Tumor suppressor gene
tTA	Tetracycline transactivator protein
TTF1	Thyroid transcription factor 1
UbC	Ubiquitin C promoter
WAP	Whey acidic protein

Acknowledgements

Foremost, I would like to thank my mentor, Scott Lowe, for having provided me with such a nurturing environment to grow as a young scientist. Thank you for believing in me, for encouraging me to embark on challenging projects, and for providing me with the ample resources to do them. In just a few years I have learned an immeasurable amount under your tutelage.

I would like to thank the members of my thesis committee, Greg Hannon, Lloyd Trotman, Scott Powers and David Stewart, for all of your guidance, patience and encouragement over the years. Your expert advice and genuine interest in my progress have always been a source of reassurance and support. And to my external examiner, Ramon Parsons, thank you for taking the time to read my thesis and attend my defense.

My sincere gratitude to the faculty of WSBS, for having taken a chance on me despite my unconventional prior training: you have given me a truly inspiring education and I hope to safeguard that unique CSHL *je ne sais quoi* in my heart for years to come. Specifically, I would like to thank Leemor Joshua-Tor and Greg Hannon for their influential mentorship.

Thank you to the administrators of the Watson School, Dawn, Alyson, Kim and Keisha, for years of tender loving care… And I still believe the Entering Class of 2007 is the best class ever! Thank you to all 13 of you for being such awesome classmates and housemates.

Thank you to collaborators Jim Hicks, Camila Dos Santos, Mikala Egeblad, and Senthil Muthuswamy for your interest in my projects and your expert advice on matters specific to breast cancer research. I would like to thank Yong Hannah Wen for help with pathology.

I owe so much of what I learned during the first two and a half years in the Lowe lab to the knowledgeable mentorship of Uli Bialucha. Thank you for your patience and friendship.

I would like to thank all members of the Lowe lab, past and present, that I have had the privilege of knowing. I hope the many friendships we developed will last a lifetime. There have been too many to mention every colleague, but a few special thanks…

To the numerous Lowe lab postdocs who contributed so much to this unforgettable chapter of my life, thank you for generously sharing your passion, perspective and expertise: Luke Dow, Jess Bolden, Johannes Zuber, Cornelius Miething, Tom Kitzing, Michael Saborowski, Amaia Lujambio, Agustin Chicas, and Ross Dickins.

To Lynn "the Real Boss" Michel for taking such great care of everyone, to Mona Spector and Young Park for your helpful advice and experienced points of view.

To the best flunch crew a girl could ask for: Amy, Katie, Johannes and Luke. Thank you for always being there to make me laugh on the good, the mundane and the most often discouraging day in the life of a grad student. Amy Rappaport and Katie McJunkin, I simply cannot fathom the Lowe Lab without the both of you in it. I will forever treasure the memory of our countless hours spent together in and out of the lab.

To Susi Weissmueller, the best baymate ever. Thank you for putting up with all my crazy.

To the other CSHL-era graduate students, thank you for your friendship, supportive camaraderie and the late nights in lab: Christof Fellmann, Zhen Zhao, Claudio Scuoppo, Özlem Mert, Nilgün Tasdemir, Chun-Hao Huang, Prem Premsrirut, and Wen Xue. Many thanks to Ted Kastenhuber, it has been fun having another person on the breast cancer team since last summer!

To Sarah Ackermann and Jamie Plevy for keeping us all sane.

To our many mouse techs for help with colony management and for teaching me so many tips about mouse work: Janelle Simon, Danielle Grace, Laura Lintault Kraehling, Sha Tian, Erika Antinis-Ginnetta, Jackie Cappellani and Merri Taylor. I gratefully acknowledge Eileen Earl and her amazing crew who took such great care of my mice that were left behind at the Hillside facility after our move to Sloan.

My sincerest thank you to Justin Cross for your close friendship and generous mentorship in the MSKCC-era of my thesis. I cannot imagine what this past year and a half would have been like without you – and the several hundred cups of English tea you brewed for me – on the 12th floor.

To my wonderful friends in the Hannon lab: Colin, Fred, Elvin, Felix, and especially to Paloma Guzzardo for so much more than could ever possibly be described in words. To Kristen, Stephane, and Dani for making Long Island that much more like a place one might call home.

To my parents, my sister, and my extended family for your tireless love and unflinching support. To my dear friends Dino, Laura, Judith, Niels, Karin, Naomi, Marine, Dorothée, Daniele, Sid, Dorje, Carolyn, Bernard, Aunt Nadine, the Stillwells, and Peter & Laura for having been part of this six year journey from both near and afar.

Many thanks to John P. Morris IV, Luke Dow, Dino Mavrakis and Justin Cross for help with editing my thesis.

This dissertation work was supported by a Star Centennial Scholarship and an NIGMS-NIH Training Grant through the Watson School, HHMI funding and a joint MMHCC grant for breast cancer research.

I. Introduction

BREAST CANCER

Breast cancer is the most frequently diagnosed cancer in women in the United States, with an estimated 226,870 new cases in 2012 (American Cancer Society 2012). Despite the fact that recent scientific and clinical advances have led to a constant decline in breast cancer mortalities, it remains the second leading cause of cancer deaths with an estimated yearly mortality rate of 40,000 patients. The decline can be attributed in part to early detection, diagnosis, and surgery, coupled with improvements in postsurgical adjuvant treatments including hormonal, cytotoxic and molecular based therapies.

Breast cancer is a clinically heterogeneous disease, the complexity of which relates to the diversity of molecular abnormalities driving the tumorigenic process. This collection of diseases displays distinct histopathological features, genetic and genomic characteristics, and diverse prognostic outcomes and responses to therapy (Vargo-Gogola and Rosen 2007). Currently, there is an ideological shift in the treatment of many cancer types, from an approach where the histology and tissue of origin were the guiding principles in the choice of therapy towards a strategy involving the identification of oncogenic driver mutations and selective treatments in the clinic using specific targeting agents. This paradigm change has been enabled by the emergence of next-generation DNA sequencing technologies that have allowed for the identification of recurrent genetic aberrations and the concurrent development of highly selective inhibitors against the products of genes that are activated by these alterations (Bernards 2012). Major advances in the areas of breast cancer disease classification and targeted therapy will be briefly discussed below.

BREAST CANCER PATHOLOGY AND MOLECULAR PROFILES

Until very recently, pathological examination was the gold standard for diagnosis in breast cancer and its role also encompassed the elucidation of etiology, pathogenesis, clinicopathological correlation, and prognostication (Leong and Zhuang 2011). Historically, the selection of adjuvant systemic therapy for early breast cancer patients relied on risk assessment as delineated by the TNM classification (Dinh et al. 2007). Developed in the 1940s, the TNM staging system for solid cancers classifies malignant tumors based on the size of the primary tumor (T), the involvement of regional lymph nodes (N) and distant metastasis (M) (Brierley 2006). Furthermore, the Scarff-Bloom-Richardson grading system for breast cancer was developed based on microscopic observations based on tubule formation, mitotic activity, and cellular pleomorphism (Bloom and Richardson 1957). Subsequent refinement and incorporation into the Nottingham Prognostic Index resulted in a robust scoring system that predicted long-term survival for patients (Haybittle et al. 1982). Additionally, risk-assessment incorporated both patient-related (such as age and menopausal status) and tumor-related prognostic factors (such as tumor size and grade) (Gelber et al. 2003).

Technological advances in molecular biology, and the accompanying realization that breast cancer is a heterogeneous group of diseases, has shifted the focus of pathobiology towards the improvement of diagnostic tools with increased attention being paid to the identification of morphological features and immunohistochemical markers of prognostic relevance (Leong and Zhuang 2011). Incorporating the expression status of hormone receptors and human epidermal growth factor receptor (HER2) as prognostic factors marked the first emphasis towards predictive markers that reflect both the molecular make-up of the tumors and represent the actual targets for therapies such as tamoxifen and

aromatase inhibitors against the estrogen receptor (ER) and the humanized monoclonal antibody trastuzumab (Herceptin, Genentech) that targets HER2 (Fendly et al. 1990; Dinh et al. 2007). Despite efforts invested towards the identification of other immunohistochemical biomarkers to further refine breast cancer diagnosis and treatment, few have proven to be of value in multivariate analyses and only ER, progesterone receptor (PR), and HER2 expression have remained essential components of pathological examination (Leong and Zhuang 2011).

To better understand the phenotypic diversity breast cancers present in their natural history and responsiveness to therapy, researchers sought to characterize tumors through a detailed interrogation of inter-tumor variation in gene expression patterns (Perou et al. 2000; Sorlie et al. 2001). These emerging molecular portraits defined a new clinical and biological standard relating back to the different features of normal mammary epithelial biology: ER+/luminal-like, basal-like, HER2+ and normal breast, with important implications that ER negative breast carcinomas may encompass two biologically distinct subtypes (basal-like and HER2+) (Perou et al. 2000). Further refinement by Sorlie and colleagues led to the luminal subtype A, luminal subtype B/C, basal-like, HER2+ and normal breast-like categories (Sorlie et al. 2001). Moreover, evidence of a relationship between the expression-based subclasses of breast tumors and patient outcome was established (Sorlie et al. 2001). During the past decade, the interpretation of breast tumor biology based on molecular profiles has steadily become part of the standard medical vocabulary. In invasive ductal carcinomas (IDC), which constitute approximately 80% of all breast cancers, at least four molecular subtypes are commonly designated by the following general defining traits: luminal (ER+, PR+, and HER2–), HER2 overexpressing (ER–, PR–, and HER2+), basal-like (ER–, PR–, HER2, and CK5/6+, EGFR+), and normal breast-like (ER–, PR–, and HER2–).

Furthermore, it has been demonstrated that IDC and invasive lobular carcinoma (ILC), the second major histological type of breast cancer, present additional differences in global transcription programs (Zhao et al. 2004).

The molecular subtypes of IDC segregate by overall survival, with HER2+ and basal subtypes demonstrating the worst prognosis while luminal-A shows the most favorable outcome (Perou et al. 2000). However, it has been shown that the prognostic outcomes of each type of IDC do not differ when a pathologically complete response to therapy is achieved (Carey et al. 2007). These distinct prognostic outcomes may reflect the differential responses to chemotherapy and targeted therapies by the bulk of the tumor and sub-populations of tumor-initiating cells (Al-Hajj et al. 2004). More recently, researchers have taken molecular and genomic profiling of breast cancer a step further and looked to define intra-tumoral heterogeneity at a single-cell resolution (Navin et al. 2010; Navin et al. 2011). Continued progress towards a complete understanding of the many critical aspects of tumorigenesis, such as the cell of origin and tumor initiation and evolution from the perspectives of intra- and inter-tumoral heterogeneity, will likely provide answers to some of these seemingly contradictory phenomenon observed in the clinic.

TARGETED THERAPIES IN BREAST CANCER

Over the last past few decades, breast cancer mortality dramatically decreased in great part due to use of adjuvant systemic therapy (Berry et al. 2005; Berry et al. 2006), including chemotherapy for most patients, endocrine therapy for those with ER+ disease, and more recently trastuzumab for tumors that overexpress HER2. However, many years before the development of trastuzumab, endocrine therapy was the cornerstone in the therapeutic repertoire for treatment of metastatic, hormone receptor-positive breast cancer

(Montemurro et al. 2012). In fact, androgen deprivation therapy for prostate cancer and estrogen deprivation therapy for breast cancer represent two of the earliest targeted therapies in solid tumor oncology. While both diseases present an initial stage wherein hormone therapy is successful in controlling the disease, either through inhibition of endogenous hormone production or through inhibition of hormone receptor signaling, after a period of time both cancer types exhibit insensitivity to the effects of the first-line treatment option (Oxnard 2012).

It has been over a century since the first clinical observation that oophorectomy of a human patient with advanced breast cancer was effective in treating the disease (Beatson 1896). Tamoxifen, a selective modulator of ER that competitively inhibits the binding of estradiol and consequently disrupts mechanisms regulating cellular replication and proliferation, has been in use in the clinic since the 1970s (Jordan and Dowse 1976). Application of endocrine therapy in a non-selective manner across patient cohorts results in response rates of 30% (Buzdar and Hortobagyi 1998). In advanced tumors positive for both receptors response rates increase to 50-70%.

While tamoxifen was the staple component of breast cancer treatment for many years, research to find new strategies for treating tamoxifen-resistant hormone-dependent breast cancer led to the development of a new class of agents, aromatase inhibitors, that act to reduce estradiol production through adrenal androgen conversion by the aromatase enzyme (Harvey 1996). Aromatase inhibitors are also being actively evaluated as prevention agents for women with a history of ductal carcinoma in situ (DCIS), as well as for the treatment of women considered at high risk for developing primary invasive breast cancer (Litton et al. 2012). These early observations in targeted therapy involving mixed responses and development of resistance underscored the critical need for a better comprehension of

the molecular biology at the source of this clinical diversity and an arsenal of targeted therapies to match.

Since its FDA approval in 1998, trastuzumab has become a key component in the treatment of early and metastatic HER2-positive breast cancer (Hudziak et al. 1989; Baselga et al. 1996; Slamon et al. 2001), and demonstration of its anti-tumor activity provided the proof of principle for therapy targeted to receptor tyrosine kinases (RTKs). A member of the epidermal growth factor receptor (EGFR) family, the HER2 protein is a transmembrane tyrosine kinase receptor involved in regulation of cell growth, migration, survival and differentiation (Yarden and Sliwkowski 2001). Amplification of the gene encoding HER2 (King et al. 1985), *v-erb-b2 erythroblastic leukemia viral oncogene homolog 2* (*ErbB2*) first discovered in 1984 (Schechter et al. 1984), is the most common mechanism leading to overexpression of the receptor (Pauletti et al. 1996) and results in the constitutive signaling of downstream pathways (Yarden and Sliwkowski 2001). HER2 has been found overexpressed in 20-30% of human breast cancers and prior to the advent of HER2-targeted therapies, patients with HER2-positive disease had higher risk of recurrence after initial therapy and poor prognosis (Slamon et al. 1987; Slamon et al. 1989).

The EGFR family, which also includes EGFR (HER1), HER3 and HER4, is involved in cell-cell and cell-stroma communication through signal transduction whereby external growth factors, or ligands, affect the downstream transcription of various genes via the phosphorylation or dephosphorylation of a series of transmembrane proteins and intracellular intermediates, many of which possess enzymatic activity (Ross et al. 2009). Activation of the kinase occurs with ligand biding and subsequent hetero- or homodimerization of these receptors. HER2 is capable of acting in a ligand-independent manner when mutated or overexpressed (Yarden 2001). Its overexpression in the context of

breast cancer, which can range from 2- to greater than 20-fold, has been associated with cancer promoting phenotypes including increased cell proliferation, cell motility, tumor invasiveness, progressive regional and distant metastases, accelerated angiogenesis and reduced apoptosis (Moasser 2007). HER2 signaling has been demonstrated to promote cell proliferation through the RAS-MAPK pathway and inhibit cell death through the phosphatidylinositol 3'-kinase (PIK3)/AKT/mammalian target of rapamycin (mTOR) pathway (Yarden and Sliwkowski 2001).

In 2012, trastuzumab remained the only approved HER2-targeted therapy in the adjuvant setting (Jelovac and Wolff 2012). Data from the first generation of clinical trials combining it with various chemotherapy regimens showed significant improvements in disease-free and overall survival, and consequently a trastuzumab-containing regimen for up to one year is now considered standard for all eligible patients with HER2-positive tumors. Trastuzumab has significant clinical benefit in the adjuvant and metastatic setting but both *de novo* and acquired clinical resistance have been observed (Baselga 2001). Second generation HER2-targeted drugs are in development and in clinical trials, such as antibodies against its external domain (pertuzumab), small-molecule tyrosine kinase inhibitors (lapatinib and neratinib), anti-HER2 antibodies conjugated to toxic molecules (trastuzumab-DM1 or T-DM1), and chaperone antagonists (geldanamycin) (Perez and Spano 2012; Tsang and Finn 2012).

MOUSE MODELS OF BREAST CANCER

Human breast cancer cell lines are used extensively as preclinical models both *in vitro* and *in vivo* as xenografts. Although cell line models have not proven useful for the identification of biomarkers of chemotherapy response, and controversy remains to whether

the diversity within the available breast cancer cell lines accurately mirrors the inter-tumoral heterogeneity observed in the clinic, there is evidence to suggest that when employed under the right framework they can serve as a powerful tool for predicting the clinical performance of cancer drugs (Voskoglou-Nomikos et al. 2003; Lacroix and Leclercq 2004; Bernards 2012).

In a recent study, Neve and colleagues reported, after cross-examining the molecular profiles and genomic alterations of 51 breast cancer cell lines and 145 primary human breast tumors, that when relevant subsets of cell lines are used as a system rather than alone they can provide robust platforms for the investigation of the signaling pathways associated with therapeutic response (Neve et al. 2006). Furthermore, an argument can be made that connections between signaling pathways that have proven critical for the development of acquired resistance to targeted therapies are hard-wired in a cell autonomous manner and consequently less dependent on microenvironmental factors. Nonetheless, it remains of vital importance to complement cell line models with other approaches for predicting drug response and studying tumor biology, such as three-dimensional cell culture systems, patient-derived mouse xenograft and transgenic models of breast cancer (Bernards 2012).

Xenograft models

While xenograft models involving human breast cancer cell lines suffer from some of the same basic criticisms raised against their use in *in vitro* studies, seminal publications in the field have demonstrated their utility and direct relevance to the human disease. A series of studies from Massagué and colleagues have shown that intravenous experimental metastasis assays can be used to define metastasis gene signatures that correlate significantly with clinical data and provide valuable insights into the molecular biology

underlying the metastatic process (Minn et al. 2005; Kim et al. 2009; Zhang et al. 2009). Other investigators have also been successful in using xenographs to identify gene signatures that correlate with prognostic outcomes (Kluger et al. 2005; Montel et al. 2005).

The growth of breast cancer cell lines in an *in vivo* environment allows for experiments to incorporate the complex tumor-stromal cell interactions that facilitate disease formation and progression (Vargo-Gogola and Rosen 2007). However, the obligate use of immunocompromised mice and the resulting absence of an intact immune system may have profound effects on the tumor biology (Balkwill et al. 2005). There is increasing evidence to suggest the fundamental role of the immune system in various stages of tumorigenic transformation (Goswami et al. 2005; Schwertfeger et al. 2006; Shree et al. 2011). The transplantation of human tumor cells into a foreign microenvironment and the absence of co-evolvement of epithelial and stromal compartments of the tumor may point to some of the reasons why testing therapeutics in xenograft models has fallen short of accurately predicting treatment efficacy in human patients (Vargo-Gogola and Rosen 2007). Efforts to humanize the mouse mammary fat pad, through the reconstitution of tumor-promoting immune and fibroblast compartments (Orimo et al. 2005; Proia and Kuperwasser 2006), and the use of a panel of subtype xenografts instead of a single cell line, may eventually allow for increased predictive power. The application of xenograft transplantation methodology to perpetuate and expand breast cancer clinical isolates is a unique alternative to the use of human cell lines. While the preserved authenticity of the human genomic landscape and the retention of stromal components of patient tumor biology makes this an ideal model in design, it is inefficient in practice and access to clinical samples is limited (Vargo-Gogola and Rosen 2007). Overall, a better understanding of the role of the immune system, microenvironment and the unique traits of human breast cancer molecular subtypes is

required before informed changes can be made to improve their strength as preclinical models and ultimately overcome the obstacle of inefficient translation of major advances in basic cancer research into the clinic.

Transgenic approaches

A new era of mammary tumor research was initiated in 1984 by Stewart, Pattengale, and Leder's paper using the mouse mammary tumor virus long terminal repeat (MMTV-LTR) to promote the expression of the proto-oncogene *Myc* in the mouse mammary gland (Stewart et al. 1984). Since then, genetically engineered mouse models (GEMMs) have contributed extensively to our understanding of genes that are involved in the promotion and progression of breast cancer.

The first generation of breast cancer GEMMs were generated by targeting oncogenes such a *Myc*, polyoma virus middle T (PyMT), rat *ErbB2/Neu*, and *Hras* to the mammary gland using the MMTV-LTR and whey acidic protein (*Wap*) promoters (Sinn et al. 1987; Muller et al. 1988; Guy et al. 1992a; Guy et al. 1992b). These relatively simple transgenic models provided tools for examining how these oncogenes contribute to breast tumorigenesis, but a greater wealth of information regarding signaling interactions was obtained by interbreeding various transgenic strains together (Vargo-Gogola and Rosen 2007). Further advances in mouse modeling technology, such as the use of tetracycline-regulatable transgenes, allowed for increased precision and control in the developmental timing of the induced changes in gene function (Gunther et al. 2002). Moreover, heightened tissue and cell type selectivity was afforded through the adoption of Cre/*loxp* recombinase-mediated somatic gene deletion and activation that is driven by promoters with varied expression patterns, such as MMTV, WAP or keratin-14 (K14) (Wagner et al. 1997; Jonkers et

al. 2001; Wagner et al. 2001; Lin et al. 2004). These advances, that afforded spatial and temporal control over loss and gain of gene function, created GEMMs that could begin to replicate the development of human breast cancer *in vivo*.

In contrast to xenograft transplantation systems, GEMMs are immunocompetent and retain the endogenous tissue architecture and microenvironmental cues. Sophisticated techniques, such as the application of intravital microscopy in transgenic breast cancer models has provided a new window through which to study the processes of angiogenesis, inflammation and the many steps of metastatic disease dissemination (MacDonald and Chambers 2006; Wyckoff et al. 2007; Egeblad et al. 2008).

To determine the extent to which GEMMs faithfully reproduce the molecular features of the human disease, Perou and colleagues extended their study of the molecular profiles of human tumors to the commonly used murine models of mammary carcinoma. A comprehensive interspecies analysis, involving the gene-expression profiles for 232 human breast cancers and 122 mouse mammary tumor samples obtained from 13 GEMMs, was able to identify conserved gene expression features between murine and human tumors. Although no single mouse model recapitulated all the features of a given human breast cancer subtype, genotype correlated strongly with phenotype in the murine tumors and the shared expression features provided a framework from which to build a better understanding of how researchers might translate findings in GEMMs to the clinic (Herschkowitz et al. 2007). Recent studies have also shown that transplantation of transgenic tumors is an effective way of generating large cohorts of mice bearing well-characterized tumors with defined molecular and genetic backgrounds, thus providing a new avenue for the use of GEMMs as a preclinical model (Varticovski et al. 2007).

Owing to the diversity of human breast cancer and species differences, individual GEMMs should not be expected to faithfully recapitulate all aspects of the human disease but it is evident from the literature that over the past three decades, GEMMs have become invaluable tools for the investigation of human breast cancer genetics and pathogenesis, and that novel methods towards the optimization of their utility as preclinical models are still emerging.

PI3K/AKT PATHWAY AND PTEN

The phosphoinositide triphosphate kinase (PI3K)/AKT/mammalian target of rapamycin (mTOR) pathway is a central intracellular regulatory pathway, which is one of the most frequently activated signaling pathways in cancer. Phosphoinositide 3-kinases (PI3Ks) act by phosphorylating phosphatidylinositol lipid substrates, which in turn activate multiple effector proteins, and govern many cellular processes such as cell cycle progression, growth, differentiation, metabolism, survival and migration (Cantley 2002). Oncogenic mutations in the PI3K signaling pathway are frequently found in human cancers, including breast (Baselga 2011). These mutations generally involve either activating mutations in the genes encoding the kinases *PIK3CA* or *AKT1*, or the loss or reduced expression of the phosphatases PTEN, SHIP or INPP4B (Stemke-Hale et al. 2008). PIK3CA is found mutated in approximately 25-40% of all breast tumors (Cancer Genome Atlas Network 2012) and it has been suggested that *PIK3CA* mutations are an early even in breast cancer, more likely to play a role in breast cancer initiation than in invasive progression (Miron et al. 2010).

While HER2 and ERα have been the most commonly used targets for the treatment of breast cancer patients, activated PI3K pathway is emerging as a major target for selective

therapeutics agents (Stemke-Hale et al. 2008). A diverse set of pharmacological inhibitors has been developed to inactivate this pathway in cancer cells (Courtney et al. 2010). However, trials thus far have demonstrated that monotherapy with a single targeted inhibitor is not capable of effectively eradicating the disease (Baselga 2011). For finding effective combination therapies that can counteract the inevitable resistance mechanisms being seen against these inhibitors, physiological preclinical mouse models that can accurately predict response to treatment are essential (Klarenbeek et al. 2013).

The tumor suppressor gene *PTEN* is a negative regulator of the PI3K/Akt signaling pathway and is also found disrupted in many cancers (Cantley and Neel 1999). In fact, it is one of the most commonly lost or mutated tumor suppressor genes in human cancers (Song et al. 2012). Additionally, germ line mutations are found in several familial cancer predisposition syndromes (Liaw et al. 1997; Yin and Shen 2008). *PTEN* was initially identified as a gene frequently lost in brain, breast and prostate cancers (Li et al. 1997; Steck et al. 1997). Shortly thereafter, it was biochemically demonstrated that PTEN is a phosphatase responsible for the dephosphorylation of the messenger molecule phosphatidylinositol-3,4,5-triphosphate (Maehama and Dixon 1998) and that it was a negative regulator of the cell survival kinase Akt (Stambolic et al. 1998). In addition to its canonical role as a tumor suppressor gene in the PI3K pathway, in the context of breast cancer PTEN has been implicated in the resistance of HER2-targeted treatment (Nagata et al. 2004; Berns et al. 2007) and has been shown to have a possible microenvironmental role in tumor-stroma co-evolution (Wallace et al. 2011). PTEN has been demonstrated to be acutely dose dependent in determining cancer susceptibility, defining it as a haploinsufficient tumor suppressor gene (Alimonti et al. 2010; Berger and Pandolfi 2011).

RNA INTERFERENCE AND SHRNAS

In 1993, a new class of RNA molecules, later named microRNAs, was identified (Lee et al. 1993; Wightman et al. 1993). Through the discovery of RNA interference – a sequence-specific gene silencing mechanism mediated by double-stranded RNA – a new era of loss-of-function experimentation emerged (Fire et al. 1998), where it was possible, in principle, to reversibly suppress the expression of any gene in the genome. Although this mechanism of post-transcriptional gene silencing was first discovered in the nematode *Caenorhabditis elegans*, subsequent genetic and biochemical studies have revealed insights into the pathway and uncovered analogous mechanisms in eukaryotic organisms (Hannon 2002).

MicroRNAs form the largest class of small non-coding RNAs and are involved in the spatio-temporal control of endogenous gene activity. This mechanism of negative regulation of target gene expression at the post-transcriptional level can be hijacked by double-stranded RNA of exogenous sources to silence genes of interest in a sequence-specific manner. While transient regulation can be triggered in cultured mammalian cells through the introduction of synthetic siRNA duplexes (Elbashir et al. 2001), the use of viral vectors as a delivery vehicle for the stable expression of stem-loop structures resembling pre-miRNAs creates a renewable source of silencing reagents that can be transduced into almost any immortalized or primary cell type at controlled copy numbers (Brummelkamp et al. 2002; Paddison et al. 2002).

By embedding an artificial hairpin-like structure into the physiological backbone of an endogenous miRNA (human miR-30), short hairpin RNAs (shRNAs) have been engineered to be recognized as a natural substrate. The hybrid pri-mRNAs expression cassette, which retains all the *cis*-acting sequences required for pri-miRNA processing, are processed through the canonical RNAi pathway and consequently allow for target

inhibition through the production of synthetic mature small RNAs (Silva et al. 2005). Further spatio-temporal control has been incorporated through the use of the RNA polymerase II-dependent promoter (Dickins et al. 2005; Stegmeier et al. 2005). Moreover, combining shRNA knockdown with tetracycline-regulated expression systems (Gossen and Bujard 1992; Gossen et al. 1995), as well as the use of fluorescent reporters, has conferred additional versatility to the use of this tool for conditional gene expression in both *in vitro* and *in vivo* studies (Premsrirut et al. 2011; Zuber et al. 2011a).

II. An oncogenomics-based *in vivo* RNAi screen for novel tumor suppressors genes relevant to breast cancer

INTRODUCTION

All cancers are a consequence of alterations in the DNA of a once healthy cell (Greenman et al. 2007; Stratton et al. 2009). Forward genetic screens can be used to identify the key tumorigenic drivers within loci that show copy number variation in human patients (Zender et al. 2008). This approach is founded on the hypothesis that chromosomal regions lost in human cancers are enriched for TSGs. Genomic instability, that is a characteristic of tumorigenesis, leads to the deletion and amplification of chromosomal regions. Such copy number alterations constitute one of several types of genetic aberrations that manifest in a cancer genome including specific DNA sequence mutations, structural rearrangements (translocations) and alterations in epigenetic profiles (Chin and Gray 2008). It can be postulated that deletion of regions enriched for TSGs will confer a proliferative and/or survival advantage to a cell and thus will be selectively maintained during tumor evolution (Bignell et al. 2010). In this manner, identifying recurrent alterations of the cancer genome can lead us towards a focused search for novel cancer genes (Velculescu 2008).

Significant advances in sequencing technology over the past decade have allowed for an exponential increase in the resolution at which cancer cells can be analyzed (Futreal et al. 2001; Wood et al. 2007; Mardis 2008; McLendon R et al. 2008). The first fully sequenced cancer genome of a cytogenetically normal acute myeloid leukemia was published in 2008 (Ley et al. 2008). The genomes and transcriptomes of the primary and metastasized lesions

of an estraogen-receptor-α-positive metastatic lobular breast cancer have also been sequenced at depth (Shah et al. 2009).

A major challenge lies in translating such a vast catalogue of genomic information into clinical use (Chin and Gray 2008). Due to spontaneous mutagenesis, inherent chromosomal and genomic instability of cancerous cells, and association through genetic linkage, all genomic alterations displayed in cancers are not necessarily relevant to the progression of the disease itself (Zender et al. 2008). Previous studies by the Lowe laboratory have demonstrated that *in vivo* RNAi screening approaches allow for the efficient filtering of oncogenomic data and the identification of novel TSGs (Zender et al. 2008; Bric et al. 2009; Scuoppo et al. 2012). A similar methodology has also been applied towards the identification of oncogenes among frequently amplified regions of the genome (Sawey et al. 2011).

In order to perform an *in vivo* RNAi screen for TSGs relevant to breast cancer, we sought to develop an orthotopic transplantation model. Although constructing a high-throughput platform proved challenging, a small gene-by-gene screen was conducted and *Nf1*, a gene that encodes neurofibromin 1 (NF1), was identified and validated in our mouse model as a putative TSG in HER2-driven breast cancer. Transgenic strains with shRNAs targeting *Nf1* were subsequently generated for further studies.

RESULTS

Generating a list of candidate tumor suppressor genes and an shRNA library

Regions of copy number variation can be identified using high-resolution array-based comparative genomic hybridization (CGH). In collaboration with Jim Hicks and Michael Wigler at Cold Spring Harbor Laboratory (CSHL), a candidate TSG list was

generated from the analysis of genomic deletion and amplification frequencies of 247 primary breast cancers and 43 breast cancer cell lines using representational oligonucleotide microarray analysis (ROMA) (Lucito et al. 2003; Hicks et al. 2006; Zender et al. 2008).

In an effort to selectively identify recurrently deleted genes from the array data, criteria were established requiring deletions to represent focally deleted chromosomal regions of less than 5Mb and a minimum frequency of at least 5% within the overall dataset. Focal deletions were in most cases less than 1Mb in length. With the aid of supporting evidence from the literature, the original list was further refined to a focused set of 144 genes [Table 2.1]. Mouse orthologs were identified using the open source database BioMart (www.biomart.org) (Haider et al. 2009), reducing the list to 112 candidates. Thirty-seven additional genes were curated from a Genentech study of high-resolution CGH analysis of 51 breast tumors to supplement this list (Haverty et al. 2008), resulting in a total of 149 candidate genes. Unfortunately, the ROMA breast cancer dataset was too small to segregate the patient samples by their molecular annotation without losing statistical significance, preventing us from compiling a list of candidate TSGs specific to the HER2 overexpression clinical subtype. However, later in this chapter, attempts to screen these candidate genes in a model of HER2-positive breast cancer will be discussed at length. In future iterations of RNAi screens seeking to identify cancer genes and drug targets relevant to human breast cancer, it will be critical to integrate the molecular profiles of clinical samples into the fundamental design of the project.

The neural network siRNA algorithm BIOPREDsi developed by Novartis (http://www.biopredsi.org/) was used to design five unique shRNA sequences targeting the mouse ortholog of each candidate gene (745 shRNAs total) (Huesken et al. 2005) [Table 2.2]. We have previously shown that stable suppression of gene expression can be achieved

Table 2.1 ROMA recurrent deletion tumor suppressor candidates

Chromosomal regions	*Gene names*
chr5:16,723,108-17,775,055	MYO10
	BASP1
chr8:11,108,957-14,105,148	MTMR9
	AMAC1L2
	BLK
	GATA4
	NEIL2
	FDFT1
	CTSB
	DUB3
	DLC1
	SGCZ
chr8:34,256,633-36,524,467	UNC5D
chr8:39,328,853-41,933,548	ADAM18
	ADAM2
	INDO
	INDOL1
	C8orf4
	ZMAT4
	SFRP1
	GOLGA7
	GINS4
	AGPAT6
	NKS6-3
	ANK1
	has-mir-486
	MYST3
chr9:37,004,824-38,655,208	PAX5
	ZCCHC7
	GRHPR
	ZBTB5
	PAF53
	C9orf105
	EXOSC3
	WDR32
	MCART1
	ALDH1B1
	IGFBPL1
	ANKRD18A

chr9:78,799,360-83,235,988	TLE4
	RASEF
chr10:69,209,947-70,876,569	DNJC12
	SIRT1
	HERC4
	FLJ14437
	ATOH7
	MAWBP
	HNRPH3
	RUFY2
	SLC25A16
	CXXC6
	CCAR1
	STOX1
	DDX50
	DDX21
	PRG1
	VPS26
	SUPV3L1
	HKDC1
	HK1
	TACR2
chr11:46,327,487-48,083,630	DGKZ
	MDK
	CHRM4
	AMBRA1
	ARHGAP1
	ZNF408
	F2
	CKAP5
	LRP4
	ARFGAP2
	PACSIN3
	DDB2
	ACP2
	NR1H3
	MADD
	MYBPC3
	SPI1
	SLC39A13
	PSMC3
	RAPSN
	CUGBP1

	PTPMT1
	KBTBD4
	MTCH2
	AGBL2
	FNBP4
	NUP160
	PTPRJ
chr11:56,305,352-57,532,499	OR5AK2
	AGTRL1
	TMLS1BP1
	SSRP1
	P2RX
	SLC43A3
	RTN4RL2
	UBE2L6
	SERPING1
	YPEL
	CLP1
	HEAB
	ZDHHC5
	has-mir-130a
	MED19
	CTNND1
chr11:71,383,633-71,895,665	RNF121
	IL18BP
	NUMA1
	LRRC51
	FOLR3
	FOLR1
	FOLR2
	INPPL1
	PHOX2A
	SKD3
chr11:73,675,366-74,237,477	P4HA3
	PGM2L1
	KCNE3
	POLD3
	CHRDL2
chr11:83,312,841-84,692,488	DLG2
chr13:19,212,114-20,340,806	PSPC1
	ZNF237
	ZNF198
	GJA3

	GJB2
	GJB6
	TTC10
	IL17D
	LOC221143
	XPO4
chr17:26,402,098-28,056,700	NF1
	OMG
	EVI2A
	EVI2B
	RAB11FIP4
	hsa-mir-193A
	hsa-mir-365-2
	C17orf40
	RHOT1
	RHBDL4
	ZNF207
	PSMD11
	CDK5R1
	MYO1D
Genentech (Haverty et al.) candidates	NOX3
	TIAM2
	CLDN20
	ANGPT2
	MFHAS1
	PPP1R3B
	hsa-mir-124a-1
	RP1L1
	SOX7
	PINX1
	XKR6
	LONRF1
	DLC1
	GATA4
	NEIL2
	FGF20
	EGR3
	TNFRSF10A
	EFHA2
	PTK2B
	hsa-mir-383
	MAML2
	MMP1

	CASP4
	CASP5
	COP1
	CHEK1
	hsa-let-7a-2
	SMAD9
	POSTN
	CCNA1
	RB1
	hsa-mir-16-1
	hsa-mir-15a
	PCDH9
	SQSE29775
	EDNRB
	SCEL
	CHES1
	STX8
	RCV1
	GAS7
	MYH1
	MAP2K4
	MYOCD
	ZNF18
	LOC91353
	LRP5L

Table 2.2 Candidate tumor suppressor gene shRNA library – 149 genes/745 shRNAs

Acp2.1364	Ank1.153	Cdk5r1.1759	Ctsb.1897	Egr3.118
Acp2.1824	Ank1.2400	Cdk5r1.1993	Ctsb.2102	Egr3.182
Acp2.191	Ank1.2613	Cdk5r1.3373	Ctsb.215	Egr3.235
Acp2.933	Ank1.4409	Cdk5r1.4051	Ctsb.3129	Egr3.38
Acp2.95	Ank1.923	Cdk5r1.545	Ctsb.3229	Egr3.538
Adam18.1508	ArfGAP2.1212	Chek1.1720	Cugbp1.1414	Evi2a.1073
Adam18.1630	ArfGAP2.1892	Chek1.2012	Cugbp1.1755	Evi2a.723
Adam18.334	ArfGAP2.2677	Chek1.2128	Cugbp1.1790	Evi2a.845
Adam18.456	ArfGAP2.2688	Chek1.2348	Cugbp1.206	Evi2a.896
Adam18.492	ArfGAP2.323	Chek1.729	Cugbp1.329	Evi2a.960
Adam2.160	Arhgap1.2092	Chrdl2.1172	Ddb2.1336	Evi2b.1040
Adam2.2398	Arhgap1.2352	Chrdl2.1313	Ddb2.364	Evi2b.2989
Adam2.323	Arhgap1.3018	Chrdl2.1388	Ddb2.736	Evi2b.375
Adam2.394	Arhgap1.381	Chrdl2.824	Ddb2.946	Evi2b.821
Adam2.490	Arhgap1.896	Chrdl2.836	Ddb2.971	Evi2b.84
Agbl2.1512	Atoh7.235	Chrm4.1208	Ddx21.1441	Exosc3.329
Agbl2.2907	Atoh7.272	Chrm4.1484	Ddx21.1487	Exosc3.374
Agbl2.3337	Atoh7.278	Chrm4.2267	Ddx21.395	Exosc3.620
Agbl2.3368	Atoh7.373	Chrm4.2706	Ddx21.4037	Exosc3.715
Agbl2.650	Atoh7.387	Chrm4.431	Ddx21.4419	Exosc3.980
Agpat6.1823	Basp1.136	Ckap5.2579	Ddx50.1347	F2.1531
Agpat6.2187	Basp1.495	Ckap5.3361	Ddx50.1476	F2.1630
Agpat6.2465	Basp1.655	Ckap5.3671	Ddx50.1637	F2.1685
Agpat6.476	Basp1.661	Ckap5.3923	Ddx50.2437	F2.1820
Agpat6.711	Basp1.662	Ckap5.6478	Ddx50.2468	F2.1850
Agtrl1.1869	Blk.1785	Cldn20.381	Dgkz.1156	Fdft1.1009
Agtrl1.1960	Blk.2172	Cldn20.418	Dgkz.1166	Fdft1.1861
Agtrl1.1968	Blk.385	Cldn20.443	Dgkz.2104	Fdft1.782
Agtrl1.2532	Blk.625	Cldn20.634	Dgkz.3338	Fdft1.932
Agtrl1.3374	Blk.94	Cldn20.641	Dgkz.3491	Fdft1.997
Aldh1b1.1927	Casp4.1126	Clp1.1006	Dlc1.1594	Fgf20.418
Aldh1b1.2190	Casp4.1254	Clp1.1386	Dlc1.2161	Fgf20.448
Aldh1b1.2247	Casp4.1277	Clp1.162	Dlc1.3806	Fgf20.512
Aldh1b1.524	Casp4.402	Clp1.702	Dlc1.4074	Fgf20.595
Aldh1b1.88	Casp4.733	Clp1.711	Dlc1.5485	Fgf20.602
AMBRA1.3565	Ccar1.261	Clpb.1556	Dlg2.2184	Fnbp4.1674
AMBRA1.3831	Ccar1.2906	Clpb.3761	Dlg2.249	Fnbp4.2253
AMBRA1.533	Ccar1.645	Clpb.3946	Dlg2.4827	Fnbp4.3353
AMBRA1.534	Ccar1.691	Clpb.4074	Dlg2.6459	Fnbp4.4464
AMBRA1.599	Ccar1.713	Clpb.444	Dlg2.961	Fnbp4.4649
Angpt2.1082	Ccna1.1058	Ctnnd1.110	Ednrb.1478	Folr1.1242
Angpt2.1279	Ccna1.1214	Ctnnd1.2122	Ednrb.1720	Folr1.202
Angpt2.1641	Ccna1.163	Ctnnd1.2260	Ednrb.1954	Folr1.65
Angpt2.1662	Ccna1.376	Ctnnd1.3138	Ednrb.3631	Folr1.650
Angpt2.806	Ccna1.923	Ctnnd1.900	Ednrb.3701	Folr1.92

Folr2.1075	Grhpr.468	Inppl1.945	Mdk.474	Myo10.7990
Folr2.355	Grhpr.628	Inppl1.1072	Mdk.631	Myo10.956
Folr2.52	Grhpr.771	Inppl1.1627	Mdk.639	Myo1d.1890
Folr2.680	Herc4.2552	Inppl1.3469	Mdk.642	Myo1d.1939
Folr2.740	Herc4.2657	Inppl1.4434	Med19.1091	Myo1d.2145
FoxN3.1482	Herc4.3413	Inppl1.457	Med19.1097	Myo1d.4761
FoxN3.2207	Herc4.3568	Kbtbd4.1039	Med19.1147	Myo1d.720
FoxN3.2386	Herc4.574	Kbtbd4.2145	Med19.1328	Myocd.2874
FoxN3.2514	Hk1.209	Kbtbd4.2232	Med19.1776	Myocd.3969
FoxN3.708	Hk1.2369	Kbtbd4.2266	Mfhas1.2757	Myocd.4206
Gas7.3443	Hk1.2537	Kbtbd4.2359	Mfhas1.3288	Myocd.4499
Gas7.3501	Hk1.2599	Kcne3.571	Mfhas1.4081	Myocd.658
Gas7.4460	Hk1.2630	Kcne3.840	Mfhas1.4869	Myst3.2590
Gas7.4483	Hkdc1.1016	Kcne3.88	Mfhas1.4961	Myst3.3127
Gas7.6555	Hkdc1.3367	Kcne3.894	Mmp13.1241	Myst3.3485
Gata4.2478	Hkdc1.3425	Kcne3.981	Mmp13.1284	Myst3.4554
Gata4.2882	Hkdc1.3426	LONRF1.1065	Mmp13.1662	Myst3.6844
Gata4.2989	Hkdc1.359	LONRF1.1533	Mmp13.1906	Neil2.1184
Gata4.343	Hnrph3.1561	LONRF1.2779	Mmp13.2534	Neil2.1850
Gata4.416	Hnrph3.1599	LONRF1.2852	Mtch2.1392	Neil2.440
Gins4.1105	Hnrph3.1684	LONRF1.3622	Mtch2.2058	Neil2.787
Gins4.1294	Hnrph3.1899	Lrp4.4384	Mtch2.2245	Neil2.923
Gins4.621	Hnrph3.486	Lrp4.604	Mtch2.409	Nf1.3226
Gins4.723	Igfbpl1.1968	Lrp4.6063	Mtch2.850	Nf1.6052
Gins4.822	Igfbpl1.504	Lrp4.7106	Mtmr9.1156	Nf1.6074
Gja3.1067	Igfbpl1.560	Lrp4.7332	Mtmr9.1627	Nf1.9045
Gja3.139	Igfbpl1.624	Madd.1519	Mtmr9.1653	Nf1.9930
Gja3.1391	Igfbpl1.792	Madd.1688	Mtmr9.1837	Nox3.1135
Gja3.809	Il17d.1054	Madd.2701	Mtmr9.995	Nox3.1514
Gja3.968	Il17d.1173	Madd.3130	Mybpc3.1176	Nox3.1550
Gjb2.1905	Il17d.379	Madd.4588	Mybpc3.1367	Nox3.30
Gjb2.2099	Il17d.806	Maml2.208	Mybpc3.3497	Nox3.894
Gjb2.2264	Il17d.920	Maml2.2143	Mybpc3.3608	Nr1h3.1739
Gjb2.569	Il18bp.1004	Maml2.3352	Mybpc3.4122	Nr1h3.1845
Gjb2.599	Il18bp.1134	Maml2.3492	Myh1.2060	Nr1h3.1853
Gjb6.1082	Il18bp.1266	Maml2.92	Myh1.2590	Nr1h3.563
Gjb6.1252	Il18bp.1368	Map2k4.218	Myh1.283	Nr1h3.788
Gjb6.1382	Il18bp.857	Map2k4.3198	Myh1.4540	Numa1.1262
Gjb6.775	Indo.1030	Map2k4.3242	Myh1.5641	Numa1.1391
Gjb6.882	Indo.1053	Map2k4.3553	Myh2.1129	Numa1.4538
Golga7.1249	Indo.1367	Map2k4.420	Myh2.221	Numa1.6275
Golga7.1353	Indo.1368	Mcart1.1792	Myh2.2240	Numa1.7111
Golga7.142	Indo.1381	Mcart1.2770	Myh2.23	Nup160.2099
Golga7.146	Indol1.1567	Mcart1.3405	Myh2.3767	Nup160.255
Golga7.1685	Indol1.2425	Mcart1.3560	Myo10.1124	Nup160.5392
Grhpr.1009	Indol1.2564	Mcart1.3803	Myo10.1685	Nup160.5556
Grhpr.361	Indol1.296	Mdk.227	Myo10.6841	Nup160.992

Omg.1201	Polr1e.2910	Rab11fip4.2924	Rtn4rl2.203	Slc43a3.2572
Omg.1378	Polr1e.388	Rapsn.1568	Rtn4rl2.457	Slc43a3.868
Omg.1700	Polr1e.999	Rapsn.442	Rtn4rl2.905	Smad9.1349
Omg.368	Postn.1066	Rapsn.682	Rtn4rl2.967	Smad9.2944
Omg.800	Postn.1649	Rapsn.871	Rufy2.156	Smad9.2965
P4ha3.1187	Postn.2709	Rapsn.96	Rufy2.2013	Smad9.3054
P4ha3.1382	Postn.2764	Rasef.1619	Rufy2.4145	Smad9.4358
P4ha3.1587	Postn.848	Rasef.1733	Rufy2.870	Sox7.1012
P4ha3.305	Ppp1r3b.2670	Rasef.2360	Rufy2.8828	Sox7.1623
P4ha3.669	Ppp1r3b.2720	Rasef.3787	Scel.1412	Sox7.2541
Pacsin3.1067	Ppp1r3b.2793	Rasef.982	Scel.2134	Sox7.3030
Pacsin3.1329	Ppp1r3b.340	Rb1.2317	Scel.2294	Sox7.3201
Pacsin3.1598	Ppp1r3b.3999	Rb1.3736	Scel.253	Srgn.202
Pacsin3.1685	Psmc3.1232	Rb1.4191	Scel.2892	Srgn.411
Pacsin3.740	Psmc3.1524	Rb1.508	Serping1.1194	Srgn.536
Pax5.154	Psmc3.318	Rb1.901	Serping1.1674	Srgn.661
Pax5.328	Psmc3.59	Rcvrn1.1005	Serping1.1772	Srgn.865
Pax5.601	Psmc3.947	Rcvrn1.231	Serping1.291	Ssrp1.1022
Pax5.852	Psmd11.1021	Rcvrn1.557	Serping1.998	Ssrp1.1100
Pax5.914	Psmd11.1081	Rcvrn1.576	Sfrp1.1803	Ssrp1.329
Pbld.1197	Psmd11.1122	Rcvrn1.838	Sfrp1.1887	Ssrp1.431
Pbld.1333	Psmd11.1149	Rfwd2.1866	Sfrp1.1978	Ssrp1.702
Pbld.1434	Psmd11.139	Rfwd2.2025	Sfrp1.3781	Stx8.1328
Pbld.1530	Pspc1.1714	Rfwd2.3664	Sfrp1.3903	Stx8.2538
Pbld.660	Pspc1.180	Rfwd2.3816	Sgcz.1008	Stx8.3979
Pcdh9.1446	Pspc1.2288	Rfwd2.4896	Sgcz.2367	Stx8.3995
Pcdh9.4411	Pspc1.880	Rhbdl3.1333	Sgcz.401	Stx8.93
Pcdh9.5145	Pspc1.993	Rhbdl3.1692	Sgcz.909	Supv3l1.1295
Pcdh9.5219	Ptk2b.1393	Rhbdl3.3158	Sgcz.950	Supv3l1.1425
Pcdh9.623	Ptk2b.1460	Rhbdl3.3319	Sirt1.1708	Supv3l1.1936
Pgm2l1.1544	Ptk2b.3282	Rhbdl3.3465	Sirt1.1779	Supv3l1.496
Pgm2l1.2972	Ptk2b.3571	Rhot1.1737	Sirt1.1921	Supv3l1.532
Pgm2l1.3051	Ptk2b.551	Rhot1.1869	Sirt1.2191	Tacr2.1357
Pgm2l1.3250	Ptpmt1.1078	Rhot1.3285	Sirt1.688	Tacr2.1531
Pgm2l1.7527	Ptpmt1.1080	Rhot1.334	Slc25a16.1575	Tacr2.1780
Phox2a.1307	Ptpmt1.1140	Rhot1.4055	Slc25a16.2535	Tacr2.1816
Phox2a.1316	Ptpmt1.1201	Rnf121.416	Slc25a16.2639	Tacr2.228
Phox2a.1373	Ptpmt1.884	Rnf121.60	Slc25a16.3108	Tiam2.2834
Phox2a.1415	Ptprj.4708	Rnf121.740	Slc25a16.322	Tiam2.3111
Phox2a.543	Ptprj.5046	Rnf121.768	Slc39a13.1018	Tiam2.5046
Pold3.1213	Ptprj.5347	Rnf121.791	Slc39a13.1544	Tiam2.5567
Pold3.2223	Ptprj.538	Rp1l1.4559	Slc39a13.2027	Tiam2.5675
Pold3.2668	Ptprj.7284	Rp1l1.5608	Slc39a13.2236	Tle4.1870
Pold3.427	Rab11fip4.1840	Rp1l1.5895	Slc39a13.778	Tle4.286
Pold3.641	Rab11fip4.2058	Rp1l1.6565	Slc43a3.1040	Tle4.3126
Polr1e.1726	Rab11fip4.2291	Rp1l1.6697	Slc43a3.2221	Tle4.3521
Polr1e.2529	Rab11fip4.290	Rtn4rl2.1030	Slc43a3.2483	Tle4.822

Ube2l6.1022	Zmat4.1785
Ube2l6.192	Zmat4.1806
Ube2l6.461	Zmat4.604
Ube2l6.620	
Ube2l6.630	
Unc5d.1851	
Unc5d.2469	
Unc5d.2930	
Unc5d.2952	
Unc5d.3319	
Vps26a.138	
Vps26a.1860	
Vps26a.2089	
Vps26a.713	
Vps26a.732	
Wdr32.2157	
Wdr32.2235	
Wdr32.3030	
Wdr32.3807	
Wdr32.6353	
Xkr6.1012	
Xkr6.310	
Xkr6.379	
Xkr6.852	
Xkr6.886	
Xpo4.1196	
Xpo4.2016	
Xpo4.2146	
Xpo4.2658	
Xpo4.375	
Zbtb5.1220	
Zbtb5.1228	
Zbtb5.2090	
Zbtb5.3265	
Zbtb5.379	
Zcchc7.430	
Zcchc7.503	
Zcchc7.588	
Zcchc7.831	
Zcchc7.859	
Zdhhc5.135	
Zdhhc5.2488	
Zdhhc5.4273	
Zdhhc5.542	
Zdhhc5.85	
Zmat4.1079	
Zmat4.1166	

in vivo by utilizing a murine stem cell virus (MSCV) based retroviral vector that expresses a human miR-30-based shRNA (Dickins et al. 2005). This pLMS (MLS) vector also contains a constitutively expressed green fluorescent protein (GFP) marker, used to identify transduced cells [FIGURE 2.1a]. As described further in Materials and Methods, shRNAs were generated from a pool of 97mer oligonucleotides and subcloned into pLMS. Sanger sequencing of individual bacterial clones following retransformation of the pLMS pools allowed identification of individual shRNAs. This enabled the assembly of a sequence validated library and access to shRNAs targeting individual genes for follow-up analysis.

The positive selection *in vivo* screen design is based on two assumptions: a) shRNA-mediated silencing can mimic the loss of TSGs; b) if reduced protein levels of a candidate TSG confers a growth or survival advantage, that shRNA will be selectively enriched during tumor growth. To identify enriched shRNAs the following work-flow is employed: 1) once a tumor has developed, genomic DNA is isolated and shRNAs contained in the retrovirus are cloned out using sequence specific primers to the human miR-30 backbone; 2) changes in shRNA representation are assessed by comparing abundance of each shRNA in the initial population to its presence in the resulting tumor; and 3) over-represented shRNAs indicate the possible identification of a novel TSG. To avoid results obtained through off-target effects, it is important that more than one shRNA against any particular gene scores in the assay. Short hairpin RNAs also need to show specific target knockdown by qRT-PCR or by Western blot if an antibody is available. All positive hits identified from the pooled screening approach must also be validated *in vivo* as single shRNAs. A caveat to this screening approach is that the lack of an effective shRNA will result in a false negative result where a valid candidate TSG will be missed due to insufficient knockdown. Efforts to

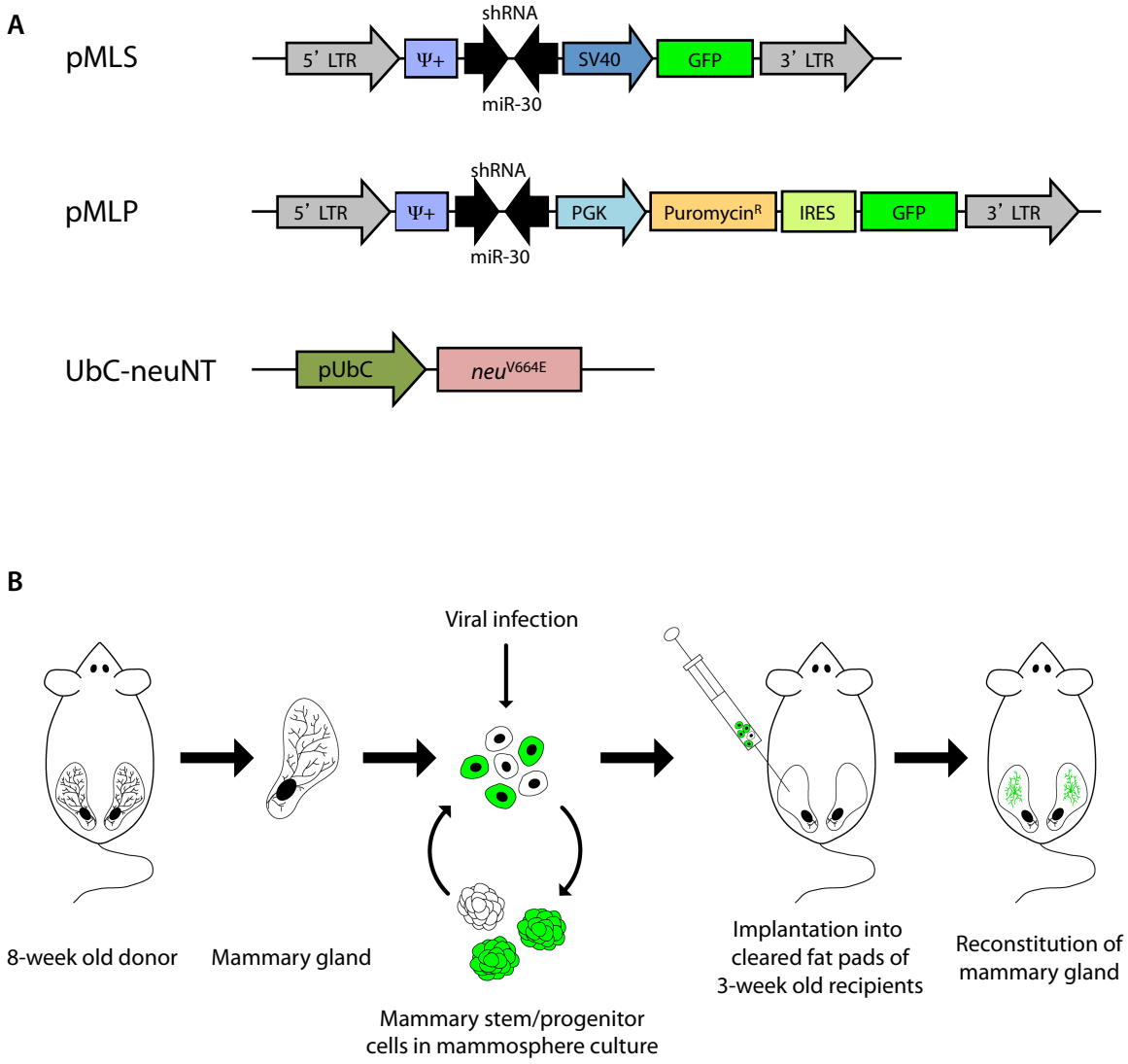

Figure 2.1 Viral constructs and orthotopic transplantation model schematic. (A) Retroviral constructs pMLS and pMLP for constitutive, GFP-reporter tagged expression of miR-30 shRNAs; Gateway 3rd generation lenti-viral vector with UbC promoter driving mutant rat *neu* overexpression. (B) Transplantation-based mosaic and modular mouse model incorporating the gland-reconstituting capacity of primary mammary stem/progenitor cells.

ameliorate shRNA design and efficacy has been an on-going area of research by other members of the laboratory (Fellmann et al. 2011).

Screening platform development

There are several important criteria for designing a well-adapted *in vivo* cancer model system for the purpose of conducting a positive selection screen. Firstly, it must be physiologically relevant to the human disease, reflecting both the genetics and histopathology of the cancer. Secondly, representation of the screening library should be maintained following transplantation of the cell population, taking into account 'tumor seeding' rates. Thirdly, a robust screening assay, in this case tumor development, which provides a clear window for detection of disease acceleration over baseline. In sum, each tissue and disease type present unique mouse modeling challenges that require careful consideration in order to maximize the utility of *in vivo* experimentation.

One advantage of a 'mosaic' transplantation model, where transduced mouse cells are orthotopically transplanted into a wild type recipient mouse, is that a physiological disease microenvironment is faithfully maintained (Zender et al. 2008; Bric et al. 2009; Zuber et al. 2009; Zuber et al. 2011b). With the exception of inherited genetic mutations, most tumorigenic cells arise surrounded by healthy, normal stromal tissue. Mosaic models also allow for a great deal of flexibility for the modular introduction of transgenes and RNAi constructs, as well as fluorescent and bioluminescent reporters that allow for easy tracking of the developing tumor. Importantly, primary cells with defined genetic manipulations are genetically tractable in a manner in which xenograft models relying on human cancer cells lines are not.

We sought to exploit the observation that the majority of murine mammary gland development occurs postnatally in a method that would combine the gland-reconstituting capacity of mammary stem/progenitor cells (MaSCs) with *ex vivo* genetic manipulation via viral transduction. Initial attempts to develop an orthotopic transplantation-based, modular and mosaic mouse model of breast cancer consisted of the following features and steps [also shown schematically in Figure 2.1b]. Beginning at three weeks of age, the endogenous mammary epithelium begins to develop into and populate the fat and connective tissue of the mammary gland, a process which is compete by ten weeks of age (Richert et al. 2000). Primary MaSCs would therefore be isolated from the mammary glands of adult donor female mice, approximately 8-12 weeks in age. The primary cells would be maintained in mammosphere *in vitro* culture to enrich for the stem/progenitor cells prior to introducing shRNA plasmids via lentiviral infection. Transduced cells would be implanted into the cleared fat pads of three-week-old syngeneic recipient animals. The clearing process removes the native stem cell population, allowing for the transplanted cells to reconstitute the mammary epithelium during puberty. Previous studies have shown that a single mammary stem cell transplanted into the developing gland of a prepubescent mouse is capable of reconstituting the entire gland (Shackleton et al. 2006; Stingl et al. 2006). Tumors would then develop in an immune-competent, wild type animal in the presence of the appropriate stromal and microenvironmental cues.

Although the intended model was optimal for positive selection, as it allows for implanted cells to fully integrate into the native glandular and stromal architecture before oncogenic transformation, it proved too complex to scale to a high-throughput screening platform. Side-by-side comparisons demonstrated that in our hands one freeze-thaw process could greatly reduce the efficiency of reconstitution following orthotopic

implantation of MaSCs (data not shown). The low yield of MaSCs per donor mouse made it prohibitively labor-intensive to harvest sufficient quantities of cells to conduct well-controlled experiments. While preserving as many of the original design elements as possible, we sought to find feasible alternatives.

The multi-potent mammary progenitor cell line Comma-D was a strong candidate to replace the primary cells for *in vivo* RNAi screening (Medina et al. 1986). Comma-D cells are capable of reconstituting a functionally normal mammary gland when transplanted into a cleared fat pad of a recipient mouse. However, these cells begin to transform after approximately twenty passages in culture and have two well-defined mutations in *TP53* – a substitution of tryptophan for cysteine at codon 138 and a deletion of the first 21 nucleotides at exon five – that have been suggested as the sources of genomic instability and susceptibility to neoplastic transformation *in vitro* (Jerry et al. 1994; Barcellos-Hoff and Ravani 2000). The lack of genetic tractability and the heterogeneity following passages *in vitro* caused dual concern for building a screening system, as genomic instability could cause a high rate of transformation *in vitro* and variation among the cells could compromise even shRNA library infection efficiency and representation. Diluting *c-Myc* overexpressing Comma-D cells into MaSCs to directly assess differences in the reconstituted gland morphology was used to test their mammary gland reconstitution capability. Twelve weeks after implantation, we observed that a higher percentage of Comma-D cells gave a more hyperplastic, branched ductal morphology [Figure 2.2]. In contrast, those glands with a predominantly MaSC population closely resembled endogenous control glands. The high rate of transformation raised the possibility that each reconstituted gland would contribute many initiating tumor cells and consequently confound the assay.

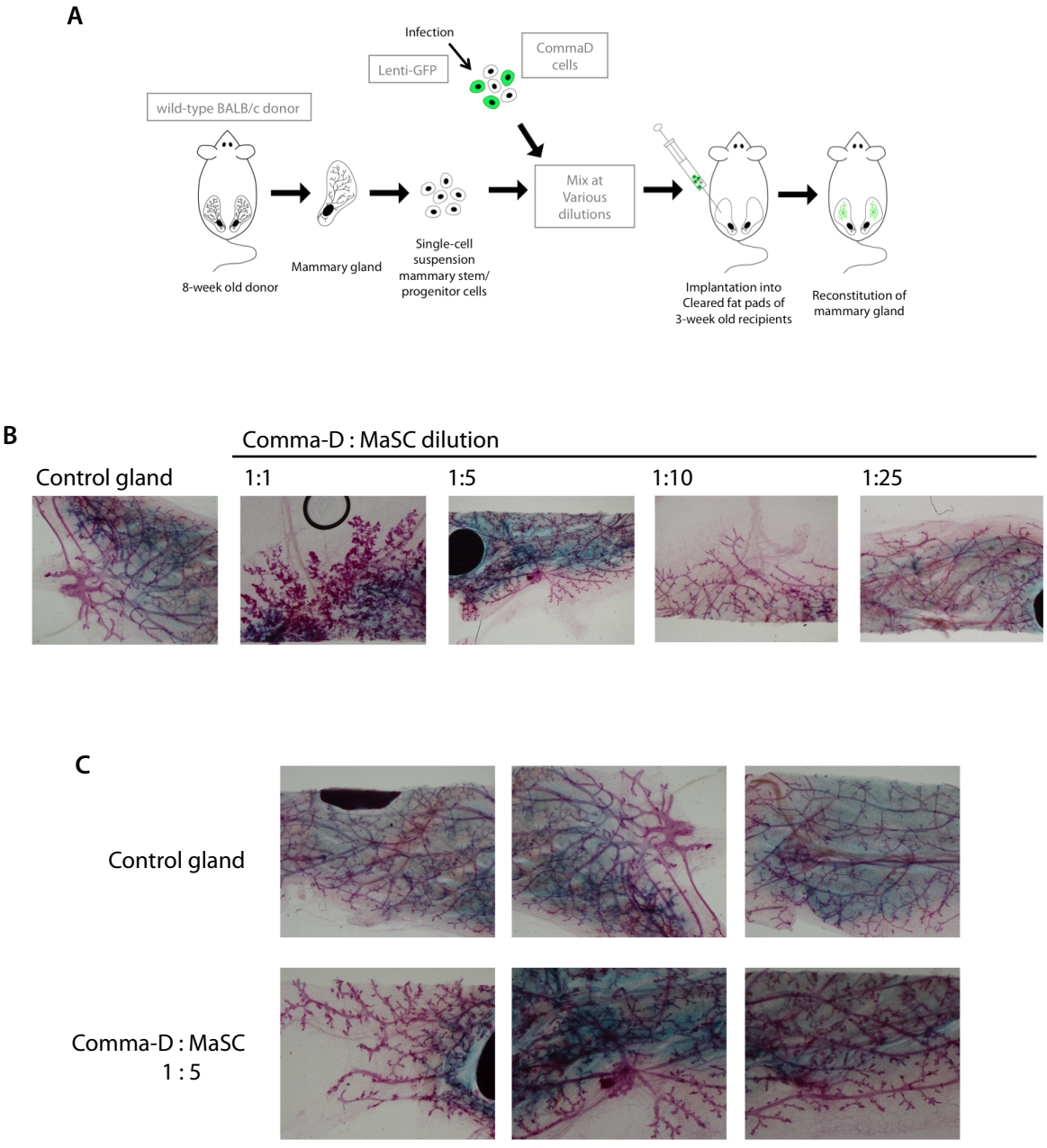

Figure 2.2 Modified orthotopic transplantation model with Comma-D cells and MaSCs. (A) Schematic of experimental set-up for mixing *c-Myc* overexpressing Comma-D cells at various dilutions into population of MaSCs. (B) Reconstituted mammary glands were harvested approximately 12 weeks after implantation and stained with carmine to reveal ductal structures. (C) Detailed view comparing endogenous control mammary gland to 1:5 dilution of Comma-D to MaSCs; a increase in hyperplastic branching is visible.

NMuMG cells are non-transformed mouse mammary epithelial cells that were originally derived from normal glandular tissue of an adult NAMRU mouse (Owens 1974; David et al. 1981; Hall et al. 1982). They were the next choice for a mouse mammary epithelial cell line because at low-passage NMuMG cells have been demonstrated to have typical epithelial morphology, display no cytologic instability, and also form structurally normal continuous basal lamina *in vivo* when injected into athymic nude mice (David et al. 1981). They have been used extensively in the literature to study transforming growth factor-beta (TGF-β) signaling and epithelial to mesenchymal transition (EMT) (Piek et al. 1999; Deckers et al. 2006). One major disadvantage of the NMuMG cell line, however, is the discontinuation of its syngeneic NAMRU strain, whereas Comma-D cells can be re-injected into syngeneic BALB/c mice (Medina et al. 1986).

There was no clear evidence in the literature to suggest that NMuMG cells had lost functional p53, an important step in tumorigenesis in many tumor types. Mutations in *TP53* occur at a frequency of ~23% in breast cancer, where is it the second most frequently mutation gene after PIK3CA (26%) (COSMIC) (Forbes et al. 2011). We reasoned that depletion of p53 in NMuMG cells might accelerate disease and serve as a clinically relevant positive control for the screen. To verify that NMuMG cells express functional p53, the parental cell line was treated with the DNA damaging agent Adriamycin that is known to promote stabilization of p53 and downstream activation of p21 (Watring et al. 1974). As expected Adriamycin treatment (0.25μg/mL) induced a dramatic upregulation of p53 and p21, an effect that was abrogated in the presence of a potent shRNA targeting p53 (shRNA-p53.1244) (Dickins et al. 2005; Xue et al. 2007) [Figure 2.3]. We were unable to detect $p19^{ARF}$ by Western blot but could not rule out this may be due to technical difficulties with the antibody. Alternatively, gain of replicative potential in culture often comes as a consequence

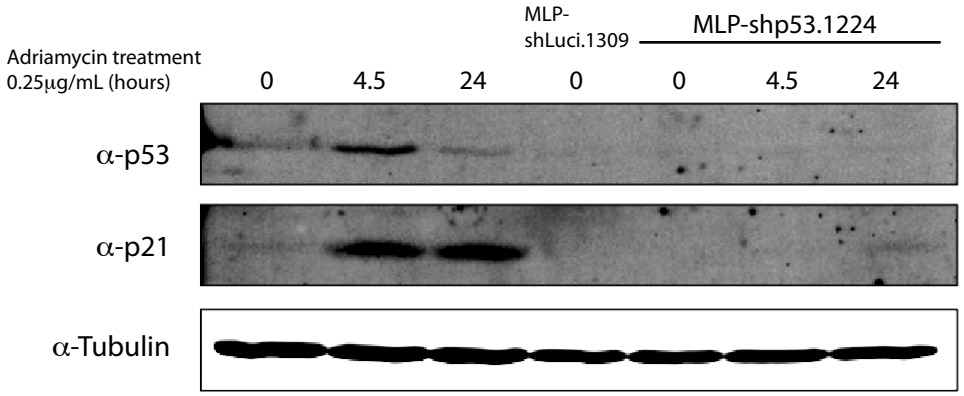

Figure 2.3 Induction of p53 and p21 in NMuMG cells. Western blots against p53 and p21 on protein lysate from NMuMG cell either native or trasduced with shRNA. Cells were retrovirally infected with pMLP constructs and puromycin selected before treatment with adriamycin. Luciferase.1309 is a neutral control shRNA.

of the loss of the INK4A/ARF locus (Collado et al. 2007), and this could be expected as a step in the immortalization process of this cell murine line cell.

The first three elements in defining an RNAi screening platform are the sensitized background, shRNA pool size and positive controls. We considered the use of overexpressed c-Myc and HER2, as well as a mutant PI3 kinase catalytic subunit p110α (PIK3CA^{H1047R}), as the sensitizing oncogenic stimulus. Ideally, since the candidate genes in our library were identified from patients comprising multiple different subtypes of breast cancer, the screen would be performed in multiple sensitized backgrounds in order to identify context specific as well as common TSGs.

We began by lentivirally transducing NMuMG cells with a construct containing the mutant rat ortholog of *ERBB2*, *neu*^{V664E} (*NeuNT*), driven under the control of the Ubiquitin C (UbC) promoter. *Neu* has been commonly used in transgenic mouse models of HER2-positive breast cancer to mimic the effects of HER2 overexpression frequently seen in patients (Muller et al. 1988; Bouchard et al. 1989). Our data showed that overexpression of Neu^{V664E} initiated tumor formation in NMuMG cells injected into the fat pads of nude mice [Figure 2.4], in contrast to parental NMuMG cells that do not form tumors at long latency (over 3 months post-injection; data not shown).

We discovered that an shRNA targeting the TSG *phosphatase and tensin homolog (Pten)* was highly efficient in accelerating the disease onset and tumor size in *NeuNT* overexpressing NMuMG cells, even more strongly than shRNA-p53.1244 [Figure 2.5]. Further testing confirmed this result but also uncovered that the window for detection of disease acceleration between RNAi of a real positive control or candidate TSG and the appearance of baseline disease driven by the aggressive oncogenic stimulus was less than four weeks (data not shown). Factoring the inevitable variability of *in vivo* experimentation,

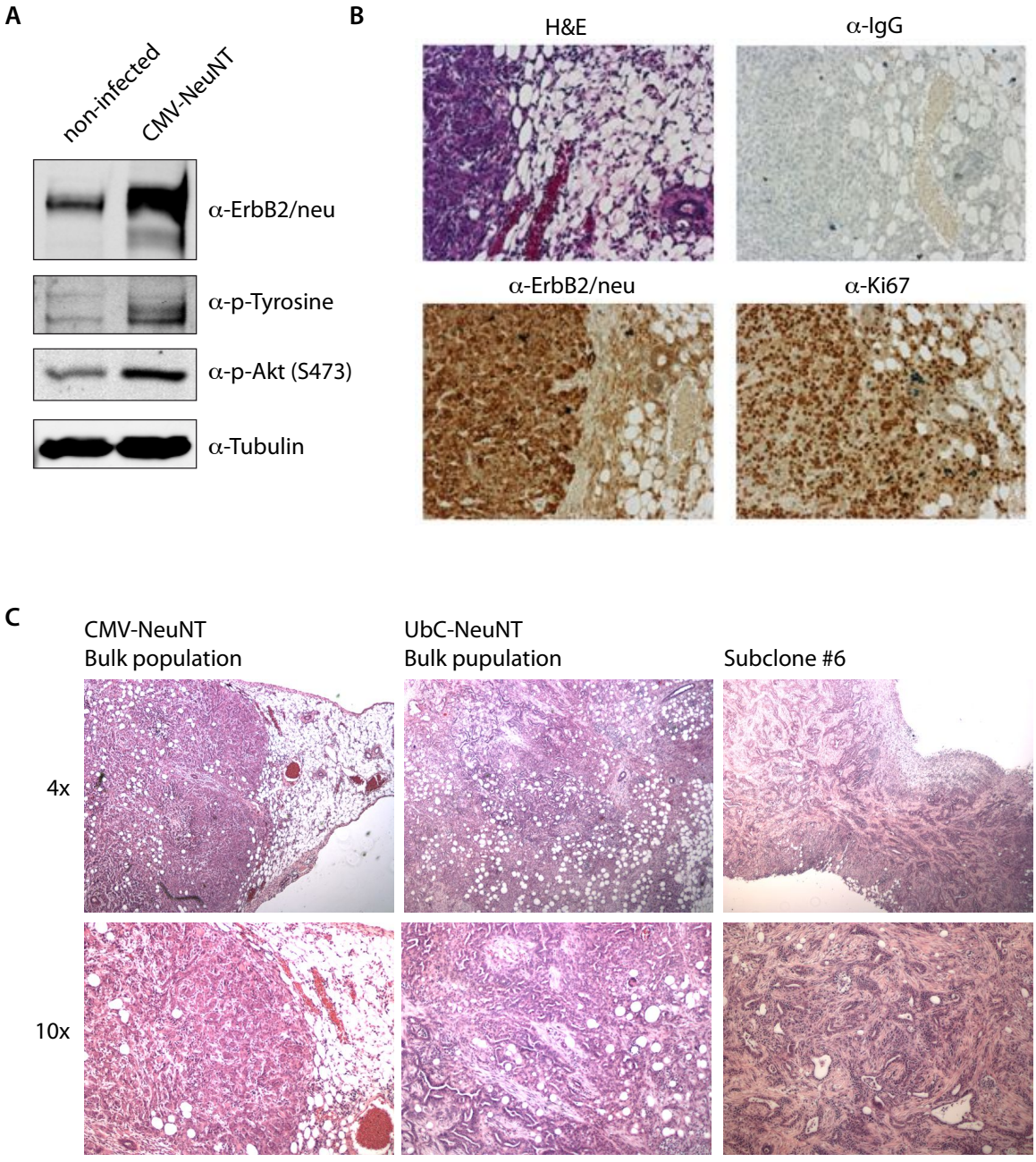

Figure 2.4 NMuMG cells overexpressing NeuNT. (A) Western blots on protein lysates of NMuMG cells overexpressing NeuNT from CMV promoter. (B) IHC on tumors sections from CMV-NeuNT overexpressing NMuMG cells transplanted into nude mice. (C) H&E staining of tumor sections from orthotopic transplantation of NMuMG cells expressing NeuNT from either CMV or UbC promoters; UbC-NeuNT subcloned cells (clonal line #6) gave more glandular and differentiated morphology compared to UbC-NeuNT bulk population.

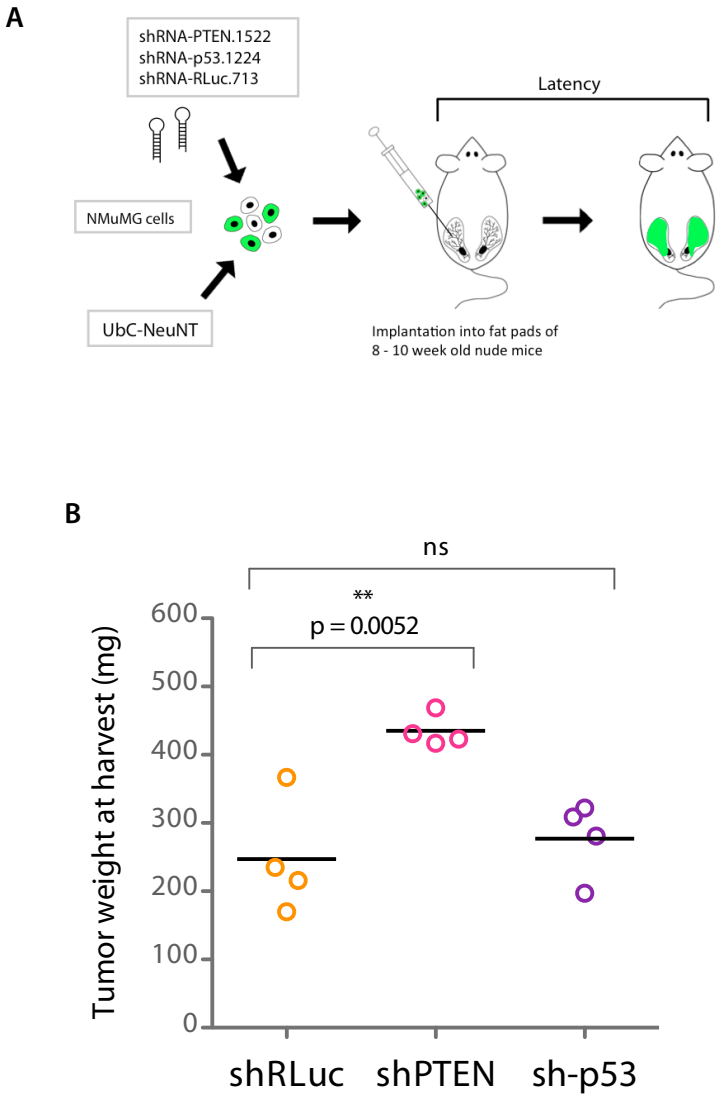

Figure 2.5 Establishing positive control for screening: shRNA targeting PTEN cooperates with NeuNT in NMuMG cells. (A) Schematic of transplantation assay; NMuMG cells transduced with UbC-NeuNT, pMLP-shRNAs introduced at high copy number and puromycin selected before transplantation. (B) Average tumor weight per cohort (n=4 tumors) at harvest, two-tailed unpaired t test.

several weeks represented an insufficient period of time for conducting a positive selection screen of any complexity with the requisite sensitivity. However, pilot *in vivo* assays using GFP reporter tagged shRNA-Pten.1522 demonstrated a quantifiable success in increasing its representation within a tumor as compared to neutral shRNA controls (data not shown). We posited that decreasing the strength of the *NeuNT* cDNA overexpression might address this lack of dynamic range. Deriving clonal cell lines to standardize and quantify oncogene expression levels, reducing the multiplicity of infection (MOI) during lentiviral transduction, and using a weaker promoter were among several strategies we tested in an attempted to increase the temporal resolution of our orthotopic transplantation assay by delaying the onset of disease driven by the sensitizing driver alone.

Our first attempt to address these issues involved replacing the bulk population of transduced cells that was potentially comprised of diverse oncogene expression levels and cellular phenotypes. By deriving clonal lines we were able to cross-compare *NeuNT* expression levels, observe growth rates *in vitro* and verify for cobblestone epithelial morphology indistinguishable from the parental population [Figure 2.6a]. Two sub-clonal lines with moderate oncogene expression, compact epithelial cellular morphology and moderate growth rates – NMuMG UbC-NeuNT Clone #6 and #7 – were expanded and tested *in vivo* along side the parental bulk-population [Figure 2.6b-c]. In both bulk populations and clonal lines, shRNA-Pten.1522 showed reproducible acceleration of tumor formation compared to a neutral control shRNA that targets Renilla Luciferase (RLuc.713). Ultimately, however, the latency of tumor onset and tumor growth rates were still too aggressive to envisage a positive selection screen, as assessed by the failure to observe enrichment of a potent shRNA targeting an established TSG such as *Pten* when introduced into cells with a 50-fold excess of a neutral shRNA construct [Figure 2.6d].

Several promoters tagged with GFP were tested for expression levels in NMuMG cells in an attempt to identify a weaker substitute for the UbC promoter (data not shown). A suitable replacement was not found but we were reassured to find that the Cytokeratin-19 (CK-19) promoter expressed well in these cells, confirming their luminal cellular origins.

In a further attempt to reduce the aggressiveness of the spontaneous disease, a wild type sub-clonal line of NMuMG cells dubbed "NMEC#6" (NMuMG Mammary Epithelial Cells Clone #6) was transduced with lower titers of UbC-NeuNT lentivirus to decrease the number of viral integrations and clones were isolated following antibiotic selection. Low-expressing NeuNT clones were identified by 'In-Cell' Western blot for ErbB2/neu expression [Figure 2.7a]. Since empirical observations from *in vitro* work with the parental NMuMG cells indicated heterogeneity in cellular morphology, several NMEC clonal lines were produced and tested (data not shown). NMEC#6 had tight epithelial cell-to-cell junctions, cobblestone cellular morphology, a moderate growth rate *in vitro*, and importantly, maintained these traits for many passages in culture. The NMEC#6 clone was also tested *in vivo* and like the untransformed parental line did not give rise to tumors at long latency (data not shown).

NMEC#6 UbC-NeuNT clonal line #3 and #5 were tested *in vivo* with control shRNAs undiluted and in 1:50 dilution configurations, employing a combination of both GFP and dsRed flurescent marker-tagged vectors [Figure 2.7b: results shown only for clonal line #5]. The populations transduced with GFP tagged shRNA retrovirus were approximately 30% for undiluted controls and approximately 1% for 1:50 dilutions [Figure 2.7c]. Tumors were harvested 7.5 weeks after orthotopic injection and gross anatomy was observed using a dissecting microscope to assess levels of the fluorescent reporters [Figure 2.7d]. In tumors resulting from cells co-expressing shRNA-Pten.1522 were significantly

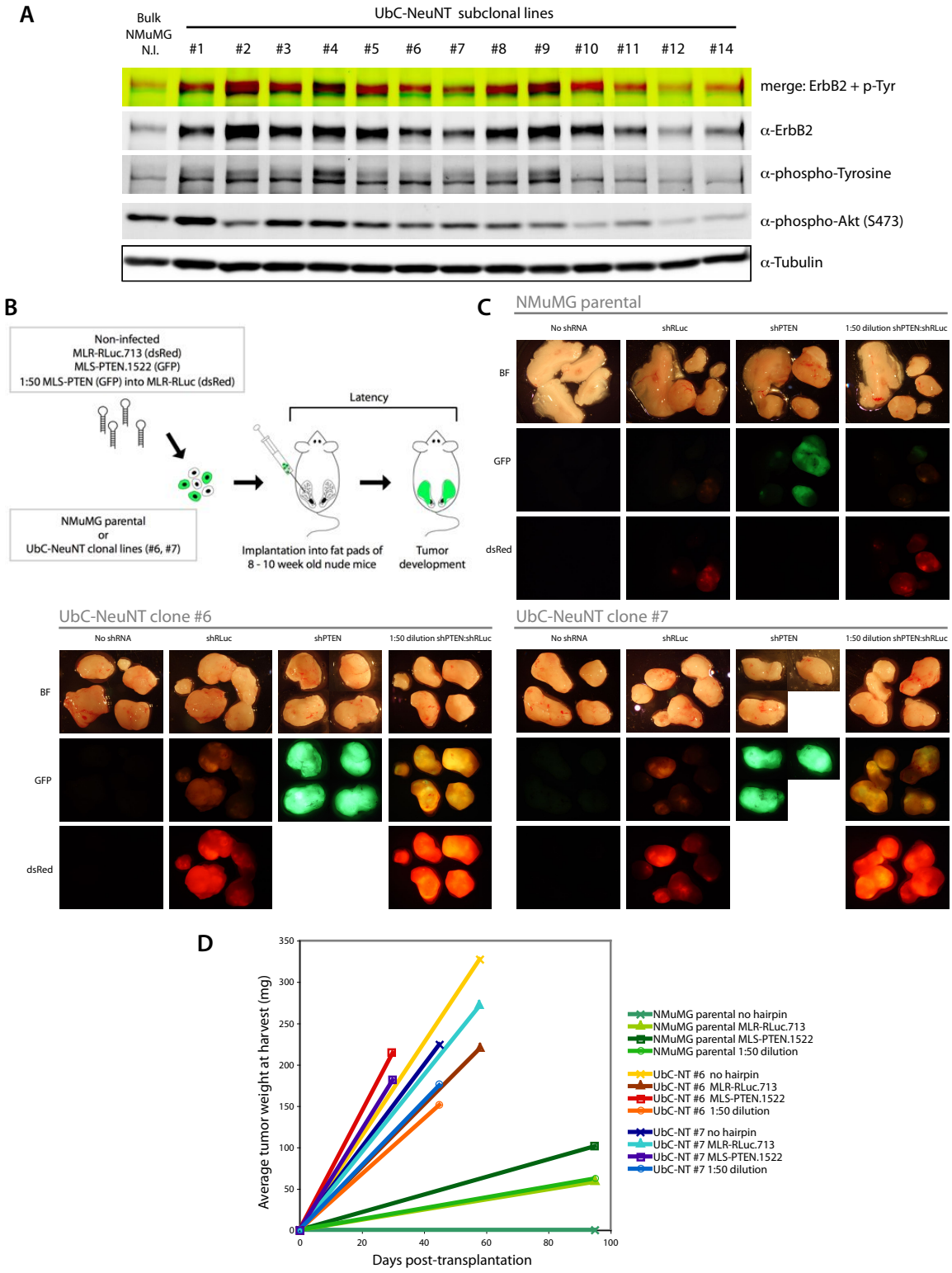

Figure 2.6 NMuMG UbC-NeuNT subclonal lines. (A) Western blot: NMuMG cells transduced with UbC-NeuNT, selected, then subcloned; #6 and #7 chosen for use *in vivo*. (B) Schematic of transplantation assay to test clonal lines #6 and #7; neutral control shRNA-RenillaLuciferase.713 in pMLR vector with dsRed reporter instead of GFP. (C) Brightfield and fluorescence images of tumors at harvest. (D) Tumor weights at harvest, per cohort (n=4).

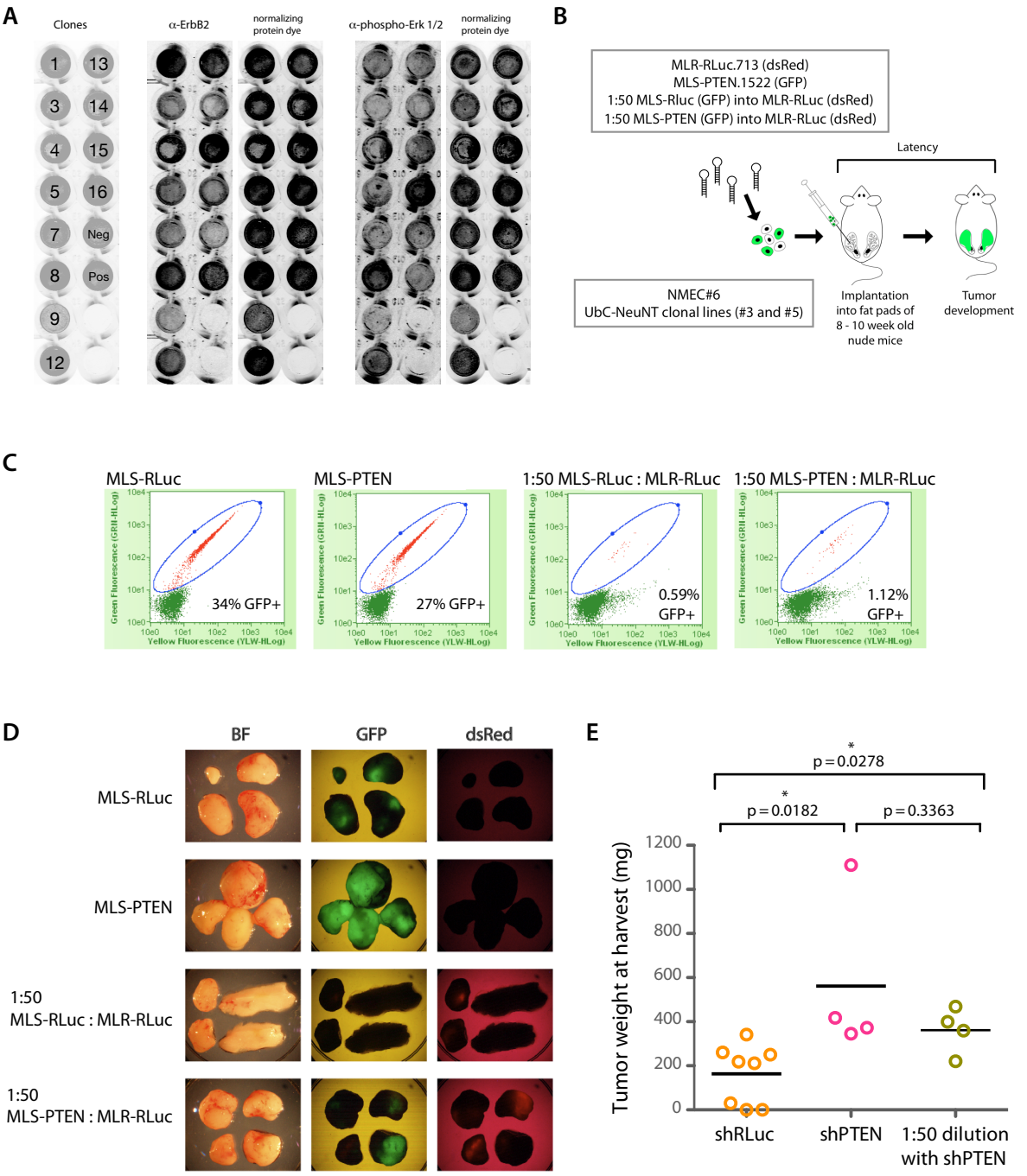

Figure 2.7 NMEC#6 UbC-NeuNT clones: *in vitro* and *in vivo* characterization. (A) In-Cell Western blot assay in fixed/permeablized whole cells, NMEC#6 cells transduced with UbC-NeuNT, then clonal lines isolated. (B) Schematic of transplantation assay; NMEC#6 UbC-NeuNT clones #3 and #5 were tested *in vivo* after retroviral introduction of shRNAs. Data for clone #5 shown: (C) Assessment of GFP positive population in each experimental condition immediately prior to transplantation. (D) Brightfield and fluorescent images of tumors harvested 7.5 weeks after transplantation. (E) Tumor weights at harvest; two-tailed unpaired t test.

larger than control tumors and there was a net increase in the GFP signal, confirming that we were able to detect the oncogenic contribution of a strong TSG shRNA over baseline in these cells [Figure 2.7e]. Similar assays were used to investigate the potential utility of c-Myc, mutant PIK3CA, human HER2, wild type mouse ErbB2 and activated mutant ErbB2(NT) as sensitizing lesions. However, these experiments all yielded inconsistent results *in vivo* (data not shown) and ultimately we chose to concentrate our efforts on optimizing NeuNT in our screening platform development.

Before embarking on a screen for all 745 shRNAs in our library, we decided to first test whether shRNA-Pten.1522 TSG activity could be successfully identified from a pool of non-neutral shRNAs. A random pool of 49 sequence-verified shRNAs from the library were assembled and spiked with either the Pten.1522 or RLuc.713 control shRNA and tested in the same *in vivo* assay as before with NMEC#6 UbC-NeuNT clonal line #5. The pMLS plasmid pools were transduced at low MOI that approximated a single retroviral integration per cell. Disappointingly, shRNA-Pten.1522 failed to enrich in this context (data not shown), and the decision was made that the system established was not suitable for large pooled-format screening. Instead efforts were focused towards testing a small set of candidates on a gene-by-gene basis.

Pilot screen

For the gene-by-gene trial, fourteen candidates were chosen from a list of 35 genes that represented an overlap between two methods of ROMA data analysis [Table 2.3]. The initial analysis had been founded on focal event counting, where the frequency and size of the chromosomal deletions detected in the CGH arrays produced a candidate list of 144 genes (of which 112 incorporated into the shRNA library). The Genentech study had been

Table 2.3 Candidate tumor suppressor genes screened in gene-by-gene pilot

Candidate	*Gene name*	*a.*	*b.*	*c.*	*pilot screen*
ARHGAP1	Rho GTPase activating protein 1	x	x	x	set 1
BASP1	brain abundant, membrane attached signal protein 1	x	x	x	set 1
Ctnnd1	catenin (cadherin-associated protein), delta 1	x	x		set 2
CUGBP1	CUG triplet repeat, RNA binding protein 1	x		x	set 2
DLG2	discs, large homolog 2 (Drosophila)	x	x	x	set 1
FNBP4	formin binding protein 4	x		x	set 1
KBTBD4	kelch repeat and BTB (POZ) domain containing 4	x		x	set 2
MAP2K4	mitogen-activated protein kinase kinase 4	x		x	set 1
MYO10	myosin X	x	x	x	set 2
Nf1	neurofibromin 1	x	x		set 2
Numa1	nuclear mitotic apparatus protein 1	x	x		set 2
PTPRJ	protein tyrosine phosphatase, receptor type, J	x		x	set 1
UNC5D	uncp5 homolog D (C. elegans)	x	x	x	set 2
ZCCHC7	zinc finger, CCHC domain containing 7	x		x	set 1

a. 5% focal deletion analysis (149 gene library)
b. high potential "priority" candidates (19 genes)
c. pinning algorithm candidates (500 genes)

used to complement that list with another 37 genes derived a list of 49 candidates. Additionally, during the process of the original library design 18 candidates had been flagged as 'high priority' based on information regarding the candidate in the literature, such as their involvement in particular pathways or as TSGs in other cancer types. These lists were compared to new set of 500 candidate genes generated by a second analysis method applied to the same ROMA datasets by Alex Krasnitz (CSHL) using a 'pinning algorithm'.

One of the more commonly applied methods of CGH profile analysis is by event counting, where a frequency plot of all loci in the sample data set is produced to visualize this basic measure of recurrence of copy number gains and losses. In many cancer types including breast, large chromosomal events are common and such simplistic methods of assessing relevance through frequency can lead to large portions of the genome being flagged. The 'pinning algorithm' was an alternative method of data analysis developed by Alex Krasnitz to allow for a more focused search for candidate driver genes where the length of any copy number variation and the potential for the overlapping events to move the calculated peak away from the actual epicenter is also taken into account. Surprisingly only 42 genes overlapped between the two candidate lists (38 with ROMA and 4 with Genentech candidates), 35 of which were part of our shRNA library, underscoring the importance in the choice of methods for the data analysis, both conceptually and computationally.

We combined the shRNA plasmids for transfection into a packaging cell line, generating small pools of five sequence-verified shRNAs targeting each gene. Knockdown efficiency of the shRNAs against each target was not tested prior to the assay. Each small pool was introduced into NMEC#6 UbC-NeuNT (clonal line #5) using a viral titer intended

to generate cell populations carrying multiple viral integrations, thus increasing the likelihood of potent gene silencing. Infection rates were determined by assessing percentage of GFP positive cells: for the first set an average of 83.4% GFP positivity (range 73-89%) and for the second set an average of 77.8% (range 72-87%). For practical reasons we conducted the *ex vivo* manipulations and orthotopic injection surgeries in two batches, each round with its own set of controls. All experimental steps were conducted in identical manner. Tumors were harvested 7 and 8.5 weeks post-transplantation for the first and second sets, respectively. None of the candidate gene shRNA pools gave statistically significant results [Figure 2.8]. In some cases there seemed to be a no selective advantage afforded by the shRNA pool in this assay since GFP negative tumors were also observed (data not shown). The screen was repeated in NMEC#6 cells expressing CMV promoter driven wild type mouse ErbB2 but this experiment similarly produced no positive selection of candidate gene pools. The overall latency was very long and we also experienced incomplete penetrance of the positive control (data not shown).

We noticed that despite a lack of statistical significance in tumor weight at harvest, the tumors resulting from the shRNA pool targeting the gene *neurofibromin 1* (*Nf1*) did present an above average tumor burden and importantly, all four tumors were GFP positive. Encouraged by these results, the *Nf1* shRNA pool was retested. Tumors were harvested and weighed two months post-transplantation and this time the increase in tumor burden was statistically significant [Figure 2.9a,b]. Crude tumor lysates were probed for NF1 protein levels and strong knockdown was observed [Figure 2.9c], but there were no major changes in histology, density of GFP positive cells or growth as indexed by Ki-67 staining [Figure 2.9d,e]. We verified protein knockdown efficacy of each shRNA individually at both high and low MOI levels in NMuMG cells [Figure 2.10a]. Owing to

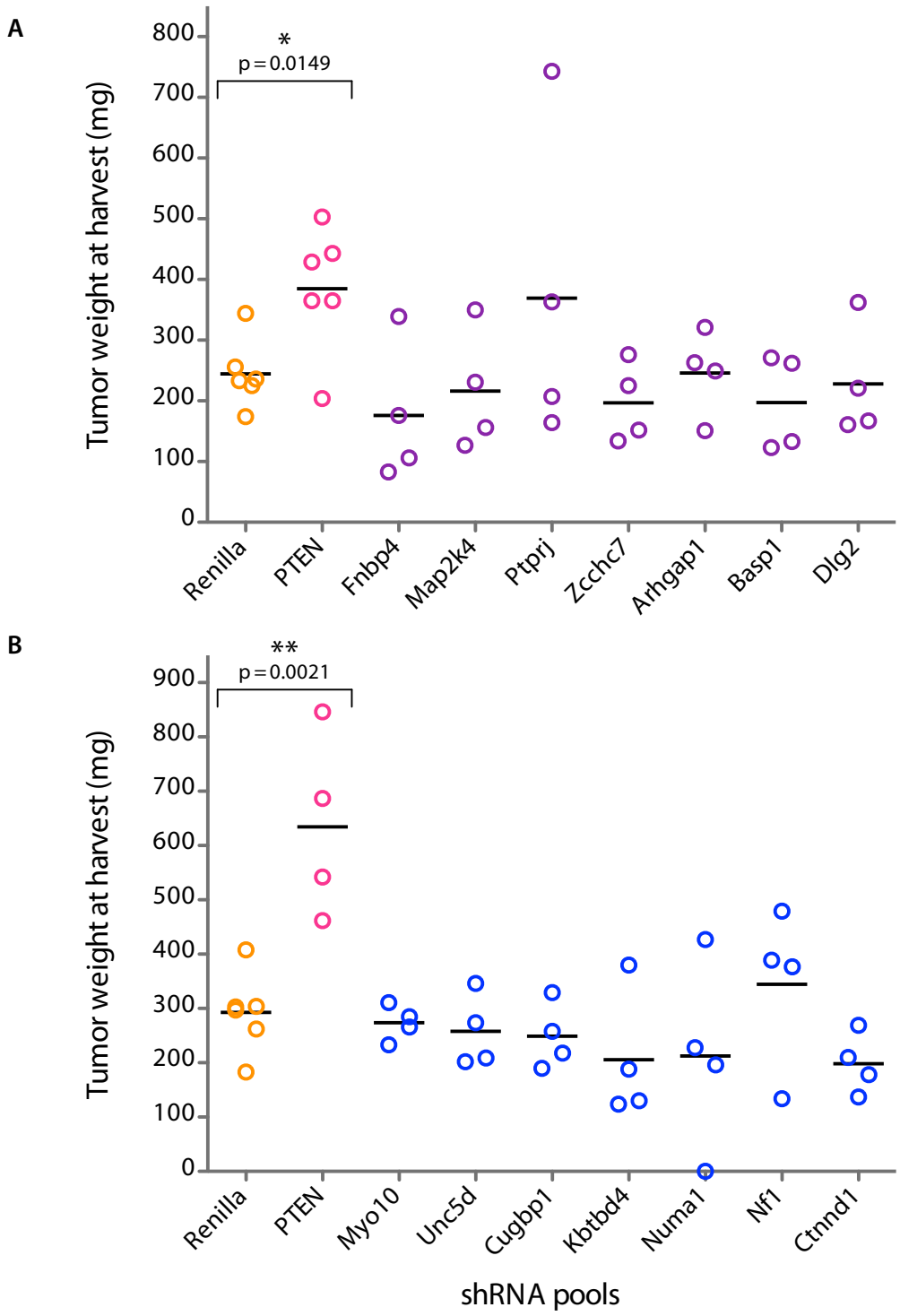

Figure 2.8 Gene-by-gene pilot screen. Nude mouse othotopic transplantation of NMEC#6 UbC-NeuNT clone #5 cells transduced with pools of 5 shRNAs targeting each candidate gene. (A) Set 1 tumor weights at harvest 7 weeks post-transplantation; RLuc vs. Ptprj not statistically significant (p value 0.2818). (B) Set 2 tumor weights at harvest 8.5 weeks post-transplantation; RLuc vs. Nf1 not statistically significant (p value 0.4746). Two-tailed unpaired t test.

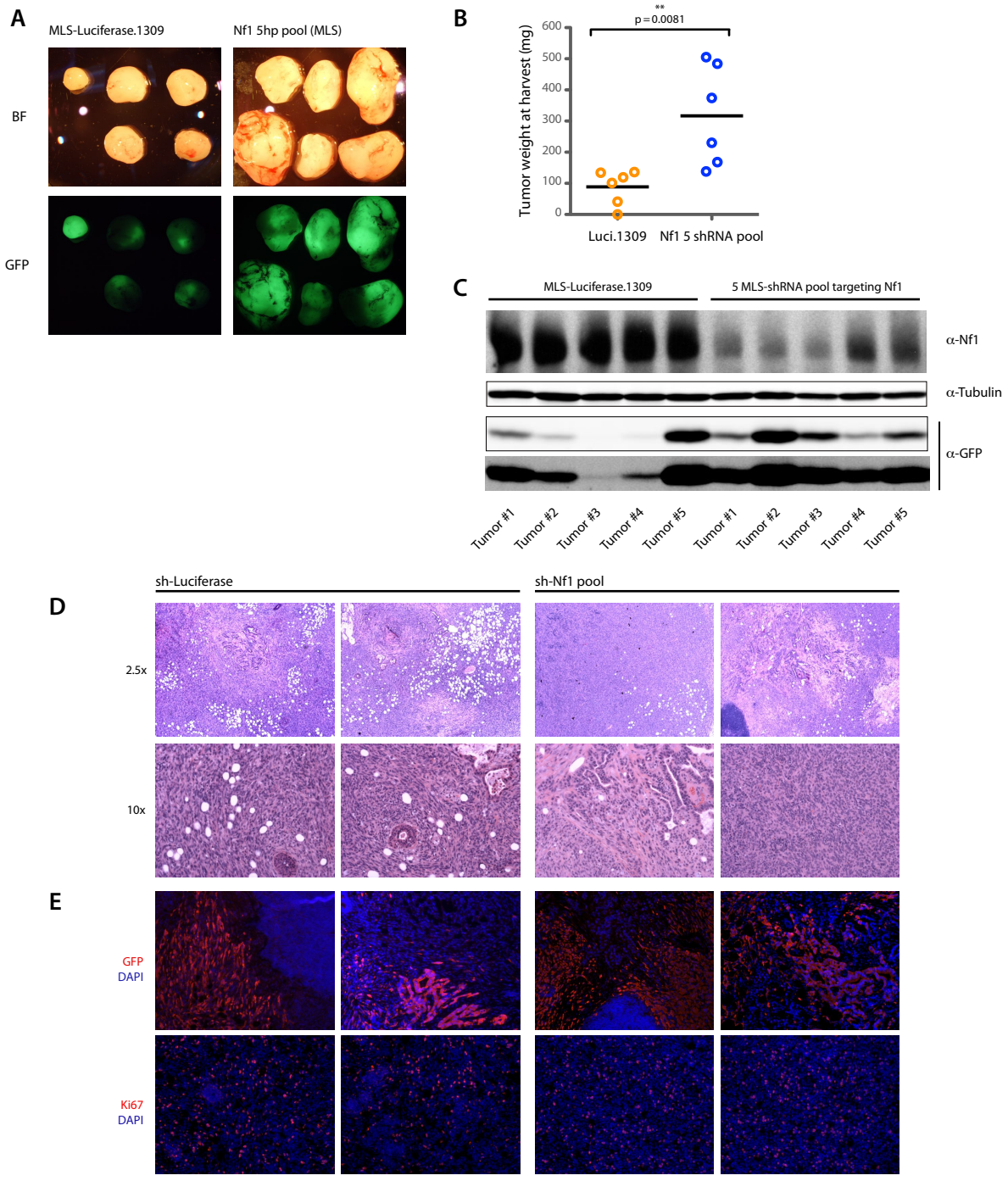

Figure 2.9 Validation of hit: NF1. (A) *in vivo* orthotopic transplantation assay in nude mice; NMEC#6 UbC-NeuNT clone #5 cells retrovirally transduced with MLS-shRNAs. (B) Tumor weight at harvest 7.5 weeks after transplantation; two-tailed unpaired t test. (C) Western blot for Nf1 knockdown in unsorted tumor tissue protein lysate. (D) H&E staining on tumor sections. (E) Immunofluorescence on tumor sections.

technical difficulties regarding the health of nude mice under experimentation we were unable to draw any robust conclusions, but accelerated tumor onset and growth was also documented in the context of PIK3CA^{H1047R} (with 5 shRNA pool) and wild type mouse ErbB2 overexpression (with two independent shRNAs alone) in NMEC#6 *in vivo* transplantation assays, albeit at a longer latency of approximately 5 months (data not shown).

NF1 is an established TSG in leukemia and is well characterized as a negative regulator of the oncogene *Ras* (Mullally and Ebert 2010). As a Ras-GTPase activating protein (GAP), its loss can lead to the constitutive activation of the Ras pathway in a manner similar to oncogenic point mutations in Ras itself (Kalra et al. 1994; Bollag et al. 1996). We investigated the *Nf1* pool shRNA tumor lysates for changes in the downstream signaling and found an upregulation in phosphorylated ERK, phosphorylated MEK, and phosphorylation of AKT at both the Thr-308 and Ser-473 sites [Figure 2.10b]. Unexpectedly, we did not perceive any of these changes in cells transduced with *Nf1* shRNAs growing *in vitro*, and similarly we also did not observe any changes in growth or cellular morphology in culture. We attributed the lack of changes in signaling to the growth factor rich culture conditions that included insulin and 10% fetal bovine serum.

In an attempt to identify differences in signaling in NMuMG cells transduced with a functionally validated and potent shRNA targeting *Nf1*, the effects of growth factor stimulation time course with epidermal growth factor (EGF) and insulin after an overnight starvation (no serum or insulin) were investigated. Neither in the presence or absence of NeuNT did we observe any changes in signaling [Figure 2.11]. Since it is conceivable that NF1 loss would result not in a strong signal upon upstream stimulation but instead allow for a prolongation of any signal downstream of Ras, we next performed a time course where

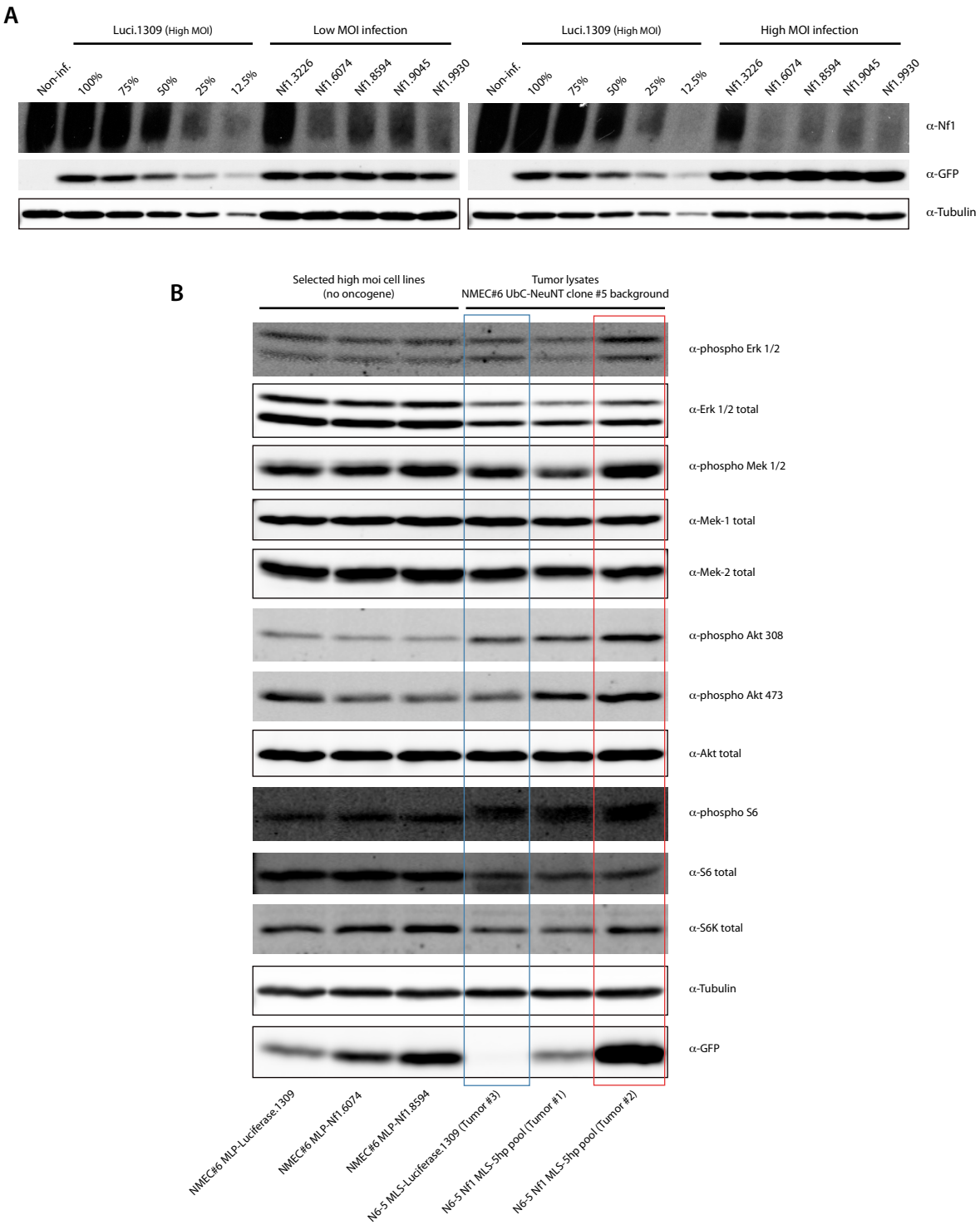

Figure 2.10 Individual NF1 shRNA knockdown levels and downstream signaling changes in NF1 knockdown driven tumor. (A) Western blots assessing Nf1 knockdown in NMEC#6 cells retrovirally infected MLP-shRNAs and puromycin selected. (B) Western blots on protein lysate from *in vitro* cultured cells and tumor lysates; blue and red boxed areas compare control tumor with *Nf1* shRNA pool tumor lysate with high percentage of GFP expressing cells; increased signal in phospho-Mek, phospho-Erk, and phospho-Akt observed.

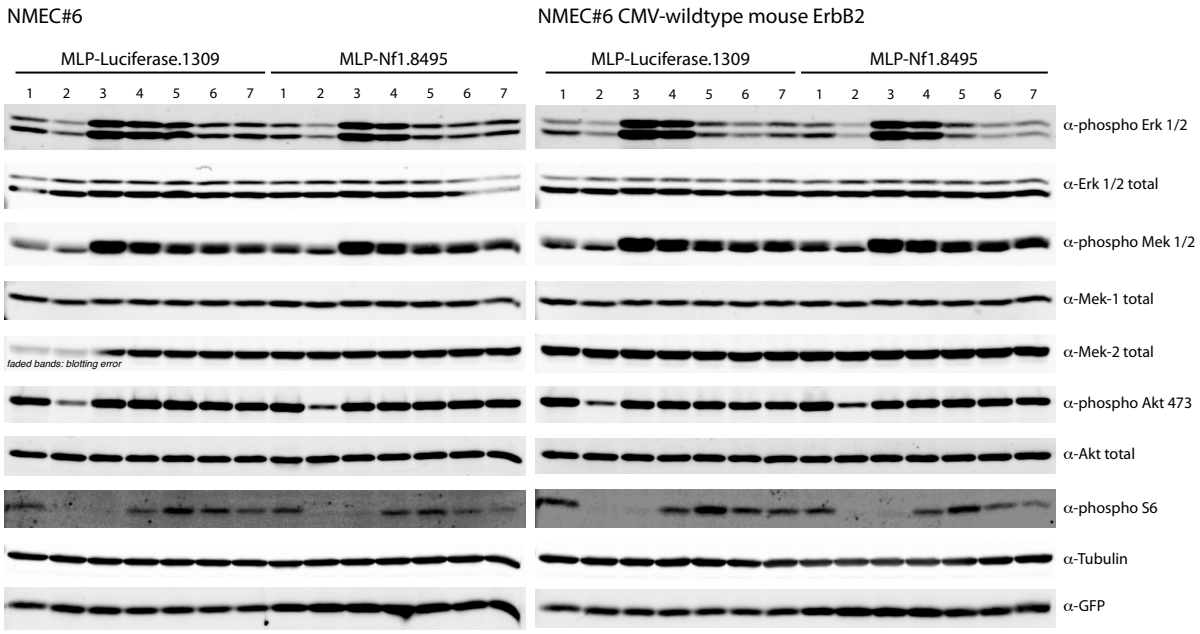

1. Growing
2. Starved overnight
3. Starved overnight, 10 min EGF/Insulin
4. Starved overnight, 30 min EGF/Insulin
5. Starved overnight, 1 hour EGF/Insulin
6. Starved overnight, 2 hours EGF/Insulin
7. Starved overnight, 3 hours EGF/Insulin

Figure 2.11 Signaling downstream of NF1 after growth factor stimulation time course. Western blots on protein lysates of NMEC#6 cells in cultrue in the presence or absence of an shRNA targeting *Nf1* and wildtype mouse ErbB2 overexpression.

cells were starved for 6 hours, stimulated with EGF/insulin for 10 minutes, then maintained in starvation conditions for a variable length of time. Once again, no significant changes were observed in downstream signaling phosphorylation by Western blot [Figure 2.12]. To generate a reagent that would allow us to study the tumor suppressive mechanism of NF1 loss *in vitro* more effectively in the future, we established a series of tumor-derived cell lines from NMEC#6 transplant tumors expressing two MLP-shRNAs against NF1 (data not shown).

The original CGH array data was re-examined to verify that *NF1* deletions, found at a frequency of 5% in this small dataset, co-occur with *ERBB2* chromosomal amplifications. There is some indication of linkage between focal deletions of *NF1* (on 17q11.2) and *ERBB2* (on 17q12), which would imply a lack of biological significance in the co-occurrence of these events within tumors. The TSG *TP53* is located on the short arm of chromosome 17 (17p13.1) and there also appears to be a frequent overlap between *TP53* and *NF1* deletions (over 10% in human breast cancer cell lines). When considering broader deletions encompassing *NF1*, they appear random with regard to *MYC* or *ERBB2* amplification but are found to co-occur in both cases (Jim Hicks, personal communication).

Making new shRNA transgenic mouse strains targeting *Nf1*

As a parallel strategy for investigating the role of NF1 in breast cancer, we generated two tetracycline-inducible shRNA transgenic mice that enable reversible silencing of endogenous NF1 expression. To do this we took advantage of previous work by Lowe lab colleagues who established a fast and reproducible pipeline for the production of these shRNA transgenic strains (Premsrirut et al. 2011; Dow et al. 2012). A gene-targeting vector can be rapidly cloned to contain the shRNA sequence of choice in an inducible expression

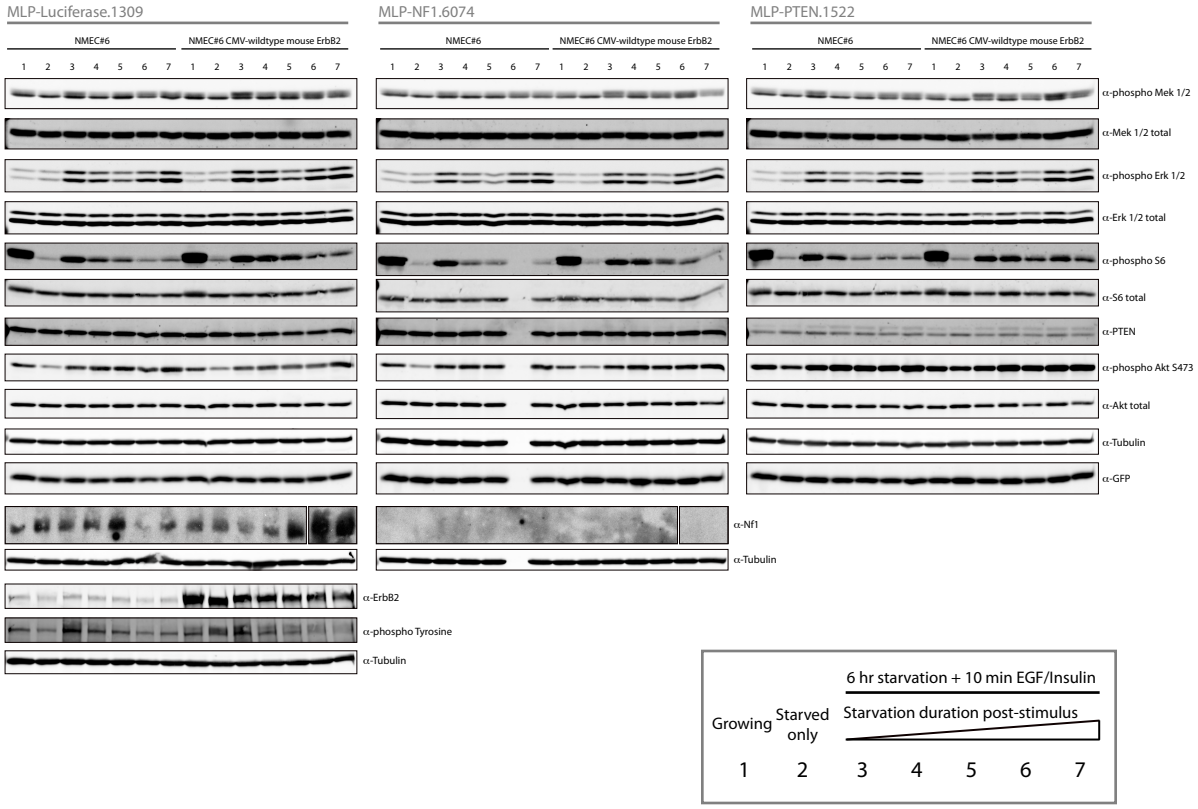

Figure 2.12 Signaling downstream of NF1 after pulsed growth factor stimulation and starvation time course. Western blots on protein lysates of NMEC#6 cells *in vitro* in the presence or absence of an shRNA targeting *Nf1* and wildtype mouse ErbB2 overexpression; shRNA-PTEN samples included in assay as a reference.

cassette flanked by FRT sites. The shRNA cassette consists of the human miR-30-based shRNA embedded in the 3′ UTR of a GFP transcript downstream of a tetracycline responsive element (TRE) promoter [Figure 2.13a]. In our case, we employed a modified targeting construct containing the TREtight promoter (TREt), which shows 40-fold lower expression in the absence of tetracycline analog doxycycline (dox) compared to the conventional TRE promoter (Clontech 2003; Backman et al. 2004). This modification had been validated in transgenic models expressing shRNAs targeting essential genes where it had been imperative that basal expression levels be reduced (McJunkin et al. 2011).

Following electroporation of the targeting vector alongside a plasmid expressing Flpe recombinase into KH2 ESCs, the TRE(t)-GFP-miR30 construct integrates into a defined locus downstream of the *collagen A1* gene (*ColA1*) on mouse chromosome 11 via recombinase-mediated cassette exchange (Beard et al. 2006; Premsrirut et al. 2011) [Figure 2.13a]. KH2 cells are 129, C57BL/6 F1 hybrid ESCs that contain not only the *ColA1* homing cassette but also a reverse tetracycline-transactivator (rtTA) cDNA expressed from the endogenous Rosa26 promoter (Hochedlinger et al. 2005; Beard et al. 2006). In this 'Tet-On' system, the presence of dox can drive expression of the GFP-shRNA cassette in the targeted KH2 ESCs (Gossen et al. 1995).

We generated targeted clones using three different NF1 shRNAs in KH2 ESCs and examined knockdown by western blot in two independent clones following 5 days treatment with dox. All three shRNAs showed robust protein knockdown [Figure 2.13b]. We decided to proceed with shRNA-NF1.6074 and NF1.8594 because these had previously been shown to be functionally active in accelerating disease in AML *in vivo* models. Three clones for each shRNA that showed compact, undifferentiated ESC morphology were placed on and off dox before assessment of GFP induction levels [Figure 2.13d]. Single-site

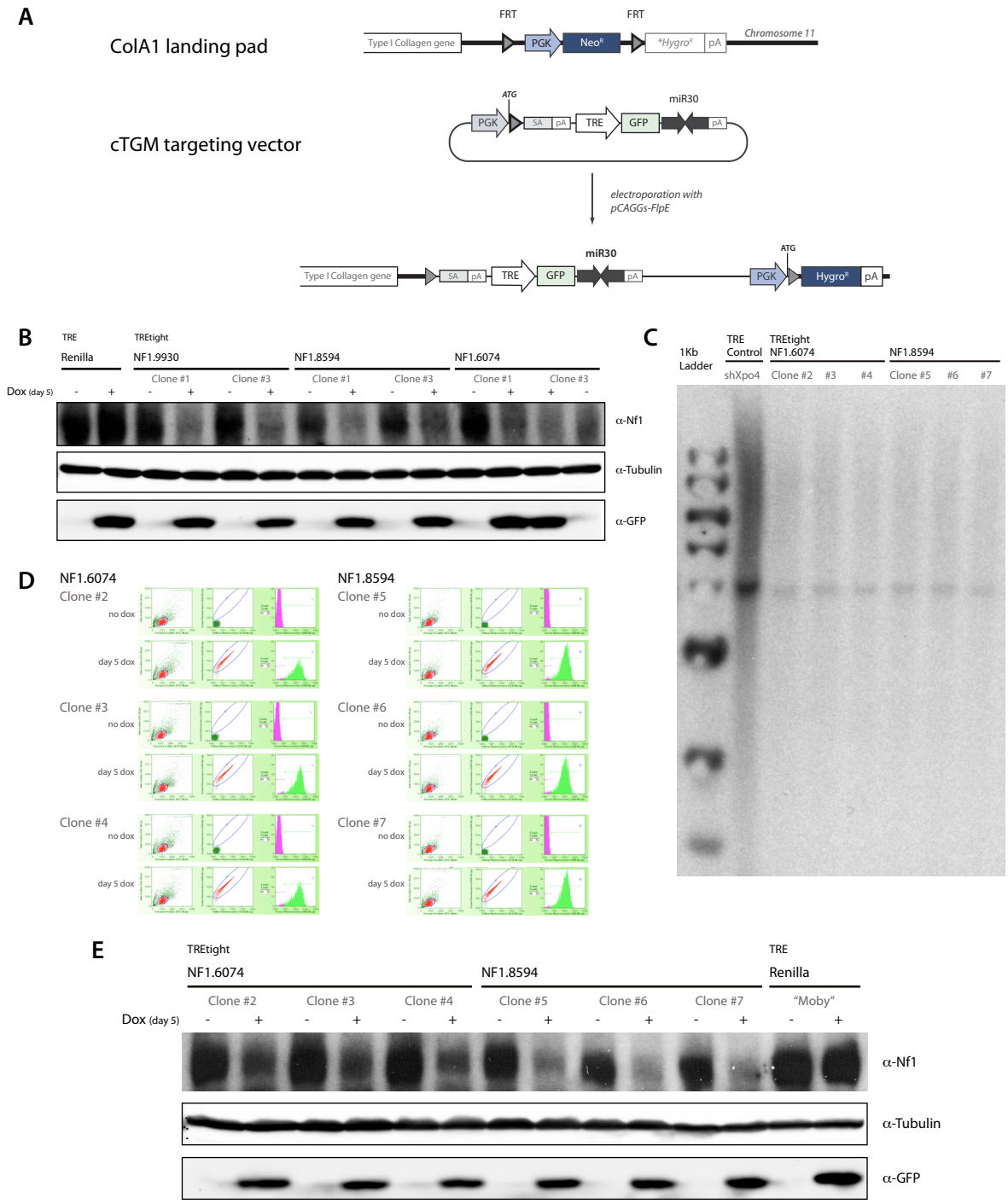

Figure 2.13 New shRNA-NF1 transgenic mouse strains. (A) Schematic of ColA1 gene targeting in KH2 ESCs; here, a modified version of the targeting vector with the TREtight promoter was used. (B) NF1 shRNA knockdown levels assessed in dox treated KH2 ESCs. (C) Southern blot to verify single-copy integration of targeting construct. (D) Induction of shRNA-GFP allele verified in dox treated KH2 ESC clones. (E) Final verification of efficient target knockdown in candidate ESC clones before tetraploid complementation; clone #4 and #7 sent for strain generation.

integration was also verified by Southern blot [Figure 2.13c]. Finally, candidate clone lysates were blotted once more to confirm protein knockdown levels [Figure 2.13e]. The clones displaying the strongest shRNA induction, protein knockdown, and healthiest undifferentiated ESC morphology were used for mouse production by tetraploid embryo complementation (Eggan et al. 2001). The production of transgenics by tetraploid complementation guarantees that recombined cells contribute to both somatic and germ line tissues in resultant male founders, permitting heritable transmission of transgenic alleles (KH2 cells are XY).

Once TtG-shNF1.6074 and TtG-shNF1.8594 founders reached sexual maturity they were crossed with C57BL/6 females in order to isolate mouse embryonic fibroblasts (MEFs) from embryos harboring both the Rosa26-rtTA-M2 (Rosa-rtTA) and TREt-GFP-miR30 alleles (Hochedlinger et al. 2005). Reversible GFP induction in the MEFs was verified by FACS analysis (data not shown). NF1 knockout strains are embryonic lethal when homozygous (Brannan et al. 1994). However, preliminary results from dox treated embryo litters did not show any phenotype in double transgenic pups, suggesting there was an insufficient knockdown of the target NF1 by either of the shRNAs tested in our model [Figure 2.14].

As the expression pattern of TREtight-GFP-miR30 had not been previously examined in detail, we sought to test the induction of the allele in the presence of Rosa-rtTA in adult female mice after two weeks of dox treatment and also to compare the GFP induction levels in various tissues types between the TRE and TREtight promoters. Additionally, we included a different rtTA allele, CAGs-rtTA3, which has a broader and stronger expression pattern than the Rosa allele (Premsrirut et al. 2011). This data is summarized in the Appendix, and indicates a limited application of the TtG-shNF1.6074 and TtG-shNF1.8594 transgenic strains for modeling NF1 loss more broadly, as neither short

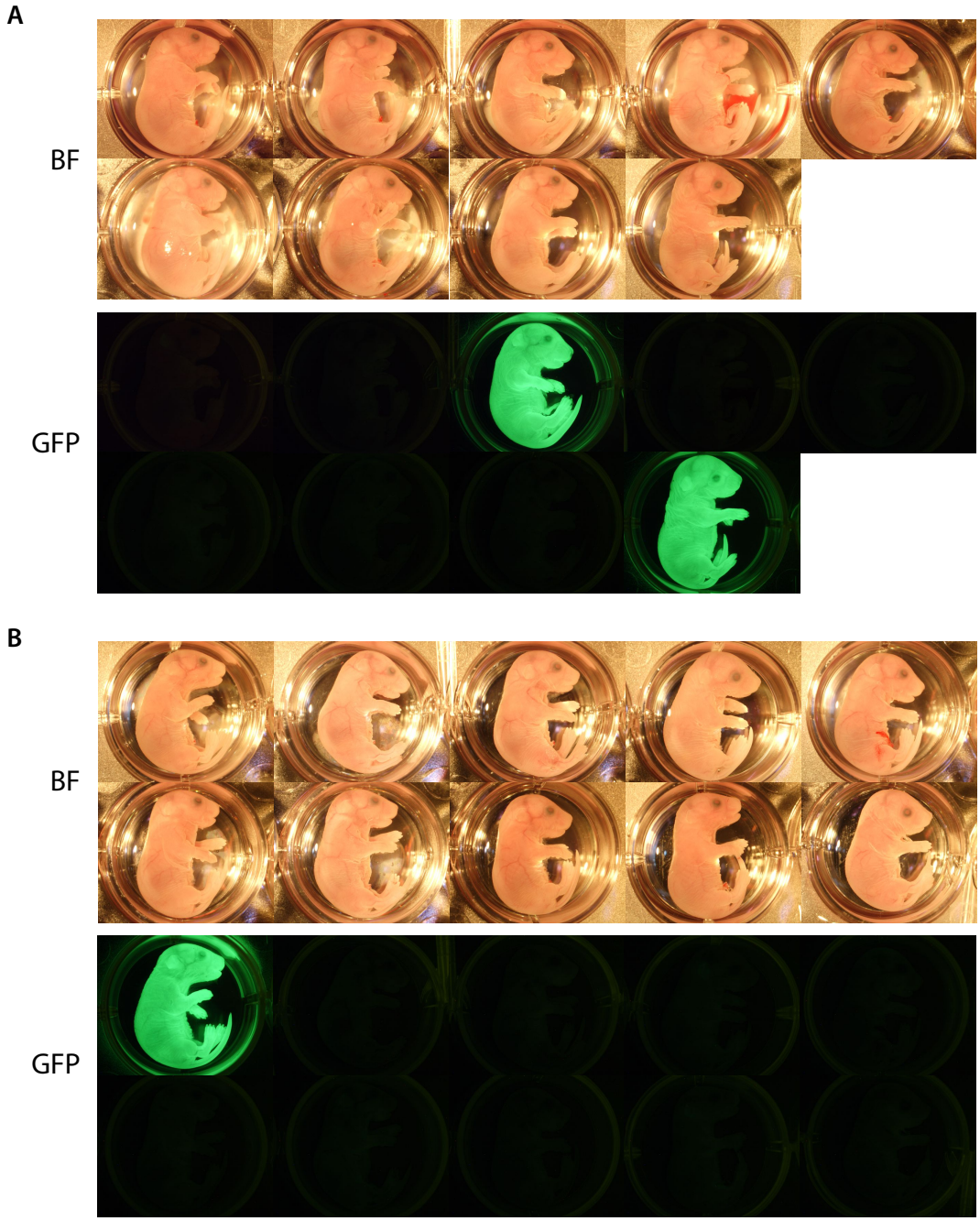

Figure 2.14 Embryonic lethality not observed in shRNA-NF1 transgenic strains. Rosa26-rtTA2 ; TREtight-shRNA E18.5 embryos after 10 days of dox treatment. Brightfield and fluorescent images of (A) TtG-shNF1.6074, litter of 11np, and (B) TtG-shNF1.8594, litter of 12np.

hairpin will be capable of sufficient suppression of its target in many tissue types while in their current configuration downstream of the TREt promoter.

The results for TREt promoter induction in the mammary gland were inconclusive. However, from previous work it had been established that TRE expresses robustly in the mammary gland when combined with CAGs-rtTA3 and MMTV-tTA (data now shown). We therefore intend to test TtG-shNF1.6074 and TtG-shNF1.8594 in the multi-allelic transgenic model described in Chapters 3 and 4. Preliminary evidence suggests that the TREt promoter, like TRE, can be induced in that model (data not shown) and experiments to validate NF1 as a tumor suppressor in this transgenic setting are currently ongoing.

DISCUSSION

This chapter describes efforts towards conducting a positive selection screen for the identification of novel tumor suppressors in breast cancer based on copy number variation data from human breast cancer genomic analysis. The approach was founded on the hypothesis that chromosomal regions frequently deleted in human cancers are enriched for TSGs. While some preliminary trials were conducted with *c-Myc*, mutant *PIK3CA* and wild type *ErbB2* with mixed results, most of our efforts centered around the use of a mutant *neu* allele as the sensitized background for modeling HER2-positive breast cancer. In the context of developing an orthotopic transplantation model, we encountered considerable difficulty in establishing the appropriate level of oncogenic stimulus. Where the other oncogenes gave incomplete penetrance even at long latency, NeuNT was too aggressive and did not allow for a large enough window for the detection of accelerated disease over baseline.

Although we were unsuccessful in developing a high throughput platform suitable for screening, we noticed that our strong positive control shRNA against *Pten* was capable

of undergoing positive selection in our *in vivo* orthotopic transplantation assay employing NMuMG cells. In an alternative gene-by-gene approach, we conducted a small pilot screen for high priority candidate TSGs frequently deleted in human breast tumor tissue, which lead to the identification of *neurofibromin 1* (*Nf1*).

When first identified in the pilot screen there was little evidence in the literature linking NF1 directly to breast cancer as a tumor suppressor gene, with the exception of one study demonstrating the failure of the human breast cancer cell line MDA-MB-231 to express NF1 (Ogata et al. 2001) and a few publications that addressed the increased risk of breast cancer in patients with the common autosomal dominant genetic disorder neurofibromatosis type I (NF-1) which is caused by inherited mutations in *NF1* (Guran and Safali 2005; Sharif et al. 2007; Brems et al. 2009; Ripperger et al. 2009; Salemis et al. 2010). Only two reports implicated spontaneous *NF1* loss to breast cancer tumorigenesis (Guran and Safali 2005; Lee et al. 2010). However, analysis of The Cancer Genome Atlas (TCGA) breast cancer data sets has revealed that 27.7% of human breast tumors have *NF1* deletions or mutations, most being heterozygous (Wallace et al. 2012). Furthermore, in basal and HER2-positive patient subtypes as high as 40% of tumors display *NF1* loss or mutation. In their study, Schimenti and colleagues examined the genomic profiles of tumors arising in inbred *Chaos3* mice that exhibit high levels of genomic instability leading to mammary tumors and found that *Nf1* was lost in 59 out of 60 tumors analyzed by CGH (Wallace et al. 2012). An earlier study by Shannon and colleagues had found that mutagen-exposed (radiation and cyclophosphamide) heterozygous *Nf1* mutant mice developed soft tissue sarcomas and breast carcinomas (Chao et al. 2005). Collectively, these studies support our preliminary finding that NF1 is a candidate tumor suppressor in breast cancer and provides

a possible explanation as to why Ras mutations are found so rarely in breast tumors (*HRAS* 1%, *KRAS* 4%, *NRAS* 2%) (Pylayeva-Gupta et al. 2011).

NF1 has been studied primarily as a tumor suppressor in myeloid malignancies but in addition to breast, but there is increasing evidence to suggest that it is also involved in solid cancers such as lung (Ding et al. 2008; De Raedt et al. 2011), colon (Cacev et al. 2005; Ahlquist et al. 2008), glioblastoma (See et al. 2012), melanoma (Whittaker et al. 2013), and ovarian cancer (Sangha et al. 2008), with implications in both disease progression and therapy resistance. Taking advantage of the strong expression of the TREt promoter in the intestinal tissues, we have crossed TtG-shNF1.6074 and TG-shNF1.8594 to the *APCmin* (*Adenomatous polyposis coli* multiple intestinal neoplasia) strain commonly used to study intestinal and colorectal neoplasms (Moser et al. 1990). Preliminary data suggests that NF1 suppression accelerates the disease phenotype with shortened tumor-free survival (data now shown) and further characterization of *NF1* as a candidate TSG in this model is ongoing.

Multiple aspects of the work described in this chapter points towards an important lesson in mouse modeling: that each model system can bring challenges unique to the tissue type and disease under interrogation. In addition, any new element introduced into the model can have unpredictable consequences on the behavior of that system. Although we proceeded with due caution and sought to avoid drawing incorrect conclusions, it was unique aspects of mammary gland biology and difficulties in titrating the oncogenic force of tumor initiating lesions that caused a series of setbacks in adapting to the murine mammary gland a blueprint previously outlined in a successful hepatocellular carcinoma tumor suppressor screen from which this study had been fashioned (Zender et al. 2008). With the experience gained within our laboratory through our work with the murine mammary

gland and various positive selection screening platforms, we believe that future iterations of this project would circumvent many of the roadblocks that were encountered.

CHAPTER CONTRIBUTIONS

Uli Bialucha compiled the initial list of breast cancer tumor suppressor genes in collaboration with Jim Hicks and members of Michael Wigler's group (CSHL) (Table 2.1). Uli Bialucha and Johannes Zuber designed the shRNAs (Table 2.2). Uli Bialucha was instrumental in the many aspects of the development of the screening platform (Fig 2.1b, Fig 2.4). Alex Krasnitz developed and applied the "pinning algorithm" on the ROMA data. Jessica Bolden ran the Southern blot (Fig 2.13c). Sang Yong Kim performed the tetraploid complementation. Saya Ebbesen conducted all other experiments.

III. A conditional RNAi transgenic mouse model for validation and characterization of novel breast cancer tumor suppressor genes *in vivo*

INTRODUCTION

HER2 amplification and subsequent overexpression occurs in 20-30% of all human breast cancers and is associated with poor clinical outcome in metastasized disease (Slamon et al. 1987; Slamon et al. 1989; Andrulis et al. 1998; Arteaga et al. 2012). Although HER2 mutations are rare, efforts to recapitulate this disease in genetically engineered mouse models (GEMMs) have focused on the use of the activated *NeuNT* allele under the control of the Mouse Mammary Tumor Virus Promoter Enhancer (MMTV), which results in the efficient induction of aggressive, multifocal mammary tumors (Muller et al. 1988; Bouchard et al. 1989). By contrast, expression of the wild type *neu* allele under the control of the same promoter gives rise to focal tumors after a much longer latency (Guy et al. 1992b). A third series of strains expressing the '*neu* deletion' (NDL) transgene carrying in-frame deletions of the oncogene were also generated and displayed an intermediate phenotype (Siegel et al. 1994; Siegel et al. 1999). The MMTV promoter enhancer has been shown to be hormonally responsive and induced during pregnancy and lactation (Henrard and Ross 1988), which may be problematic when studying a disease where hormonal regulation plays such a major role. It nonetheless remains one of the most commonly employed tissue-specific promoters for studies focused on the mouse mammary gland.

The development of sophisticated RNAi technology in mammalian systems has produced a powerful tool for the study of TSGs *in vivo*. Short hairpin RNAs targeting relevant TSGs have been designed to hijack the endogenous RNAi machinery and to allow

for the stable suppression of target gene expression through mRNA cleavage or translational repression (Dickins et al. 2005; Silva et al. 2005; Chang et al. 2006). The use of an endogenous microRNA backbone, human miR-30, has enabled the technology to be adapted flexibly for use *in vivo* for both transgenic models and through *ex vivo* viral delivery prior to transplantation (Zender et al. 2008; Bric et al. 2009; Premsrirut et al. 2011).

There are several important components that must be considered when building an effective *in vivo* tool for the investigation of genomic, molecular and cellular changes that occur in a developing tumor. Firstly, for affording organ specificity, one method is the use of tissue-specific promoters. Secondly, in most cases we seek to examine a particular interaction between two or more genetic lesions that are commonly found in the disease under investigation. Choosing the appropriate genetic background is therefore essential. For many cancer types the predominant or defining landscape of oncogenic changes have now been well characterized and can be mimicked through the overexpression of a specific oncogene, a mutant allele, or the disruption of a TSG. Genetic alterations that occur during the evolution of a tumor cell may not be simultaneous, and thus temporal flexibility and control can add a powerful dimension to the experimental model and tetracycline-inducible systems can provide that conditional control. Tetracycline inducible systems permit reversible perturbation of pathways, which can mimic the actions of a small molecule inhibitor, and help determine how addicted cancer cells have become to a particular genetic lesion. RNAi technology, namely the use of shRNAs for target knockdown, is an elegant and reversible technique for altering the protein level of a gene of interest without permanently altering the endogenous genomic locus. Lastly, imaging modalities such as fluorescence or bioluminescence can be hugely helpful in visualizing the initiation and progression of disease without sacrificing experimental animals, enabling longitudinal

monitoring and quantification. Such reporters are also beneficial for the detection of circulating tumor cells and metastatic growth at distal organs.

This chapter describes efforts to bring together an existing mouse model of HER2-positive breast cancer with the transgenic RNAi technology recently developed in our laboratory.

RESULTS

Multi-allelic model for achieving tissue specific expression of shRNA and incorporation of fluorescent markers

With the goal of building a transgenic mouse model that allowed for the temporally regulated, reversible expression of shRNAs in the mammary epithelium, we conceived of the following multi-allelic strategy [Figure 3.1]. To achieve the desired tissue-specificity, we chose the whey acidic promoter (WAP) driven Cre recombinase strain (Wagner et al. 1997). Three different promoter systems have been commonly used for studies on the mammary gland: MMTV-Cre (mouse mammary tumor virus) (Wagner et al. 1997; Wagner et al. 2001), BLG-Cre (beta-lactoglobulin) (Selbert et al. 1998), and WAP-Cre. The WAP promoter is induced during lactation following pregnancy during nursing [Figure 3.1a]. Once expressed, Cre recombinase can act on the LoxP-Stop-LoxP (LSL) cassette embedded within a CAGs-LoxStopLox-rtTA3-ires-mKate2 (RIK) allele (J. Pelletier and L. Dow, unpublished) [Figure 3.1b]. The RIK transgene contains a cytomegalovirus (CMV) early enhancer element and chicken beta actin (CAG) promoter upstream of the LSL, followed by a modified rtTA with increased dox-sensitivity (rtTA3), internal ribosomal entry site (IRES) and the fluorescent protein mKate2. mKate2 is a monomeric far-red fluorescent protein that was designed for

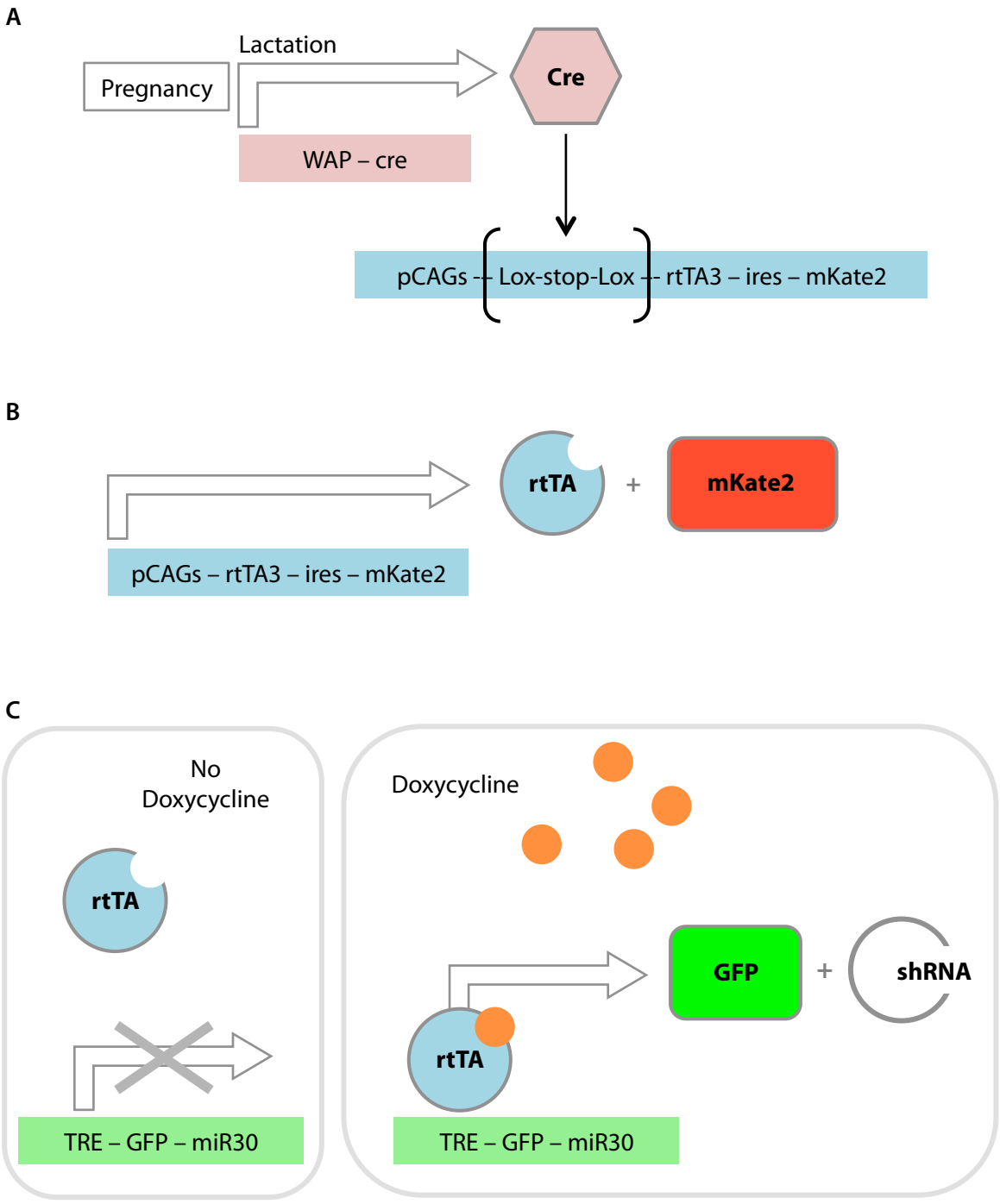

Figure 3.1 Schematic representation of lactation induced Tet-On multi-allelic transgenic system. (A) Expression of WAP promoter driven cre recombinase is parity-dependent and induced by lactation; cre excises Lox-stop-Lox cassette in pCAGs-LSL-rtTA3-ires-mKate2 (RIK) transgene. (B) CAGs promoter drives constitutive expression of rtTA and fluorescent reporter mKate2. (C) In the absence of dox, rtTA cannot bind the TRE promoter; in presence of dox, rtTA binds TRE and induces reversible expression of GFP reporter and shRNA.

imaging in living tissues (Shcherbo et al. 2009). Importantly, it is three-fold brighter than the previously published mKate protein and 10-fold brighter than mPlum.

The CAGs promoter expresses ubiquitously in most mouse tissues and can therefore drive widespread expression of downstream transgenic elements (Sawicki et al. 1998). Since the lactation-induced WAP promoter has already provided the tissue specificity, we opted for the use of a promoter upstream of the rtTA element whose expression levels would be unlikely to be modulated by changes in cellular differentiation/dedifferentiation during the course of tumorigenic transformation.

Once the luminal cells of the mammary ductal epithelium have begun expressing rtTA3, dox can be used to induce expression of the shRNA transgenic allele (TRE-GFP-miR30) (Premsrirut et al. 2011). In this Tet-On set-up, the tetracycline-responsive element promoter (TRE) is active when bound by rtTA [Figure 3.1c]. In a similar fashion to the shRNA vectors described in Chapter 2, GFP has been coupled with the expression of the shRNA. However, while GFP reporter expression in the context of the MLS retroviral vector serves to confirm the presence of the shRNA construct, here the strength of the fluorescent signal corresponds inversely to the knockdown level of the target protein (Premsrirut et al. 2011).

Lastly, in line with our decision to model HER2-positive breast cancer in Chapter 2, we overlaid the three transgenic alleles described above onto the oncogenic background of the viral MMTV promoter driven mutant rat ortholog of HER2, neu^{V664E} (MMTV-NeuNT) (Muller et al. 1988) [Figure 3.2a]. This mutated form of *neu* has a point mutation in its transmembrane domain that results in increased receptor homodimerization and constitutive activation of the kinase domain even in the absence of a ligand. It should be noted that we acquired the founder strain "TG.NK" available through the Jackson

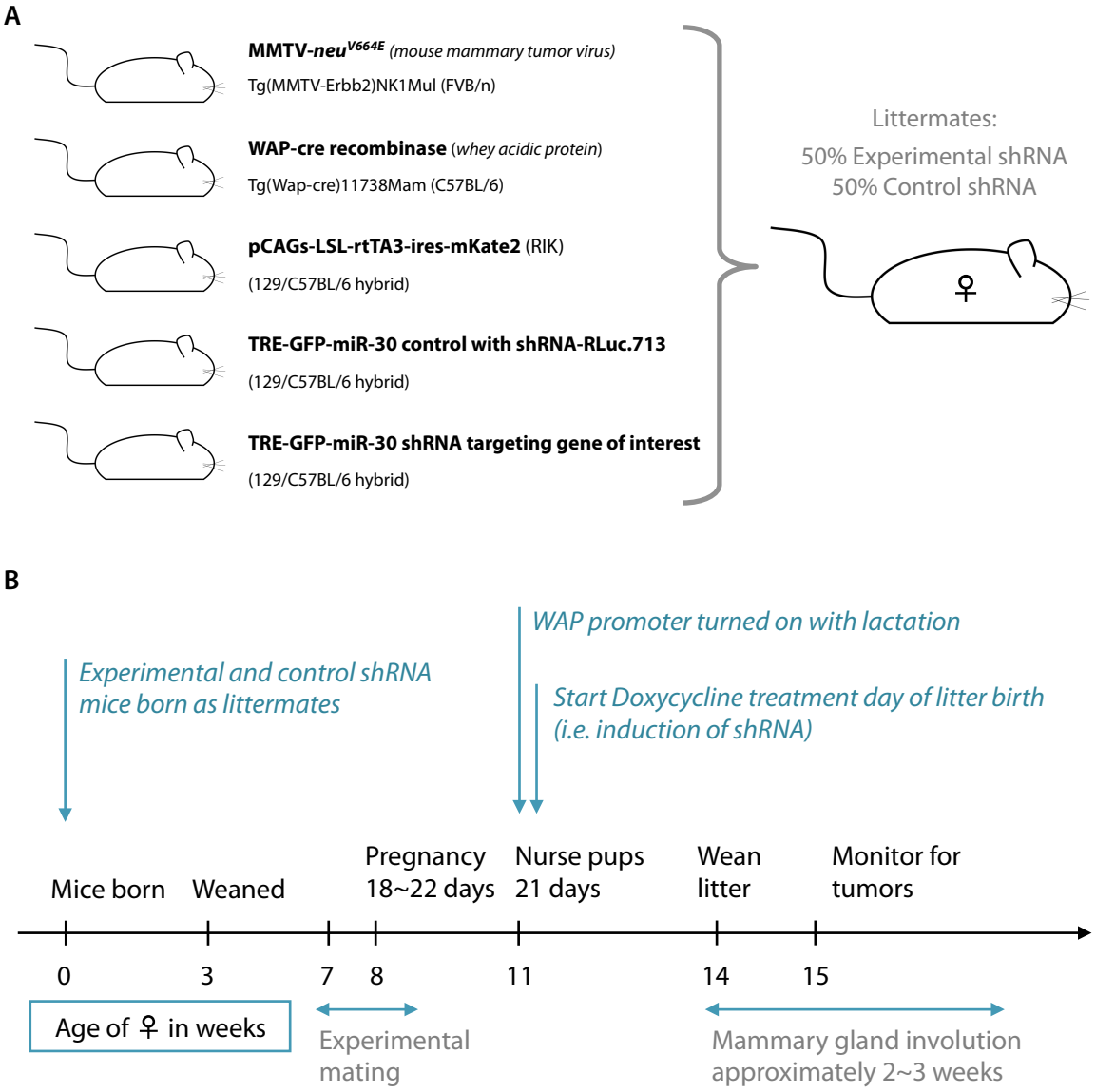

Figure 3.2 Transgenic strains and experimental timeline for induction of alleles. (A) Simplified schematic of breeding stretegy that incorporates five strains for the production of littermate controls along with experimental mice. (B) Timing of pregnancy, duration of lactation, and start of dox treatment; the designation "experimental age" in later figures corresponds to age of mice normalized to the date of birth of litter.

Laboratory (http://jaxmice.jax.org/), while most of the characterization shown in the 1988 publication focuses on strain "TG.NF". This latter strain displayed a significant ectopic expression of the transgene in male mice, notably in the salivary gland and epididymis (Muller et al. 1988).

We had previously attempted to use the MMTV-tTA allele to drive shRNA expression over the MMTV-NeuNT background but these experiments gave mixed results, notably a very long latency and incomplete tumor penetrance within cohorts (data now shown) (Hennighausen et al. 1995). While there are advantages of using a Tet-Off system, such as increased precision in the timing of target protein re-expression and reduced levels of possibly deleterious lingering dox molecules (Riond and Riviere 1988; Anders et al. 2012), and additionally the MMTV-tTA allele circumvented the need for pregnancy in the experimental outline, we remained unsatisfied with variable disease phenotypes observed.

Breeding strategy for efficient production of multi-allelic experimental mice with appropriate littermate controls

A well-planned strategy for mouse husbandry is important in allowing the efficient production of experimental animals. Since the objective is to study breast cancer, and the model system requires pregnancy, only females are useful for analysis. To minimize production of unnecessary mice, the best strategy was to first create breeder mice that contain two copies of each transgene such that all female pups that are born can be used for experimentation. In the current mouse model, we are fortunate that all of the alleles can be maintained in a homozygous state without loss of viability or fertility, although homozygous, parous MMTV-NeuNT females have a greatly shortened lifespan due to early tumor onset.

The multi-allelic model was built without undergoing the time-consuming process of backcrossing each transgenic strain onto the same mouse strain background. While the MMTV-NeuNT allele is on an FVB/n background, WAP-Cre is C57BL/6. RIK and the TG-shRNA lines were derived using F1 hybrid ESCs that are composed of 129 and C57BL/6. Interbreeding these mice introduced three strain backgrounds into the experimental cohort and the proportion at which each strain contributed to any particular animal could not be measured. To control for the variable effects of strain background on disease phenotypes (Linder 2006; Serpi et al. 2013), we sought to follow a tactic where a control shRNA strain is integrated into the breeding scheme from the start. By creating compound homozygous animals carrying one experimental and one control shRNA, both targeted to the *ColA1* locus, we could produce litters that segregated the shRNAs in a Mendelian fashion (Linder 2006; McJunkin et al. 2011; Dow et al. 2012). We currently have two neutral shRNA control strains that are routinely used: Renilla-Luciferase.713 (RLuc.713) and Luciferase.1309 (Luci.1309) [see TABLE 6.1 in Materials and Methods]. While the shRNA-Luci.1309 targets the *luciferase* gene, the RLuc shRNA has the advantage of being compatible with *in vivo* luciferase imaging as it does not repress the reporter and has been used as the control strain in the experiments described in Chapter 4 (Premsrirut et al. 2011) [Figure 3.2a]. In addition to having no known target in the mouse genome, RLuc.713 was chosen for its high level of efficient expression and processing (Zuber et al. 2011a).

Experimental timeline for induction of WAP-cre allele and shRNA knockdown

The WAP-Cre transgene has a *Cre recombinase* cDNA driven from the promoter region of the murine *whey acidic protein* (*Wap*) gene that is expressed in mammary epithelial cells in response to lactogenic hormones. High-level expression of the endogenous *Wap* gene

is confined to the last few days of pregnancy and lactation, while robust activity of the WAP-Cre transgene was detected as early as day 14 of pregnancy and most strongly during lactation (Wagner et al. 1997). The original publication reports that cells with efficient Cre activity were observed after involution, a process whereby much of the terminally differentiated epithelial cells have undergone apoptosis during the remodeling of the gland.

The molecular and cellular effects of pregnancy have been successfully mimicked in mice using hormone pellets (Ingberg et al. 2012). However, as there was no literature citing the use of hormones to mimic lactation we opted to use traditional husbandry and nursing as a means of activating the WAP-Cre transgene.

With the understanding that many of the cells that activate WAP-Cre inevitably die during post-lactation involution, we decided upon an experimental timeline that incorporated a full three-weeks of nursing after pregnancy. Experimental females with the four alleles – MMTV-NeuNT ; RIK ; WAP-Cre ; TG-shRNA – began mating at approximately 7 weeks of age when sexual maturity had been reached. They were housed in proximity to male mice prior to mating to help maintain regular estrus cycling. Although the mice were harem mated, each pregnant female was separated into a new cage before the birth of her litter, thus exact litter counts and any potential difficulties in lactation could be noted [Figure 3.2b]. The gestation period of a mouse pregnancy can vary between 18-22 days. The experimental mating colony was monitored daily and in most cases the experimental female was placed on dox treatment within 24 hours of litter birth to induce expression of the shRNA. After the experimental litters were weaned 21 days after birth, the mothers were housed randomly and remained continuously on dox treatment unless otherwise noted. Palpation for tumors began one week following weaning, though it was

rare that palpable tumor growth was observed during the first four weeks of dox treatment in any of the experiments described in Chapter 4.

The use of Adeno-Cre in place of the WAP allele was tested in the abdominal mammary fat pads of RIK mice by direct injection into the fatty tissue near the base of the ductal tree [Figure 3.3]. Further improvements to this approach could involve the use of direct intraductal injection of the virus through the nipple, a technique we would like to explore further in the future (Vonderhaar and Ginsburg 2000; Behbod et al. 2009). The use of the viral Cre could potentially activate the shRNA in a different set of epithelial cells. This could result in altered tumor phenotypes or differentiation, and would also reduce the number of cells in which the shRNA is expressed, perhaps better modeling physiological heterogeneity, although at the expense of variable transgene penetrance.

In Chapter 4, we will discuss control cohorts consisting of MMTV-NeuNT ; RIK ; WAP-Cre ; TG-shRNA mice that were kept as virgins but placed on dox at 10-11 weeks of age to approximate the treatment of the regular parous cohorts. These mice were included primarily to control for ectopic expression of the WAP promoter in the absence of pregnancy. Although the levels were insufficient to accelerate tumor onset over background, we did observe GFP positive ductal epithelium in some mice (data not shown). The timing of this ectopic activation was not investigated further. In the experiments described at the end of Chapter 2 in the context of modeling *NF1* tumor suppressive gene function, parental breeders with only one copy of WAP-Cre were used to generate littermates that harbored either a control or experimental shRNA, with or without the Cre allele. This allowed for the incorporation of controls that could undergo pregnancy and dox treatment in the same fashion as the experimental cohorts, thus normalizing the effects of

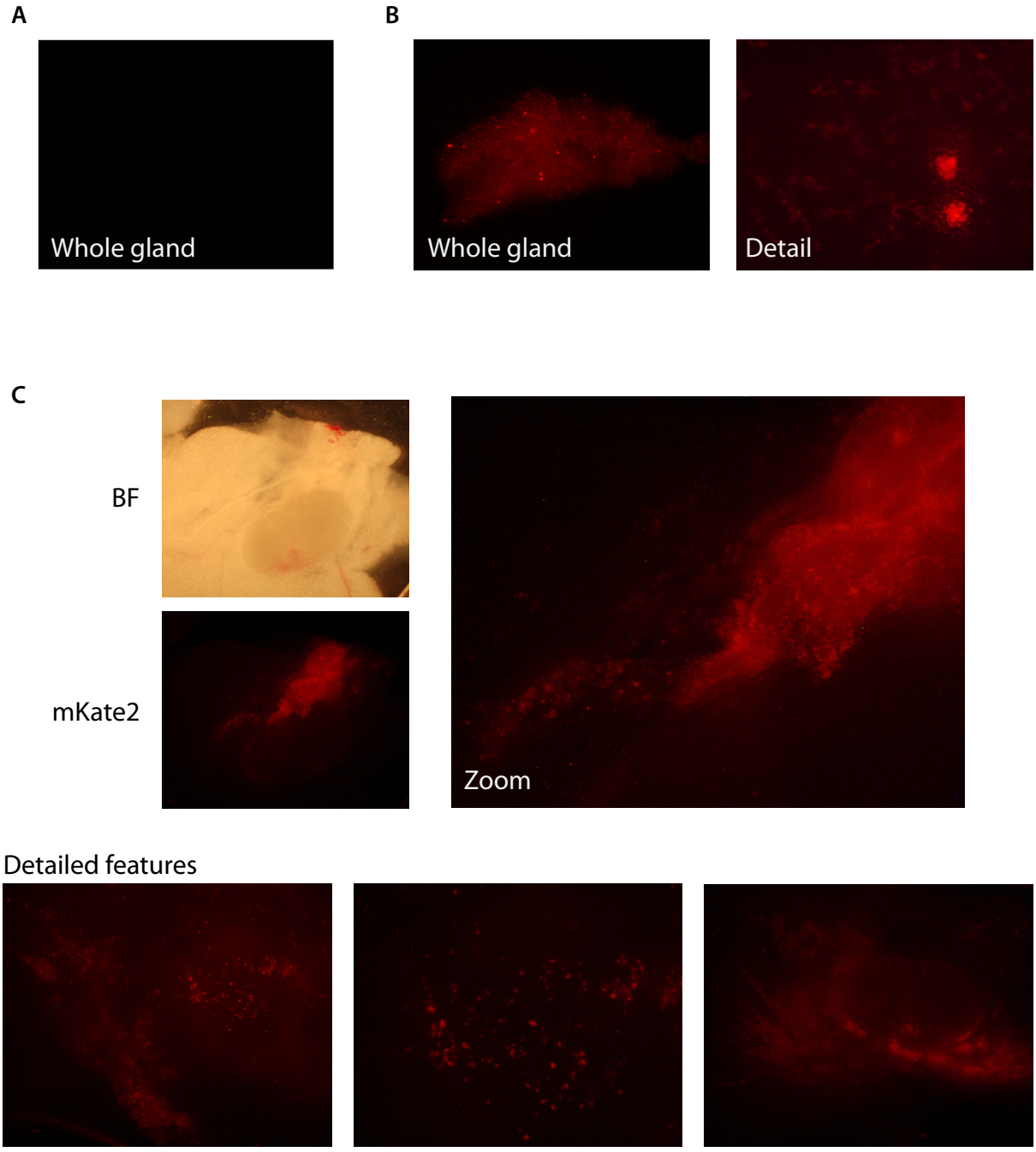

Figure 3.3 Adeno-Cre injection into mammary fat pads. (A) mKate2 signal in the mammary gland of MMTV-NeuNT parous control mouse 10 days after end of lactation; autofluorescence is not detected. (B) MMTV-NeuNT;RIK;WAP-Cre parous mouse 2 weeks after end of lactation; bright mKate2 expression is observed throughout the ductal epithelium. (C) Surgical injection of Adeno-viral cre recombinase near base of ductal in virgin RIK mice; mammary gland harvest 17 days after injection; focal and scattered expression of mKate2.

pregnancy on the mouse and on the MMTV-NeuNT transgene expression levels and patterns.

The mouse has five pairs of mammary glands that extend from the neck region all the way to the groin [Figure 3.4]. The mammary epithelial tissue does not begin to develop until puberty, at approximately 4 weeks of age and the full ductal branching is achieved at about 8 weeks. Since both the WAP-Cre and the MMTV-NeuNT transgenes express ubiquitously in all of the mammary tissue of the mouse, monitoring for tumor onset was conducted by weekly palpation of the thoracic and abdominal regions of each mouse. Anesthesia was used in cases where the precision of palpation while scruffing the animal was compromised. To facilitate the longitudinal monitoring of tumor onset and growth, a "quadrant system" was devised to section the mammary glands into four regions [Figure 3.4]. In this manner, tumor onset was scored separately for each quadrant and the number of tumor bearing quadrants could used to grossly approximate disease penetrance and progression.

Characterization of the MMTV-NeuNT ; RIK ; WAP-Cre ; TG-shRNA transgenic model: luminal epithelial expression, *in vivo* imaging and single transgene controls

Successful luminal expression of the RIK transgene after recombination by the WAP promoter driven Cre was first assessed by fluorescence activated cell sorting (FACS) using cell surface markers. A cohort of age-matched mice was prepared as shown in Table 3.1. The tri-allelic MMTV-NeuNT ; RIK ; WAP-Cre mice were littermates and biological replicates were used for the parous category. For parous animals, excess pups were euthanized to allow for normalization of litter size to 5-6 pups that were weaned after 21 days of nursing [Figure 3.5a].

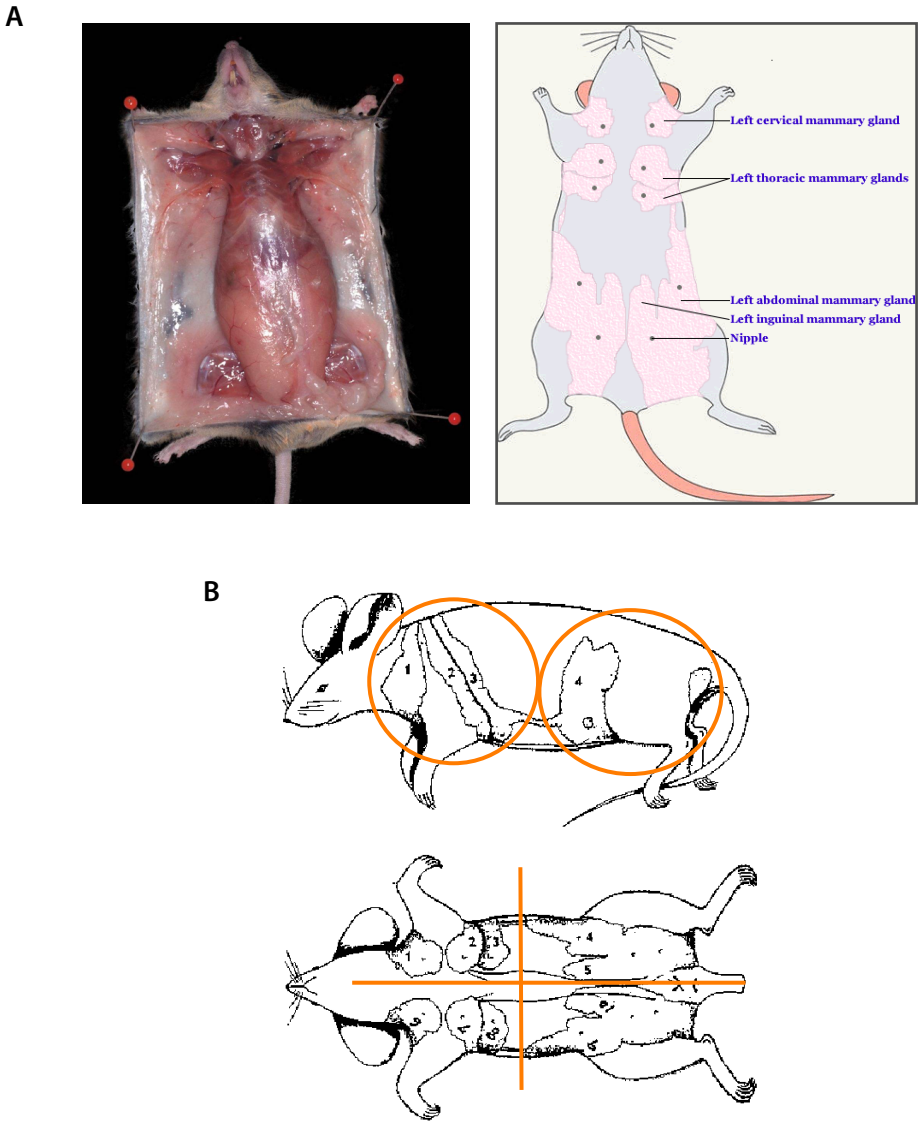

Figure 3.4 Schematic of mouse mammary glands. (A) In the mouse, five pairs of mammary fad pads are located just below the skin, which extend from the thoracic (three pairs) to the inguinal/abdominal (two pairs) regions. Each fat pad has a nipple. (B) Tumor-scoring system based on four "quadrant" regions as defined by orange lines.

Table 3.1 Experimental categories for model characterization by FACS

Strain	Virgin	Parous
MMTV-NeuNT ; RIK ; WAP-Cre	✓	✓
MMTV-NeuNT ; RIK	✓	✓
WAP-Cre	✓	✓
C57BL/6	✓	

Non-invasive, optical *in vivo* imaging was conducted using a Xenogen IVIS® Spectrum. The fluorescence marker associated with the expression of RIK, mKate2, displayed robust tissue penetration through the skin in areas where the fur had been removed [Figure 3.5b]. We observed a decrease in the fluorescence signal in the weeks following litter weaning due to involution of the mammary gland. Additionally, the expression patterns of the GFP reporter from the TG-shRNA allele were also confirmed for tissue penetrance using a separate cohort of mice [Figure 3.5c].

For FACS analysis, mammary glands were harvested 21 days after the end of lactation, a total of six weeks after litter birth. We postulated that all effects of involution and tissue remodeling would be complete at this time point, thus providing an accurate portrayal of the recombined cells that would remain in the gland. The cell surface markers CD24 and CD29 were used to define the luminal lineage of the mKate2 positive sub-population of the mammary epithelial cells [Figure 3.6]. Virgin controls showed almost no mKate2 positivity.

In the first iteration of the model, we chose to test the behavior and oncogenic background of the published transgenes in our own hands. MMTV-NeuNT$^{+/-}$ mice on a FVB/n, C57BL/6 hybrid background were generated, as well as MMTV-NeuNT$^{+/-}$; RIK$^{+/-}$ and MMTV-NeuNT$^{+/-}$; RIK$^{+/-}$; WAP-Cre$^{+/-}$ females on a mixed 129, FVB/n, C57BL/6

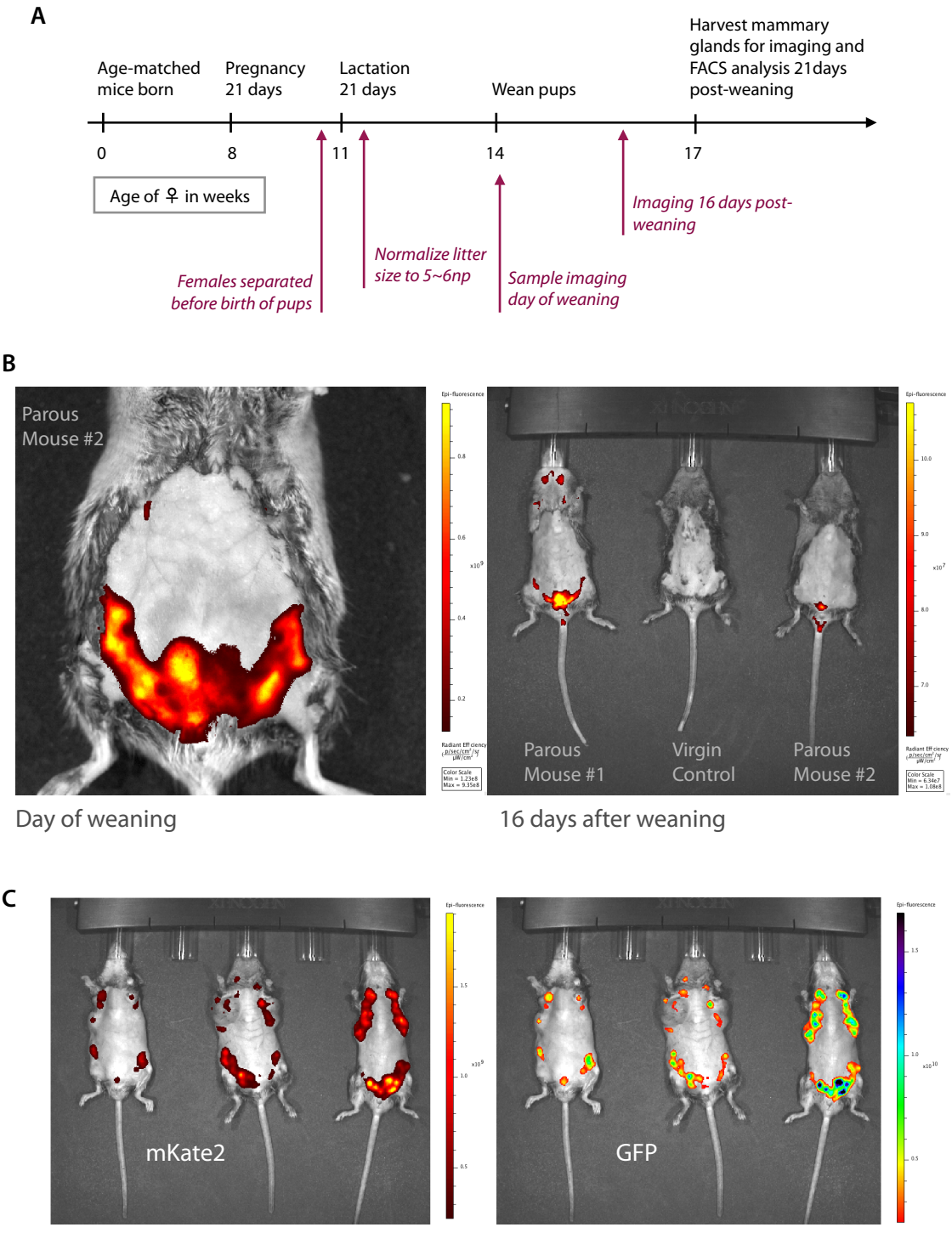

Figure 3.5 Optical *in vivo* imaging. (A) Experimental timeline for RIK induction and sample harvest for imaging and FACS analysis trial. (B) MMTV-NeuNT;RIK;WAP-Cre parous and virgin littermates imaged using a Xenogen IVIS Spectrum after removal of fur. (C) Example of GFP and mKate2 imaging from tumor-bearing MMTV-NeuNT;RIK;WAP-Cre;TG-shRNA parous mice on dox treatment.

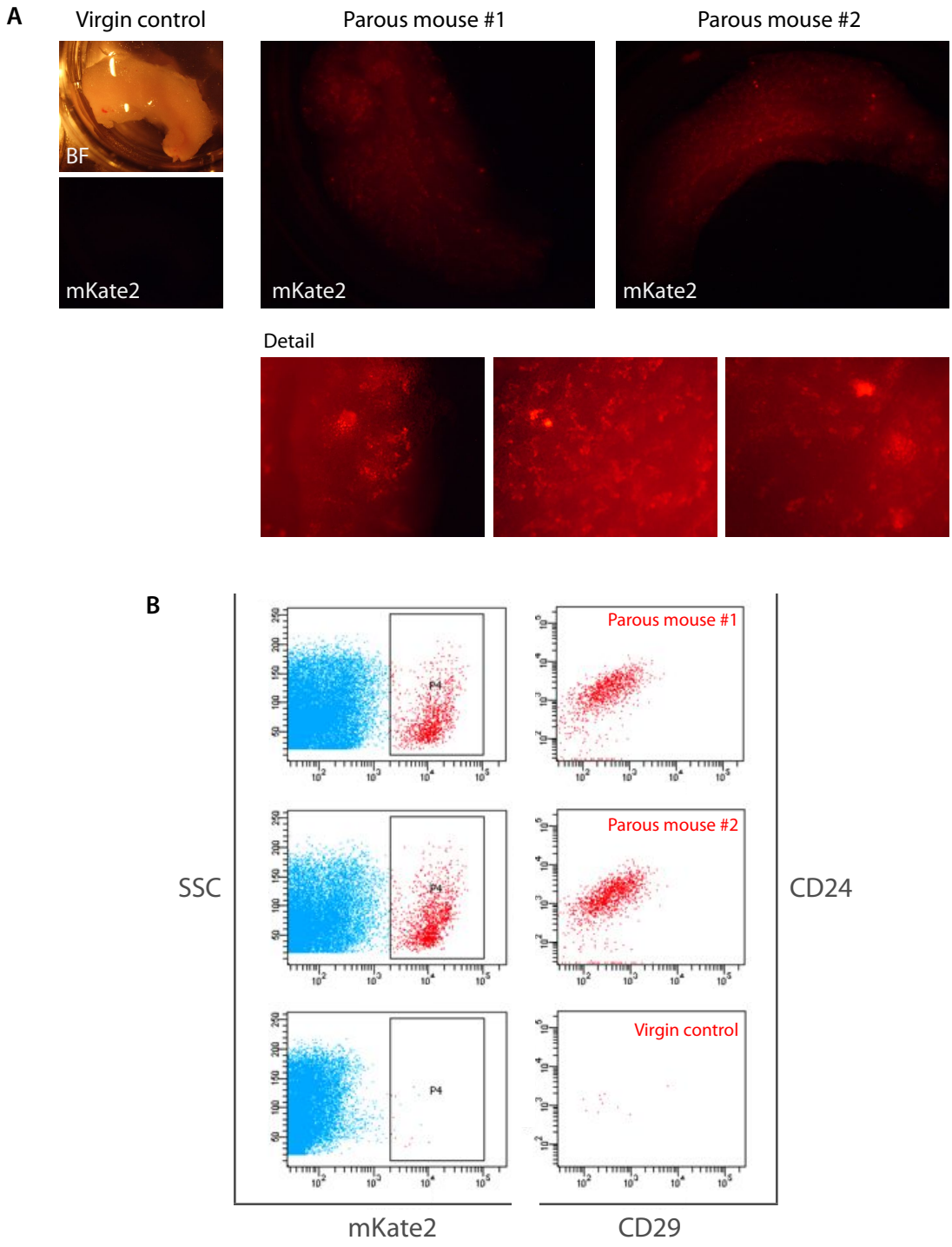

Figure 3.6 WAP-Cre induced luminal epithelial expression of mKate2 reporter from RIK allele in parous mice. (A) Verification of mKate2 signal in the mammary glands of MMTV-NeuNT;RIK;WAP-Cre parous and virgin controls. (B) FACS analsyis of epithelial cells from mammary glands of MMTV-NeuNT;RIK;WAP-Cre parous mice gated for CD24 and CD29 cell surface markers; biologial replicates for MMTV-NeuNT;RIK;WAP-Cre parous cohort, plus a virgin littermate control.

background that best resembled the undefined final strain composition of experimental cohorts described in Chapter 4. Additionally, C57BL/6 wild type mice and WAP-Cre$^{+/-}$ mice were prepared. Although these mice were not administered a dox treatment, some were kept as virgins and others underwent one pregnancy [Table 3.2]. To normalize for the variable age at which animals became pregnant (7-16 weeks; average 8.3 weeks), the term "experimental age" was used to refer to the time following the day of birth of her first litter. This nomenclature will apply to all experiments described in Chapter 4. As expected, the controls with no oncogenic transgene (C57BL/6 and WAP-Cre only) did not develop any tumors within the timeframe of this experiment (over 230 days in experimental age). Parous animals with MMTV-NeuNT remained tumor free on an average of 180 days in experimental age [Figure 3.7].

Table 3.2 Control cohorts: characterization of allelic components, background latency

Strain	Virgin (n)	Parous (n)
MMTV-NeuNT ; RIK ; WAP-Cre	5	12
MMTV-NeuNT ; RIK	4	4
MMTV-NeuNT	3	4
WAP-Cre	2	7
C57BL/6	5	3

The experimental terminal disease endpoint, determined by unbiased assessment of veterinary staff, was established as any adult mouse with a tumor size exceeding 20mm at the largest diameter. Ulcerated tumors were also a cause for euthanasia irrespective of tumor size. However, this definition had its caveats for the purposes of our experiments.

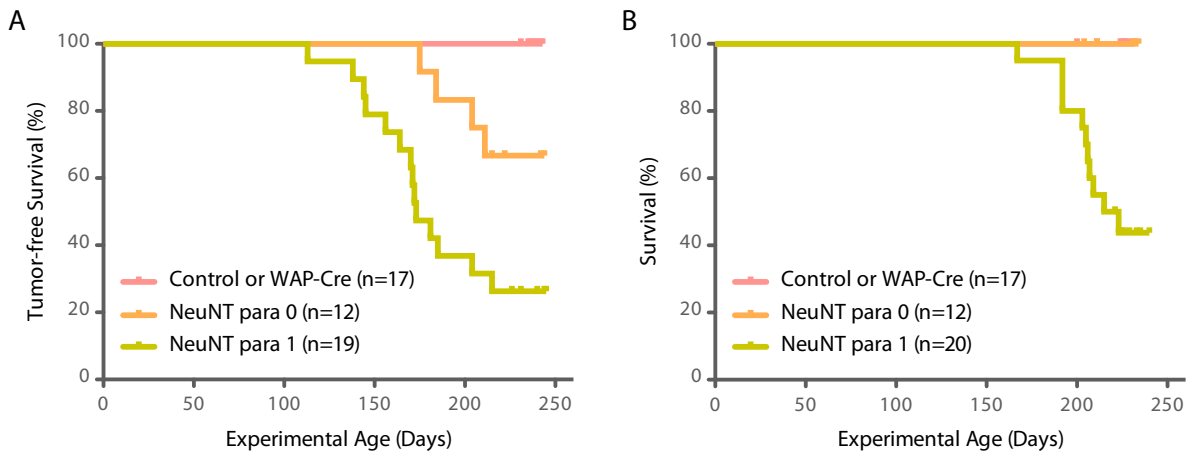

Figure 3.7 CSHL control cohorts. Kaplan-Meier suvival curves for (A) tumor-free survival and (B) overall survival of control cohorts listed in Table 3.2. Mice were segregated by presence or absence of MMTV-NeuNT transgene and subseqently by parity.

Firstly, the location of the tumor greatly influenced the distress caused to the animal, as well as visibility during routine checks by veterinary staff. Secondly, the MMTV-NeuNT model can give rise to blood-filled cysts that can balloon quickly but do not share the same disease phenotypes or consequences as more solid, epithelial primary tumors. Thirdly, in the presence of a cooperating shRNA, the model produced mice with a tumor burden representing the sum of many tumors within one animal (discussed further in Chapter 4).

DISCUSSION

We have generated and tested a new transgenic mouse model for the study of HER2 positive breast cancer that incorporates inducible RNAi technology, fluorescent reporters, *in vivo* imaging capacities, and restricted transgene expression in the luminal sub-compartment of the mammary epithelium. The multi-allelic model makes use of the WAP-Cre allele's tissue specificity and induction through lactation to temporally and spatially restrict the expression of the GFP-tagged shRNAs via the RIK allele, which allows for strong and sustained expression of the rtTA3 and mKate2 elements. The dual fluorescent marker system is particularly powerful in experiments taking advantage of the reversibility of the shRNA allele. While the GFP protein level inversely correlates to target knockdown, mKate2 tracks all cells that can express the shRNA regardless of the doxycycline treatment regimen. This is invaluable for tumor maintenance studies, as will be discussed further in Chapter 4. mKate2 expression as a Cre lineage tracer is also particularly relevant in this model where expression of the sensitizing oncogene, mutant *neu*, can drive tumor growth in cells that do not express the WAP promoter – these tumors are easily distinguished by absence of mKate2.

There are several distinct advantages and caveats to the model that should be noted. Two major advantages are the capacity to control the timing of shRNA induction and the near absence of ectopic tissue expression. In contrast, our experience with the MMTV-tTA allele were mixed. We saw high levels of GFP expression in the salivary gland and a low disease penetrance at long latency despite the presence of NeuNT and an shRNA targeting a potent TSG. It is possible that the two MMTV alleles – MTV-NeuNT and MMTV-tTA – had only a small overlapping cell population despite being driven from the same viral promoter, or that modulation of the transactivator expression levels caused by cyclical hormonal effects was deleterious towards sustained target gene suppression. A recent publication by Wagner and colleagues describes a novel MMTV-tTA transgenic strain with which it might be interesting to repeat the original experiments (Sakamoto et al. 2012). Additionally, we are looking into the possibility of testing the MMTV-cre strain in combination with our RIK allele in future iterations of this breast cancer mouse model. One caveat of our model is the dependency on pregnancy to induce lactation and expression of the shRNA allele. This makes the process more labor intensive and restricts our studies to sexually mature, parous animals; yet, the incidence of breast cancer is markedly higher in older women, many who have undergone one or more pregnancy.

Multi-allelic models such as this one rely heavily on the overlapping expression of various promoters in the cell type of interest, at the accurate and desired time in development, and with as little ectopic tissue expression as possible. The transgenes have been engineered to the best of our capacity to ensure the reliable expression of all essential elements: shRNA, oncogene, rtTA, and fluorescent markers. However, the robustness of the model can only be tested through actual experimentation as unexpected phenotypes are routinely observed. Even within our research group, we have seen examples of transgene

'silencing' and other unexpected dosage effects that are not easily explained (McJunkin et al. 2011). The RIK and TRE-GFP-miR30 strains are based on the integration of transgenic elements into a known locus of the mouse genome. This is preferable for several reasons but namely because disruption of housekeeping genes can be definitively avoided and cross-comparison of mouse strains, for example in an allelic series or between two shRNAs, can be conducted more reliably. Founder mice that are made through pronuclear injection are usually tested thoroughly as variable sites of integration can have dramatic "founder effects" on the expression levels and patterns of the same transgenic element (Lin 1966; Muller et al. 1988).

While some promoters are chosen for their tissue or cell-type specificity, others are incorporated because of their broader expression potential. In the system developed here, we are depending on the robust and efficient expression of the WAP promoter, and subsequently require linked CAGs and TRE promoter activity in the same luminal cells. Additionally, in order to observe cooperation of the shRNA target with *NeuNT* overexpression, we need to have sufficient, overlapping expression of TRE with the MMTV promoter at its particular genomic integration site. During some preliminary experiments to test the fluorescence compatibility of our model for intravital microscopy with the Egeblad laboratory in CSHL, we made the unexpected observation that a small percentage of cells that express the cre-excised RIK allele do not express the TRE-GFP-miR30 allele [Figure 3.8]. We have not yet quantified the prevalence or investigated the cause of this phenomenon since we do not believe it impacts our immediate experimental needs. It is nonetheless another reminder of how any new mouse model must be carefully tested and vetted before they can be used to probe meaningful hypotheses and draw accurate conclusions. It also

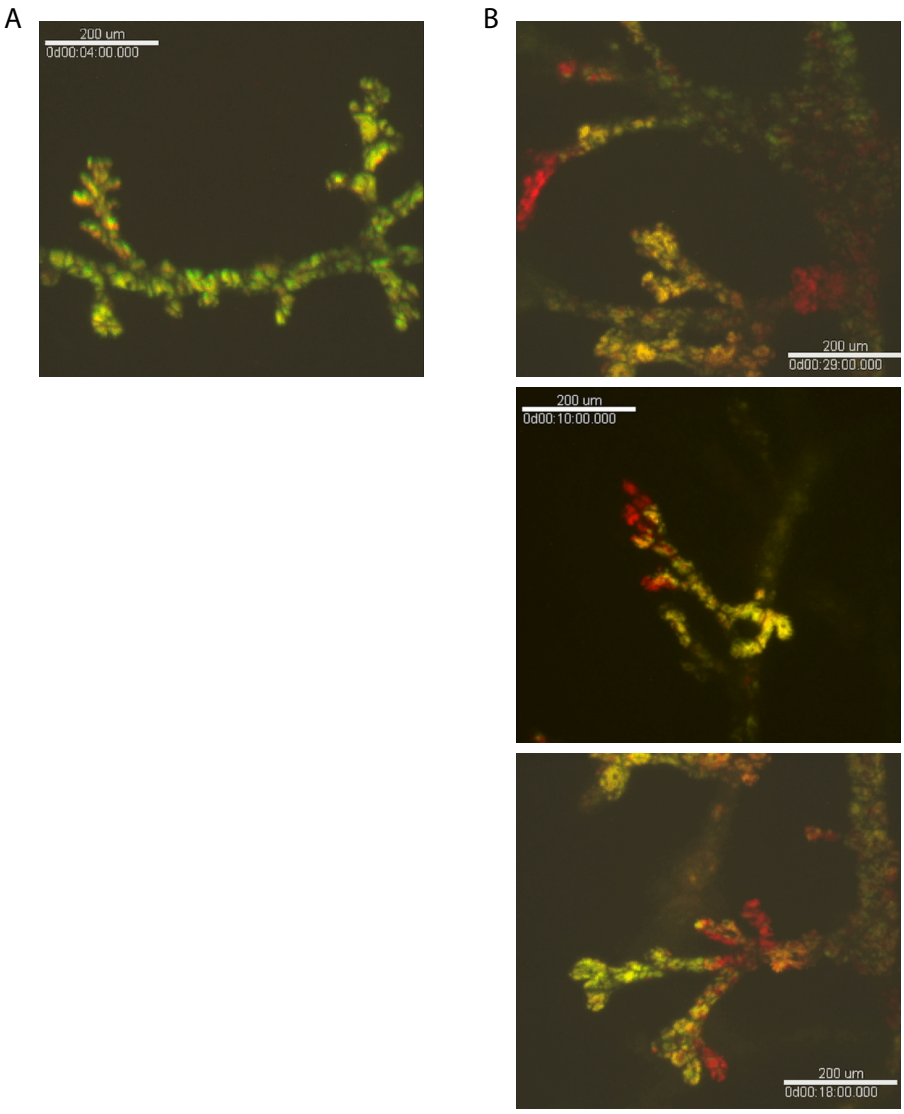

Figure 3.8 Intravital imaging. MMTV-NeuNT;RIK;WAP-Cre;TG-shRLuc.713 parous, dox treated mouse with early stage palpable tumor nodules examined using live-cell imaging for mKate2 and GFP fluorescent reporter expression. Still frames shown. (A) Example of mKate2/GFP co-expression. (B) Three examples of mKate2 only signal in terminal endbuds of mammary ductal epithelial branching adjacent to mKate2/GFP co-expressing cells.

motivates us to set up platforms that will allow for faster and more systematic methods of model building.

To this end, and to maximize the potential for the assessment of breast cancer gene function *in vivo*, we hope to pursue a secondary project in the future where we will re-derive ESCs from multi-allelic breast cancer GEMMs such as the one described in this chapter. The use of ESC re-derivation in cancer mouse models has been pioneered by Jonkers and colleagues at the Netherlands Cancer Institute (Huijbers et al. 2011) and members of our laboratory (Premsrirut et al. 2011; Dow et al. 2012). Our ESCs would be pre-engineered to harbor various cancer predisposing alleles, imaging reporters, and tetracycline-regulated transactivators, to which we would apply our transgenic *in vivo* RNAi technology pipeline to add the component of inducible, reversible suppression of endogenous genes directly into these GEMM-ESCs through *ex vivo* manipulation. We believe that bringing together these two technologies, ESC re-derivation and RNAi, will make transgenic breast cancer mouse modeling an even more flexible and scalable exercise as multiple combinations of cooperating genetic legions could be readily analyzed in parallel and the effects of tissue-specific transient gene activation or inhibition could be assessed at different stages of disease using reversible, inducible alleles. This strategy has the potential to permit the rapid generation of breast cancer mouse models while bypassing the bottlenecks of traditional breeding approaches. Importantly, this method would also allow for the scalable production of age- and gender- matched experimental animals. Other members of the Lowe laboratory have been working to adopt this strategy in the context of pancreatic cancer (Saborowski, et al. In preparation) and colon cancer (L. Dow, unpublished), with the shared objective of making the translation of cancer genomic data to the clinic a faster process and to eventually change the standards of preclinical drug trials conducted in mice.

CHAPTER CONTRIBUTIONS

Uli Bialucha chose the transgenic allele combination for the model and initiated the first mouse crosses, and also generated the experimental mice used in the MMTV-tTA experiments. Lukas Dow and Jerry Pelletier made the RIK transgenic mouse strain. Lukas Dow made and tested the TG-shRLuc control strain. Camila Dos Santos provided the protocol and technical advice for the FACS experiment (Fig 3.6). Saya Ebbesen conducted all other experiments.

IV. Exploration of *ERBB2* and *PTEN* as cooperating events using a novel inducible PTEN shRNA transgenic mouse

INTRODUCTION

In 1998 the targeted therapeutic agent trastuzumab, developed by Genentech (brand name Herceptin®), was approved by the US Food and Drug Administration for the treatment of HER2/neu-overexpressing breast cancer (Fendly et al. 1990; Robertson 1998). The recombinant, humanized anti-p185HER2 monocolonal antibody had cytostatic growth inhibitory effects on breast cancer cells overexpressing HER2 and enhanced the cytotoxic effects of chemotherapeutic agents in preclinical models (Baselga et al. 1998). HER2 has been found overexpressed in 20-30% of human breast cancers and leads to an aggressive disease with poor patient survival (Slamon et al. 1987; Yu and Hung 2000). Early clinical trials showed trastuzumab was active when used in conjunction with existing chemotherapy, and that the combination significantly prolonged the median time to disease progression, increased the overall response rate, increased the duration of response, and improved median survival time by approximately 25% compared to the use of chemotherapy alone (Cobleigh et al. 1999; Baselga 2001; Seidman et al. 2001; Slamon et al. 2001; Esteva et al. 2002). However, these trials reported less than 35% of patients with HER2-overexpresisng metastatic breast cancer responding to the drug as a single agent (Cobleigh et al. 1999; Vogel et al. 2002).

Despite over a decade of active research, an incomplete understanding of the mechanism behind trastuzumab's antitumor activity remains. Early studies suggested as possible mechanisms of action the downregulation of HER2 (Petit et al. 1997), the induction of antibody-dependent cellular cytotoxicity (ADCC) (Clynes et al. 2000), an induction of G1

arrest and the cyclin-dependent kinase inhibitor $p27^{kip1}$ (Sliwkowski et al. 1999), or the inhibition of HER2 extracellular domain cleavage preventing the production of an active truncated HER2 fragment (Molina et al. 2001). Inhibition of PI3K/Akt signaling has also been implicated, with studies demonstrating a downregulation of HER2 signaling (Hudziak et al. 1989; Yakes et al. 2002) or an increase in PTEN membrane localization and phosphatase activity leading to a decline in PI3K/Akt pathway activation and consequently an inhibition of proliferation (Nagata et al. 2004). This last study by Nagata and colleagues not only showed that PTEN antagonizes tumorigenesis but also sensitizes breast cancers to trastuzumab treatment.

The tumor suppressor gene *PTEN* opposes the activation of the proto-oncogenic PI3K/Akt signaling pathway and is found disrupted in many cancer types (Cantley and Neel 1999). *PTEN* was originally identified as a gene frequently mutated in brain, breast and prostate cancers through the mapping of homozygous deletions on human chromosome 10q23 (Li and Sun 1997; Li et al. 1997; Steck et al. 1997). Early studies reported loss of heterozygosity (LOH) of the 10q23 chromosomal region in as many as 30-40% of invasive breast carcinomas, while no LOH was seen in intraductal carcinomas, thus associating the loss of this locus with tumor progression (Bose et al. 1998; Singh et al. 1998; Feilotter et al. 1999; Garcia et al. 1999)

In the classic Knudson model of neoplastic transformation, a tumor suppressor gene begins with a somatic or inherited mutation in one allele, to which the subsequent loss of the other allele causes a selective proliferative or survival advantage (Knudson 1971; Cavenee et al. 1983; Knudson 2001). However, numerous TSGs, including *TP53* and *PTEN*, have been shown to exhibit haplo-insufficiency due to dose-dependent anti-tumorigenic functions (Berger and Pandolfi 2011). *Pten* hypermorphic mice, expressing 80% of normal *Pten* protein

levels, develop a spectrum of tumors but notably, breast tumors occur with the highest penetrance (Alimonti et al. 2010).

PTEN normally opposes the activation of phosphatidylinositol 3' kinase (PI3K) through cleavage of the D3 phosphate of phosphatidylinositol (3,4,5)-triphosphate (PIP-3), its main substrate (Maehama and Dixon 1998). Loss of PTEN function therefore results in AKT hyperactivation that leads to protection from various apoptotic stimuli (Stambolic et al. 1998). Early studies in mouse models demonstrated that the inactivation of even one *Pten* allele could lead to a dramatic impact on the survival and proliferative capacity of cells (Di Cristofano et al. 1999). It has been suggested that PTEN plays an essential and cell-autonomous role in regulating the proliferation, differentiation and apoptotic functions of mammary epithelial cells as conditional loss of PTEN in the mammary gland gives rise to precocious lobulo-avelolar development, excessive ductal branching, delayed involution and severely reduced apoptosis (Li et al. 2002).

With the goal of improving the availability of biomarkers that accurately predict responses to cancer therapy vital to the rational use of cancer drugs in the clinic, Berns and colleagues used a HER2-overexpressing breast cancer cell line BT-474 and conducted a large-scale RNAi genetic screen using a library of 24,000 shRNA retroviral vectors targeting 8000 human genes (Berns et al. 2007). BT-474 cells are sensitive to treatment by trastuzumab and respond by a reduction in proliferation. PTEN knockdown was the only gene loss that conferred resistance to the drug, in line with previous observations (Nagata et al. 2004). Fujita and colleagues also published similar findings where changes in sensitivity to trastuzumab in SKBR3 cells were examined with and without PTEN knockdown by siRNAs (Fujita et al. 2006).

Reduced or complete loss of PTEN expression has been documented in 30% of relapsed sporadic IDCs and primary ductal adenocarcinomas (Perren et al. 1999; Jones et al. 2013), in over 50% of patients treated with tamoxifen as single adjuvant therapy (Tanic et al. 2012), and as mentioned above, LOH of 10q23 has been repeatedly reported to be found in over 40% of invasive carcinomas. However somatic intragenic mutations in *PTEN* are only observed in a fraction of primary breast cancers (frequency <5%) (Saal et al. 2005), making it is unlikely that PTEN loss of function alone can serve to explain the frequent primary and acquired resistance to trastuzumab seen in patients (Nagata et al. 2004; Berns et al. 2007; Gallardo et al. 2012). However, loss of function mutations in *PTEN* or decreased *PTEN* expression lead to a hyperactivation of the PI3K pathway, and PI3K pathway activation can result from other, more frequent events found in breast cancer such as activating mutations in the p110a catalytic subunit of PI3K (*PIK3CA*) that occur in approximately 25% of primary breast cancers (Saal et al. 2005). Additionally PTEN loss and *PIK3CA* mutations are rarely present in the same tumors (Saal et al. 2005; Berns et al. 2007; Gallardo et al. 2012), and increased PI3K signaling is also capable of inducing strong trastuzumab resistance in cell culture (Berns et al. 2007).

Here, we have introduced an shRNA targeting *Pten* into our multi-allelic mouse model developed in Chapter 3 with the aim of generating an experimental system that may help further interrogate the role of the TSG *PTEN* in HER2 positive breast cancer disease progression. Mice harboring the lesions conferring PTEN knockdown and NeuNT overexpression show a dramatic acceleration to disease onset and progression, as well as shortened overall survival. There was also an increased incidence of metastatic disease in the lung. Lastly we show that PTEN loss is important for tumor maintenance in this model.

RESULTS

PTEN shRNA knockdown accelerates *NeuNT* driven disease onset and progression

Two shRNA strains targeting *Pten* were previously made and functionally tested in the context of the Eu-Myc lymphoma model (Miething, et al., In preparation). Efficient knockdown of the target and proper regulation of PTEN protein levels were shown in MEFs and in KH2 EHCs [Figure 4.1a,c]. Using the stronger shRNA strain TG-shPTEN.1522 [Figure 4.1b], we sought to test the cooperation between PTEN knockdown and oncogenic NeuNT in the multi-allelic model developed in Chapter 3. The experimental protocols previously outlined were followed as described earlier unless otherwise noted. Accordingly, control shRNA mice were produced as littermates in all cases. We are still working towards testing the second shRNA allele, TG-shPTEN.2049, to fully validate our results described in this chapter. However, in addition to *PTEN* being a well-characterized TSG, given the extensive use of the shPTEN.1522 shRNA in multiple breast cancer models as well as in many other *in vivo* cancer model systems in our research group, we are confident that the phenotypes we observe here are not due to off-target effects of this particular shRNA. Here after "TG-shPTEN" refers to the TG-shPTEN.1522 strain.

Due to consequences of the move from CSHL to Memorial Sloan-Kettering Cancer Center (MSKCC) in August 2011, the following *in vivo* experiments were performed twice, with as few changes introduced as possible in the replicate round [Table 4.1]. An acceleration of disease was seen in terms of tumor onset, with a shortened latency of tumor-free survival for mice carrying TG-shPTEN [Figure 4.2], and this was accompanied by a decreased overall survival [Figure 4.3]. The quadrant scoring system was used to define loss of tumor-free survival – a tumor in any area of the animal meant a classification as tumor bearing – and each quadrant was tracked separately. A faster progression from tumor-free

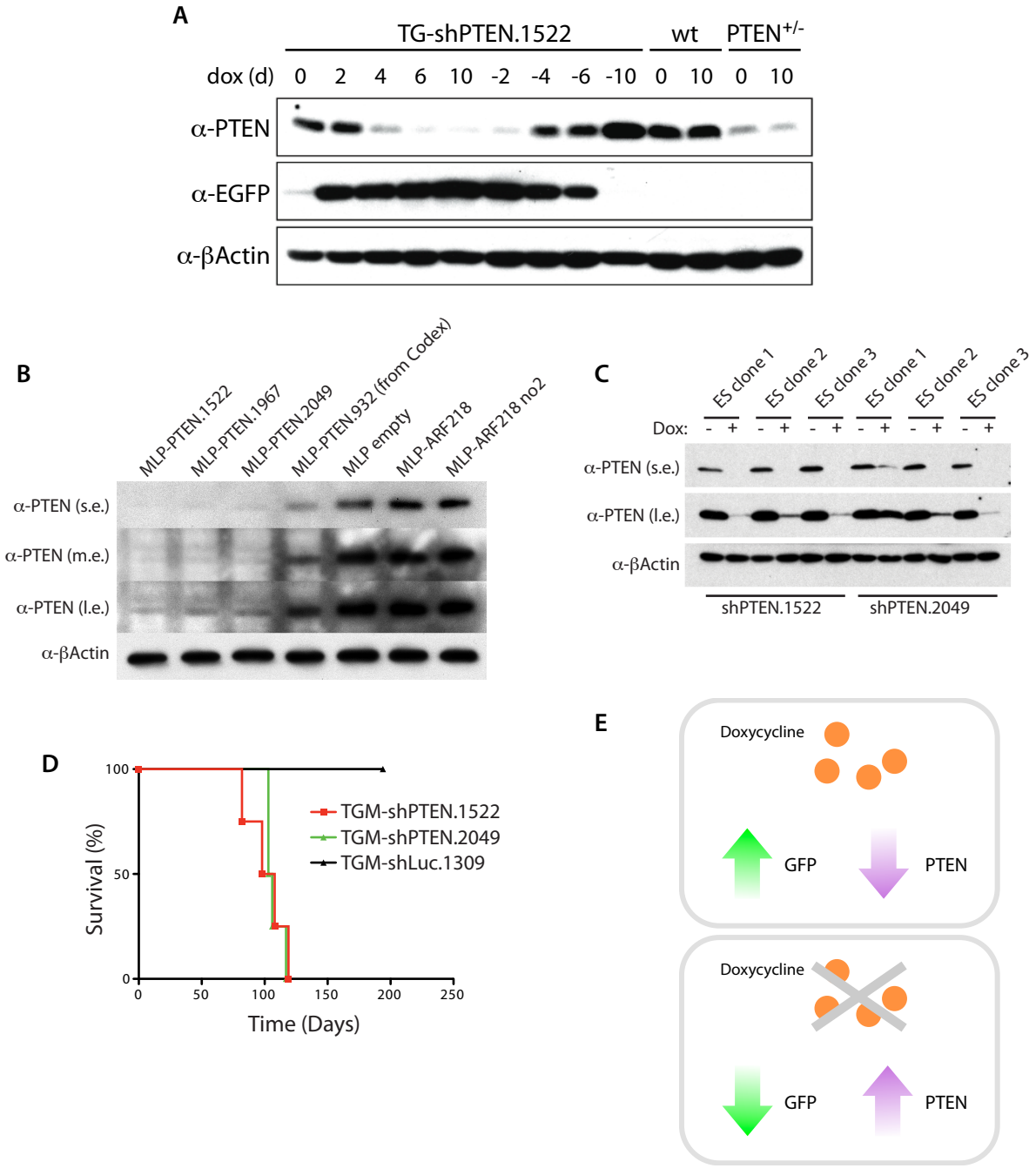

Figure 4.1 shRNA transgenic strains targeting PTEN. (A) Reverisble regulation of PTEN protein levels in dox treated MEFs derived from R26-rtTA2;TG-shPTEN.1522 embryos. (B) Western blot to assess protein knockdown efficiency of four shRNAs targeting PTEN in 3T3 cells. (C) GFP reporter protein levels correlate inversely with target protein levels in KH2 ESCs targed with shPTEN.1522 and shPTEN.2049. (D) Kaplan-Meier survival curve of TG-shRNA mice in a lymphoma mouse model. (E) Schematic of Tet-On system; GFP protein and target protein levels correlate inversely and depend on the presence/absence of dox.

Table 4.1 Experimental variables for shRLuc and shPTEN experimental cohorts

Variable		CSHL TG-shRLuc	CSHL TG-shPTEN	MSKCC TG-shRLuc	MSKCC TG-shPTEN
Age at litter birth (days)	average	76.2	77.3	74.4	75.9
	range	67~137	58~107	65~113	67~110
Litter size	average	7.8	8.2	7.0	7.5
	range	3~12	5~10	1~11	2~11
Experimental age(*) at start of dox treatment**	average	1.4	1.1	0	0
	range	-3 ~ 8	-6 ~ 7	0 ~ 1	0 ~ 2
Lactation duration	average	20.9	20.8	21.0	20-24
	range	19-22	18-22	20-22	21.1
Litter loss*** (% cohort)		0%	0%	4.4%	6.6%
Unrelated death**** (% cohort)		2.6%	0%	15.9%	3.3%

All animals listed here are parous MMTV-NeuNT ; RIK ; WAP-Cre ; TG-shRNA animals

**Experimental age defined as day of litter birth for parous animals*

***For mice under regular dox treatment protocol, where treatment begins simultaneously with nursing*

****Incidence of successful pregnancy and birth of litter followed by cannibalization or starvation of pups*

*****Deaths in young mice unrelated to breast tumorigenesis, usually during or soon after the period of lactation*

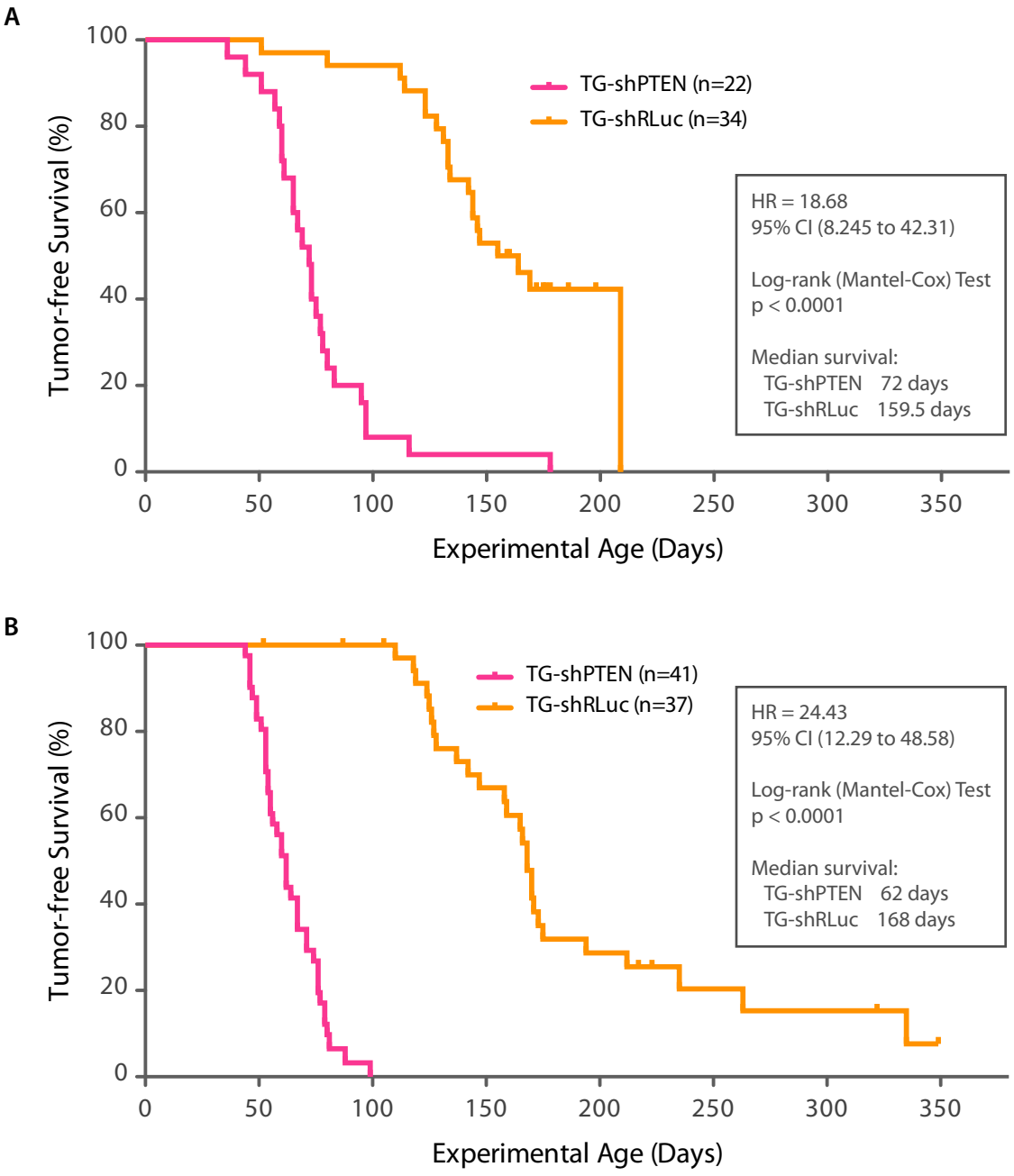

Figure 4.2 Tumor-free survival of TG-shPTEN vs TG-shRLuc mice. Kaplan-Meier survival curves for parous, dox treated MMTV-NeuNT;RIK;WAP-Cre;TG-shRNA mice monitored through weekly palpation for (A) CSHL cohort and (B) MSKCC cohort.

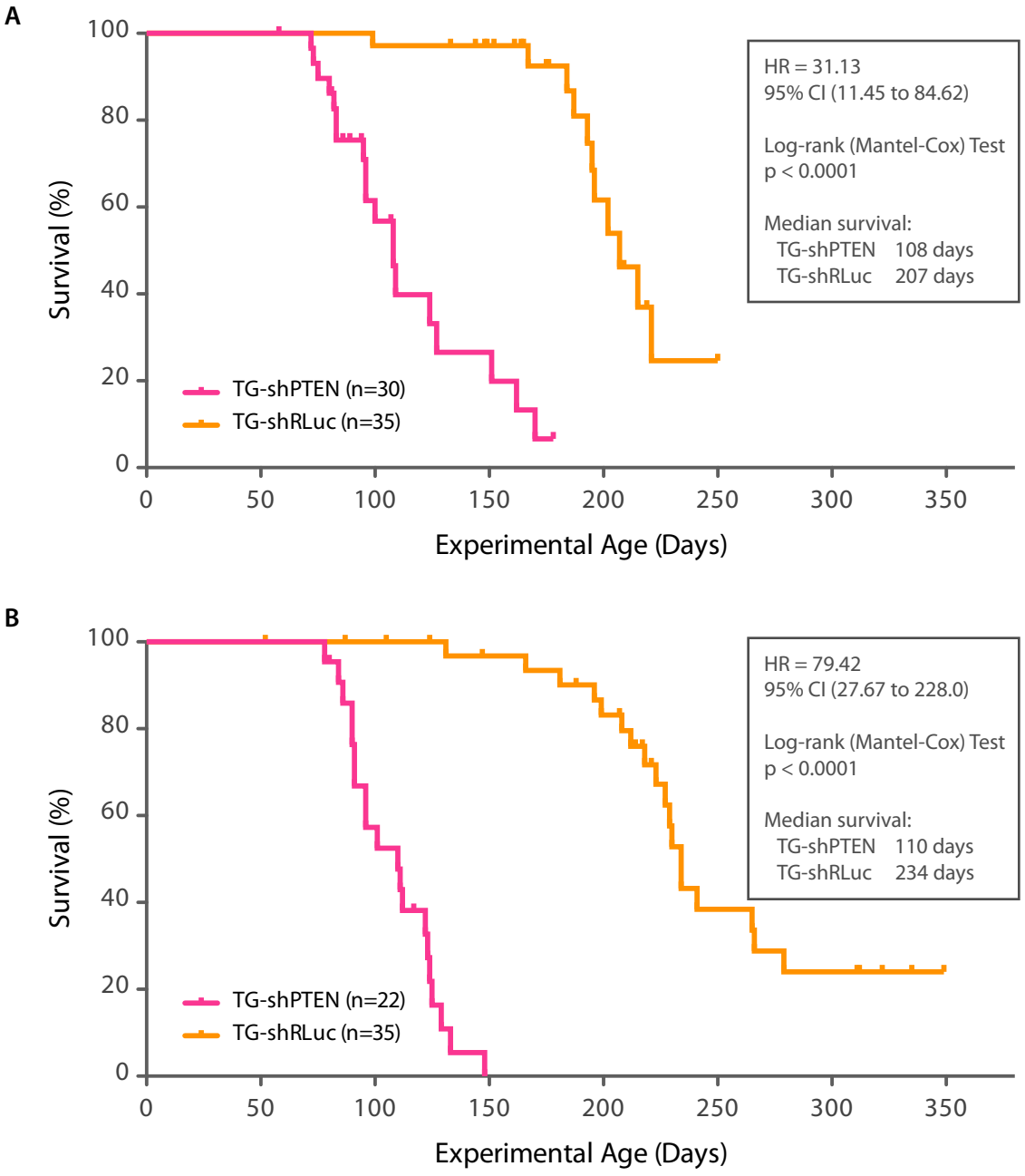

Figure 4.3 Overall survival of TG-shPTEN vs. TG-shRLuc mice. Kaplan-Meier survival curves for parous, dox treated MMTV-NeuNT;RIK;WAP-Cre;TG-shRNA mice for (A) CSHL cohort and (B) MSKCC cohort.

to a full four-quadrant penetrance of the disease was observed for TG-shPTEN mice [Figure 4.4a, 4.5]. This overall increase in tumor burden and penetrance was also quantified through the final quadrant penetrance at terminal disease endpoint and tumor burden in weight at harvest [Figure 4.4b,c].

As the data show, the combined effect of PTEN knockdown and NeuNT overexpression causes disease latency to be halved, all the while dramatically increasing the number of tumors found in each experimental animal. Additionally, while every tumor harvested from mice harboring the TG-shPTEN allele has been GFP positive, in TG-shRLuc mice only a small fraction of the tumors display fluorescence (less than 25%), indicating that PTEN knockdown is driving tumor growth in a WAP promoter expressing subpopulation of epithelial cells that are not *per se* the cell of origin for many of the MMTV-NeuNT allele driven tumors [Figure 4.6]. We concluded that the multifaceted aspect of the model's tumor growth patterns did not allow for precise quantification of tumor burden via *in vivo* fluorescence imaging, but it remains a powerful component of the system that can be used for longitudinal studies [Figure 4.7].

Although some preliminary controls had been tested in Chapter 3, there remained some uncertainty regarding which parts of the multi-allelic model would require extra controls. During the first round of experimentation at CSHL, we modulated the pregnancy status, the presence of WAP-Cre and the dox treatment in a number of small control cohorts to better pinpoint any weaknesses in the system [Table 4.2]. Through these controls we found that WAP-Cre expresses at basal levels in the absence of lactation in the mammary ductal epithelium, and that it also occasionally expresses ectopically in other tissue types such as the muscle tissue of the lung (data not shown). These control mice also served to test the efficiency of the pregnancy protocol and establish the latency of parous MMTV-NeuNT

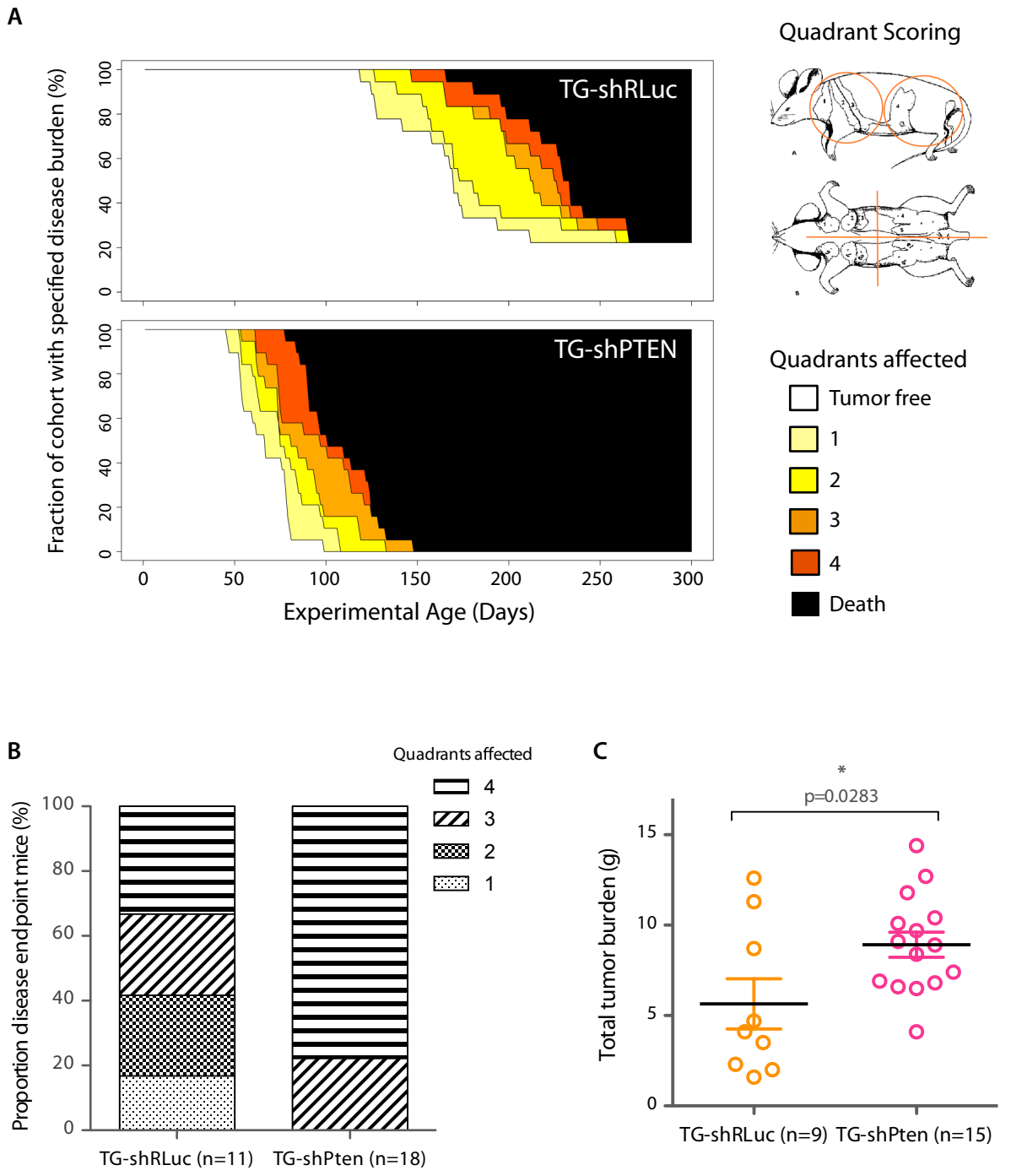

Figure 4.4 Disease progression and endpoint tumor burden in TG-shPTEN vs. TG-shRLuc mice. (A) MMTV-NeuNT;RIK;WAP-Cre;TG-shRNA parous dox treated mice from MKSCC cohort; TG-shRLuc n=21, TG-shPTEN n=19. (B) Quadrant penetrance in mice harvested at terminal tumor burden endpoint; from CSHL cohort. (C) Tumor burden in weight at terminal disease endpoint; from CSHL cohort.

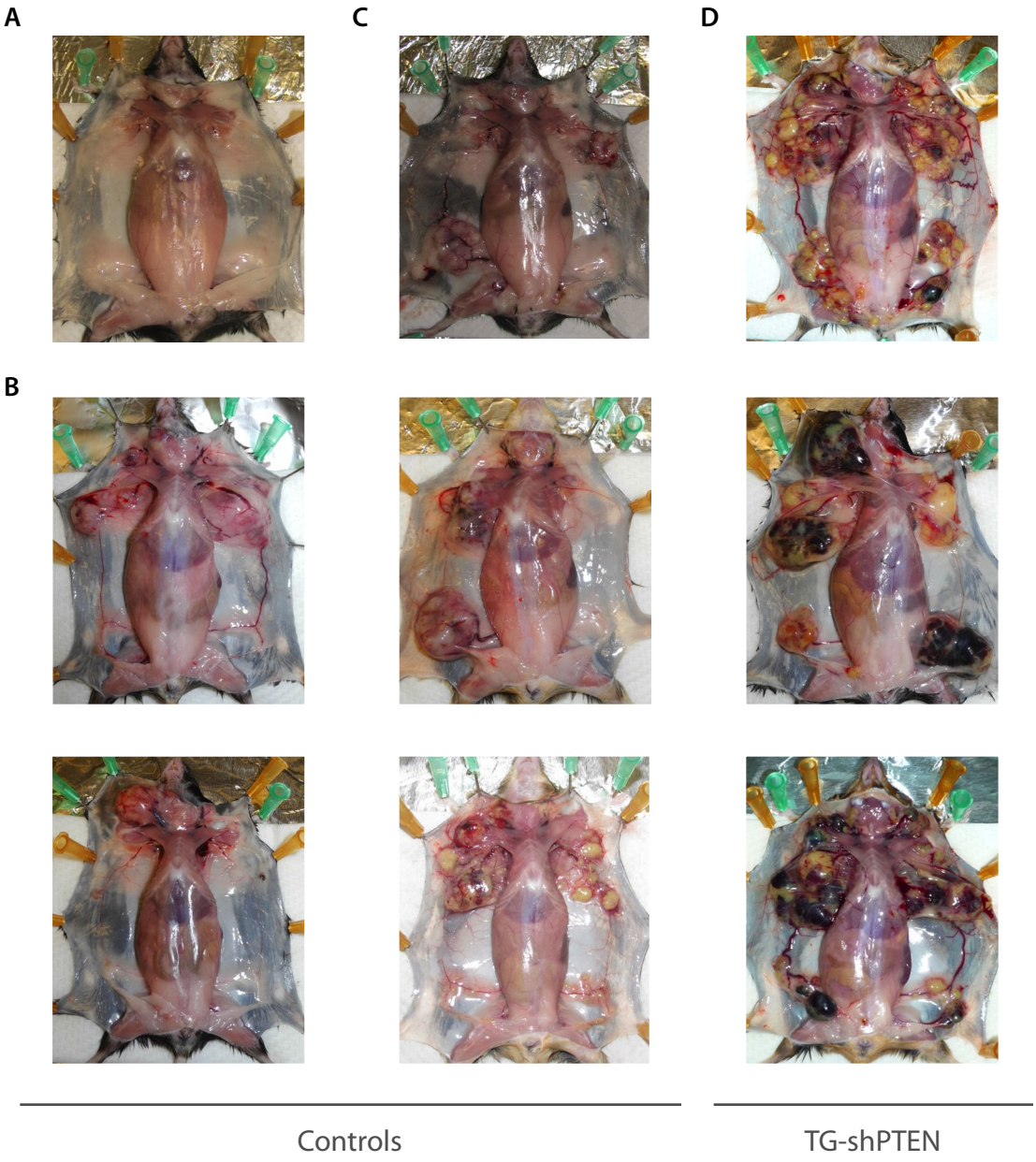

Figure 4.5 Representative images of mammary tumor burden at terminal disease endpoint. (A) c57BL/6 control mouse, no tumors at long latnecy. (B) MMTV-NeuNT, parous, no dox treatement control mice. (C) MMTV-Neu;RIK;WAP-Cre;TG-shRLuc.713, parous, dox treated control mice. (D) MMTV-Neu;RIK;WAP-Cre;TG-shPTEN.1522, parous, dox treated experimental mice. Yellow tinted color of tumors is due to high levels of GFP reporter. All animals from CSHL cohort.

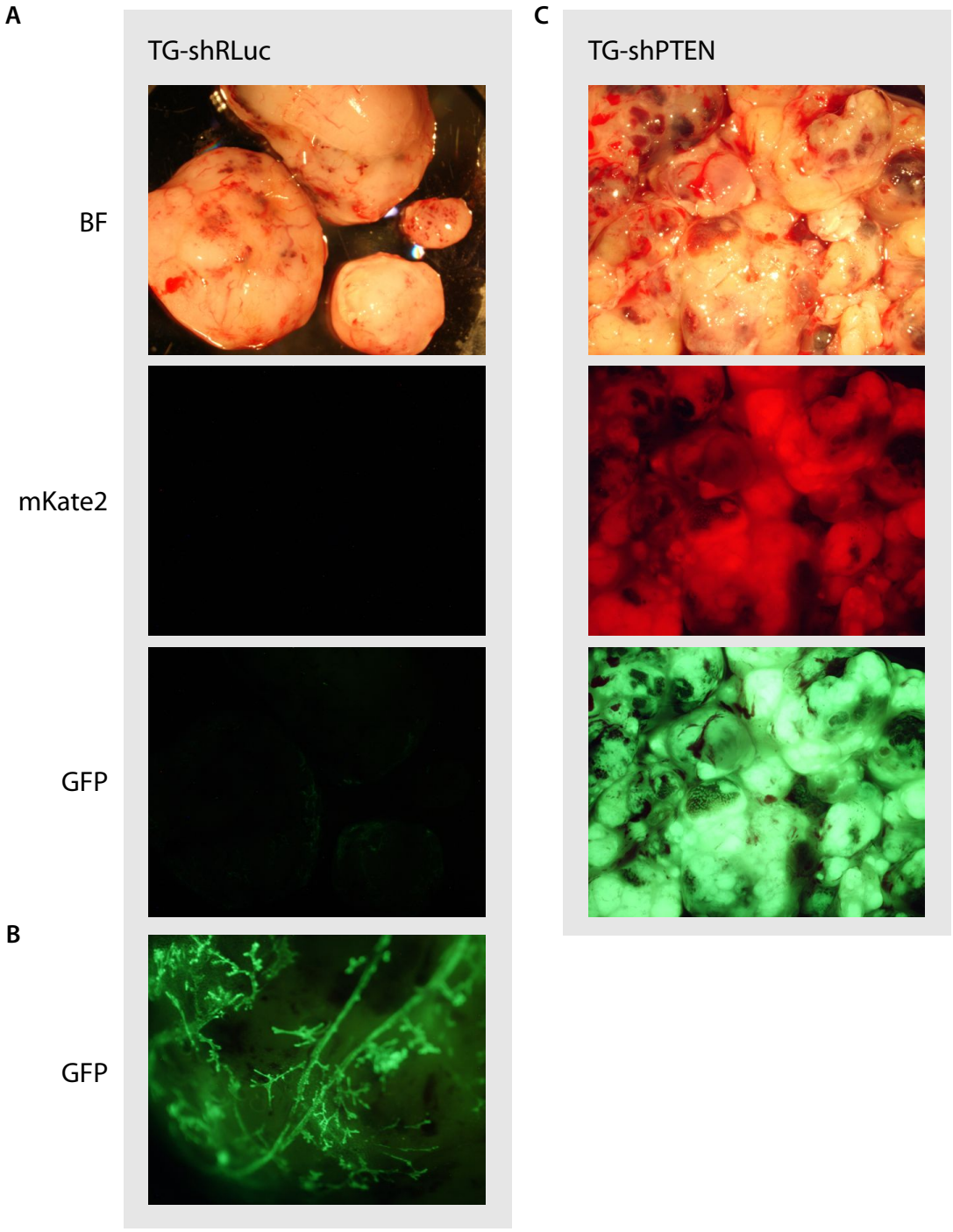

Figure 4.6 Representative images of tumors at terminal disease endpoint. Brightfield and fluoresence (GFP and RFP channels) images taken on dissecting microscope. (A) Tumors dissected from MMTV-Neu;RIK;WAP-Cre;TG-shRLuc.713, parous, dox treated control mice. Many tumors that develop in TG-shRLuc mice are negative for mKate2/GFP signal. (B) Detail of GFP reporter positive epithelial ductal structure in mammary gland fat pad tissue encasing GFP negative TG-shRLuc tumor depicted in (A). (C) Tumors dissected from MMTV-Neu;RIK;WAP-Cre;TG-shPTEN.1522, parous, dox treated experimental mice. All tumors from TG-shPTEN mice are positive for mKate2/GFP signal.

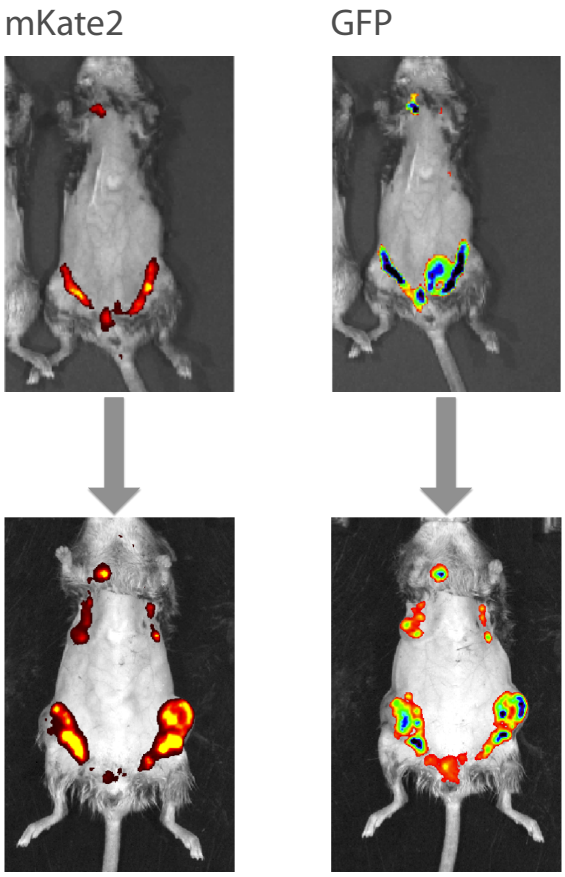

Figure 4.7 Longitudinal optical *in vivo* imaging of developing tumors using fluorescent reporters. MMTV-Neu;RIK;WAP-Cre;TG-shPTEN parous animal on dox. The bladder displays basal levels of autofluorescence in the GFP channel (visible in top right panel).

mice with a heavy contribution of C57BL/6 in their strain background. In our hands we find that the onset of NeuNT-driven disease is parity dependent [Figure 4.8].

Table 4.2 Control conditions: CSHL cohort

Condition	Control cohort for
Virgin, no WAP-Cre, no dox	NeuNT background in mixed strain setting
Virgin, on dox	WAP-Cre allele leakiness in absence of lactation
Parous, no WAP-Cre, on dox	Doxycycline treatment control
Parous, no dox	TRE leakiness in absence of dox treatment
Parous, on dox	Regular experimental condition

Four alleles unless otherwise noted

During the second round of experimentation at MSKCC, it became clear that there were additional variables to consider. We continued to monitor for the ectopic activation of WAP-Cre in the absence of pregnancy and lactation, but also modulated the timing of dox treatment vis-à-vis lactation [Table 4.3] [Figure 4.9, 4.10]. We found that delaying the induction of TG-shPTEN until after the end of lactation and involution, a period of 4 weeks, had an impact on the overall survival of mice, although the disease phenotype did not fundamentally change [Figure 4.10a]. We also included controls where MMTV-NeuNT was absent, to definitively distinguish a cooperative effect versus the impact of PTEN knockdown alone [Figure 4.9c, 4.10c]. A small cohort has only allowed for preliminary conclusions but thus far mice with TG-shPTEN in the absence of NeuNT (n=4) have not developed tumors at a latency of over 220 days in experimental age.

Table 4.3 Control conditions: MSKCC cohort

Condition	Control cohort for
Virgin, on Dox	WAP-Cre allele leakiness in absence of lactation
Parous, no MMTV-NeuNT, delayed dox	Effect of shRNA allele in absence of NeuNT
Parous, no MMTV-NeuNT, on dox	Effect of shRNA allele in absence of NeuNT
Parous, delayed dox	Effect of delayed shRNA induction
Parous, on dox	Regular experimental condition

Four alleles unless otherwise noted

Tumor pathology and primary disease phenotype

We analyzed the tumors through immunohistochemistry to gain some insight into the disease architecture at a cellular level. PTEN protein knockdown was consistently very robust in tumor tissue, which concurrently showed strong expression of GFP and mKate2. These areas also displayed strong staining for Neu/ErbB2 at the cell membrane and a high Ki-67 index, a marker for cellular proliferation [Figure 4.11]. In order to better characterize the molecular phenotype of the primary tumors, the expression pattern of luminal (CK8/CK19) and myoepithelial (CK5/CK14) markers, as well as epithelial-mesenchymal transition (EMT) markers vimentin and E-cadherin, is ongoing. Characterization of the hormone receptor status (ER/PR) of the tumors is also in progress.

We observed strong nuclear pleomorphism (3 points), a high mitotic count (3 points) and lack of tubule formation (3 points) by hematoxylin and eosin (H&E) staining of tumor sections. With a total sum of 9 points, the tumors were classified as resembling most closely a high grade, poorly differentiated tumor type with poor prognosis in humans [Figure 4.12]. With a histological likeness to patient biopsies diagnosed as "invasive ductal carcinoma, not otherwise specified (NOS)", these NeuNT-driven tumors correspond to the most common

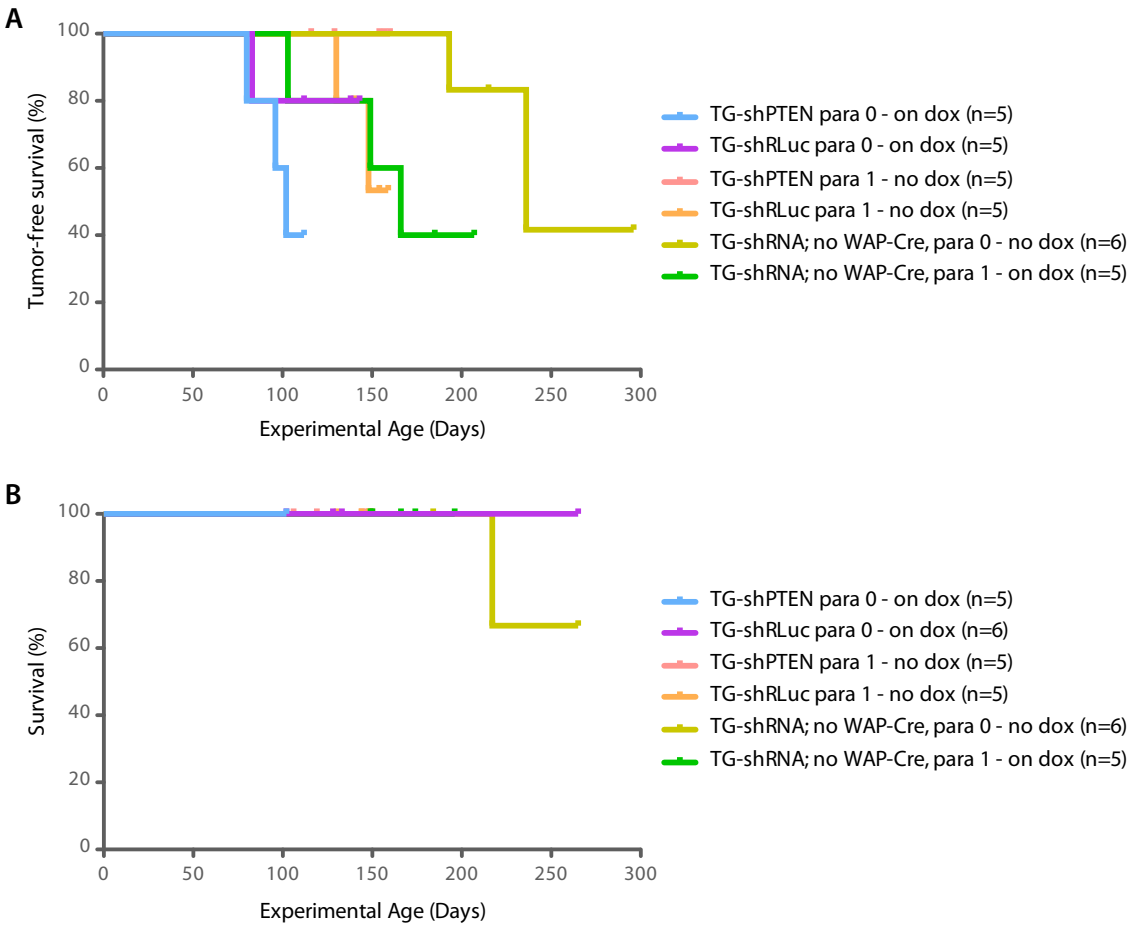

Figure 4.8 CSHL control cohorts with TG-shRNA alleles. Kaplan-Meier suvival curves for (A) tumor-free survival and (B) overall survival of control cohorts listed in Table 4.2. Mice are MMTV-NeuNT;RIK;WAP-Cre;TG-shRNA unless othewise noted.

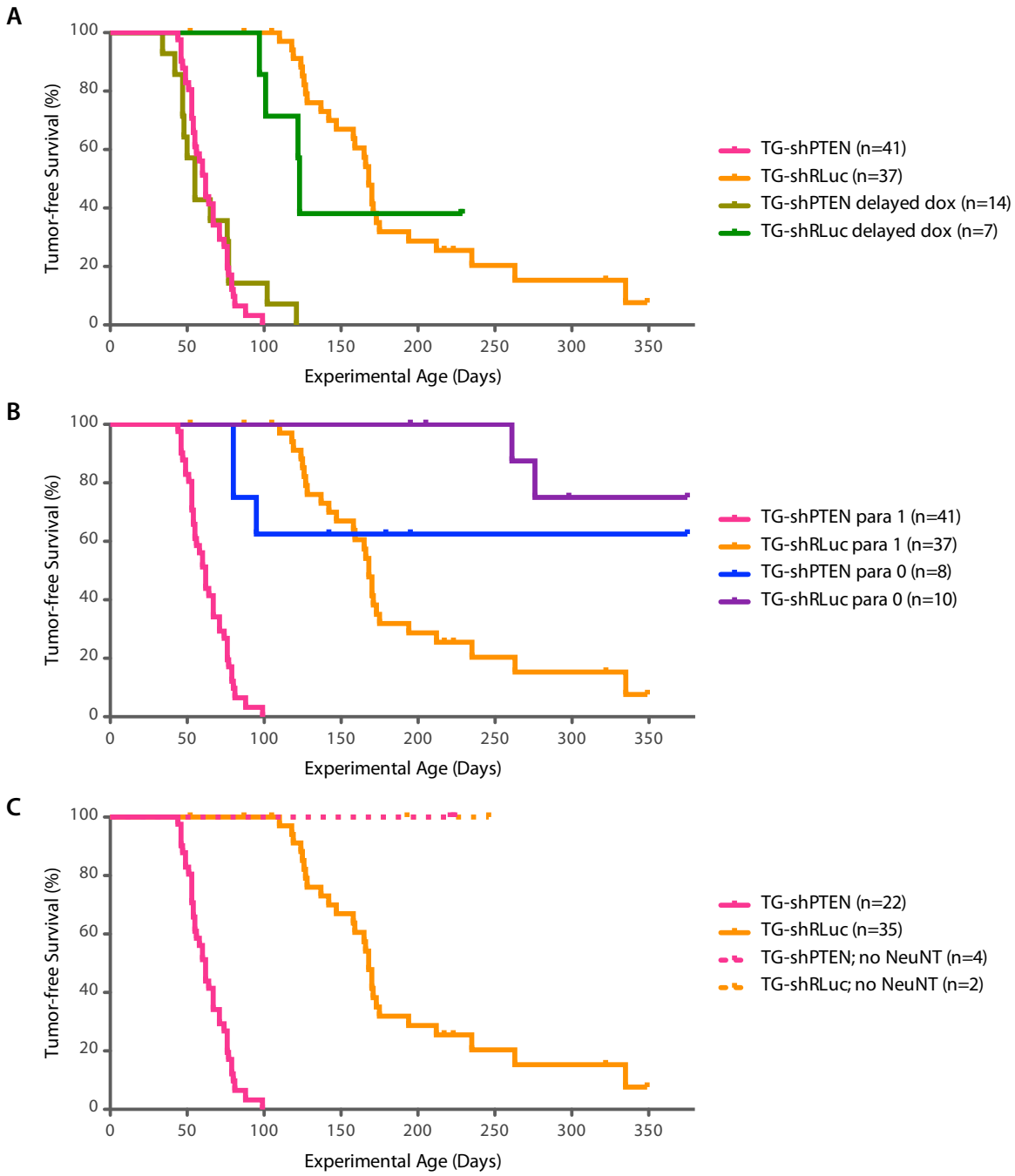

Figure 4.9 Tumor-free survival analysis of MSKCC control cohorts. Kaplan-Meier survival curves for (A) MMTV-NeuNT;RIK;WAP-Cre;TG-shRNA parous mice with delayed start of dox treatment by 3 weeks compared to main experimental cohorts, (B) MMTV-NeuNT;RIK;WAP-Cre;TG-shRNA virgin mice on regular dox treatment compared to main experimental cohorts, and (C) RIK;WAP-Cre;TG-shRNA parous mice on regular dox treatment compared to main experimental cohorts with MMTV-NeuNT allele.

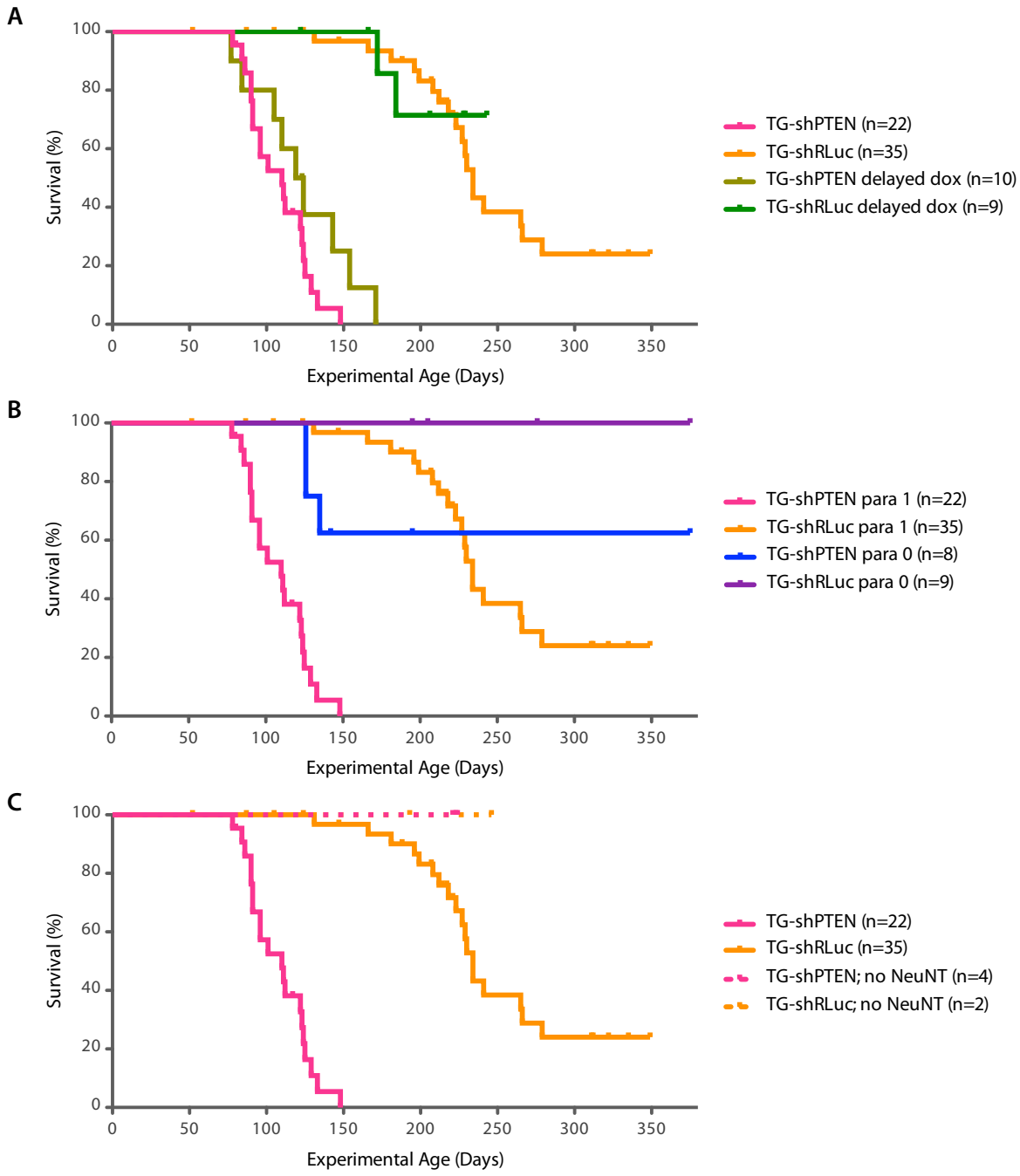

Figure 4.10 Overall survival analysis of MSKCC control cohorts. Kaplan-Meier survival curves for (A) MMTV-NeuNT;RIK;WAP-Cre;TG-shRNA parous mice with delayed start of dox treatment by 3 weeks compared to main experimental cohorts, (B) MMTV-NeuNT;RIK;WAP-Cre;TG-shRNA virgin mice on regular dox treatment compared to main experimental cohorts, and (C) RIK;WAP-Cre;TG-shRNA parous mice on regular dox treatment compared to main experimental cohorts with MMTV-NeuNT allele.

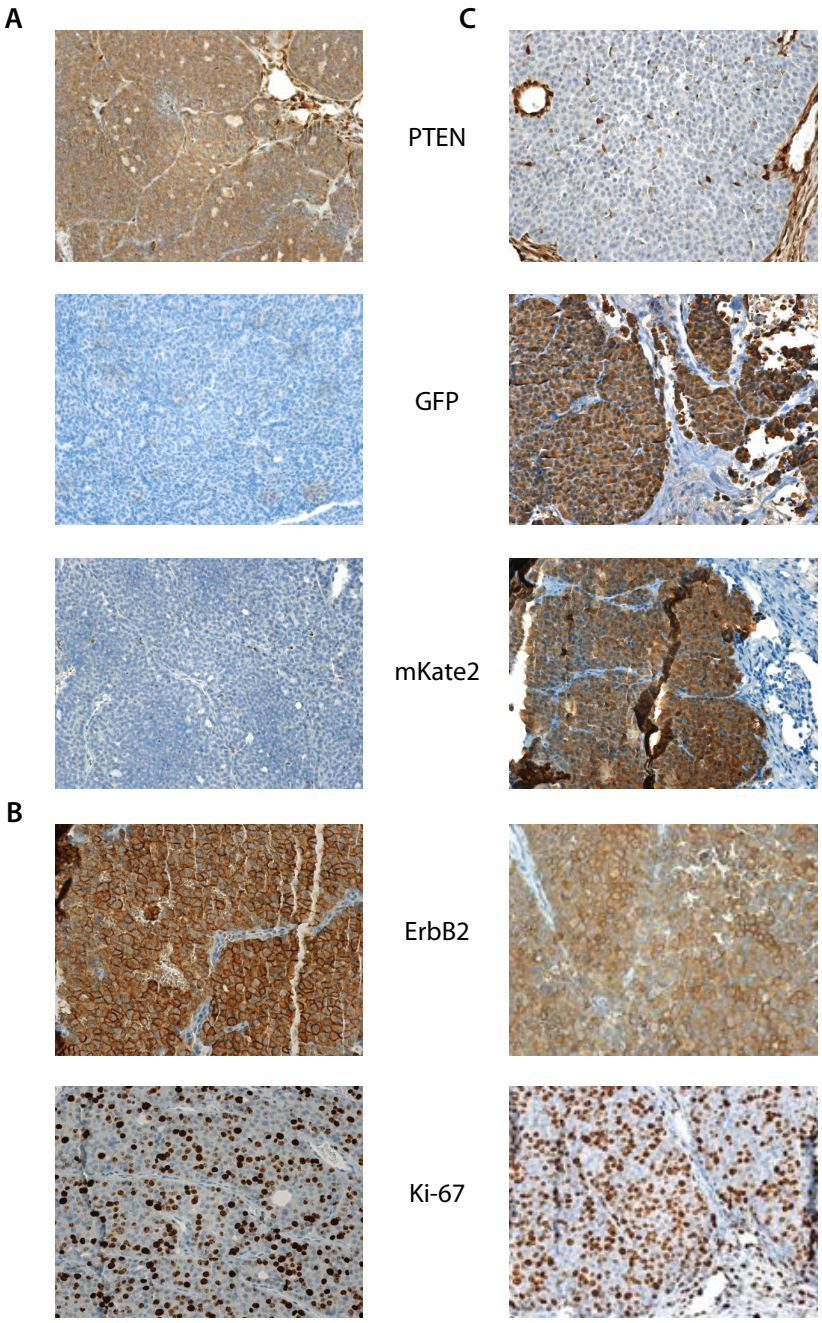

Figure 4.11 Robust PTEN knockdown observed in highly proliferative TG-shPTEN mammary tumors. Terminal disease analysis by immunohistochimistry. (A) Control tumor sample from MMTV-Neu mouse with no TG-shRNA or RIK alleles. (B) MMTV-NeuNT;RIK;WAP-Cre;TG-RLuc.713 tumor. (C) MMTV-NeuNT;RIK;WAP-Cre;TG-PTEN.1522 tumor. All images at 20x.

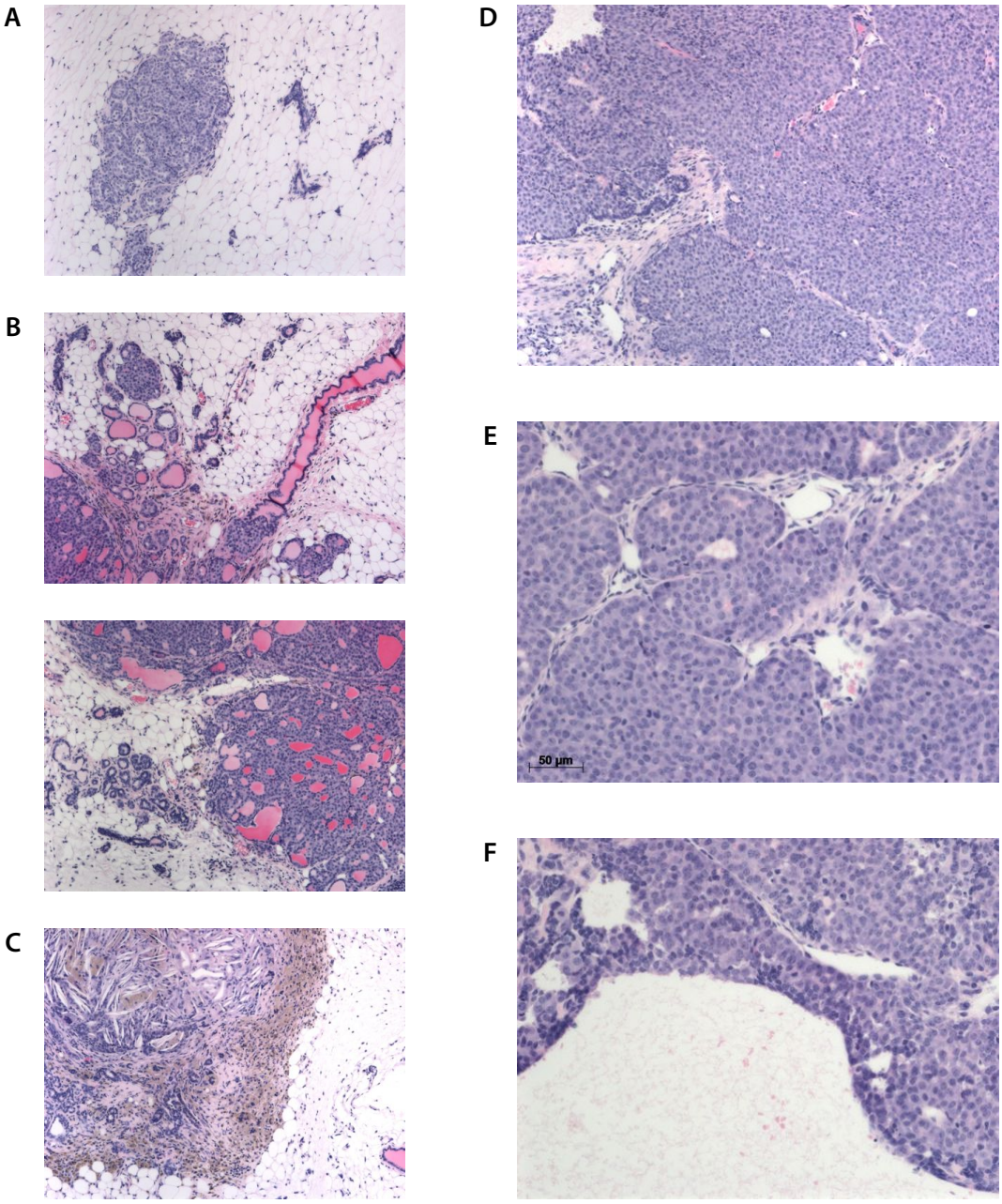

Figure 4.12 Histopathological analysis of tumors reveals highly proliferatie, undifferentiated morphology. MMTV-NeuNT;RIK;WAP-Cre;TG-shPTEN parous, on dox mouse. H&E stains of tumor sections and mammary fat pads harvested at terminal disease endpoint. (A) Example of early lesion embedded in mammary fat pad. (B) DCIS-like areas in mammary gland adjacent to advanced tumors. (C) Example of reactive stroma. (D) Dense, highly proliferative undifferentiated morphology. (E) Magnified view of highly mitotic histology. (F) Large regions of necrosis. All images at 20x, except 40x in (E,F).

type of malignant breast tumor seen in the clinic. There were no differences observed between shRLuc and shPTEN tumors harvested at terminal disease endpoint. Other features observed included large areas of necrosis, reactive stroma and evidence of ductal carcinoma in situ (DCIS) in intact mammary glands with early lesions. *ErbB2/neu* transgenics have been previously reported to frequently present microscopic fields that can be easily mistaken for human DCIS (Cardiff and Wellings 1999; Cardiff et al. 2000).

Characterization of disseminated disease

Using the fluorescent reporters we were able to track spontaneous disseminated disease to the lung, liver, bone, and spleen of TG-shPTEN animals [Figure 4.13]. Metastasis to the lung was most frequent, observed in 100% of TG-shPTEN mice, while lesions in the liver and bone were more rarely observed. If present, micromets observed in the liver were very small and would have not been detected if not for the fluorescent markers integrated into the model. Infiltration of GFP positive cells in the spleen was noted at a high frequency in mice with high tumor burden. We attributed this phenotype to a likely large quantity of circulating GFP positive tumor cells. Immunohistochemical analysis was performed on lung metastatic tumor sections to verify PTEN protein knockdown and expected expression of fluorescent markers [FIGURE 4.14]. Similar to the primary mammary tumors, there was also strong Neu/ErbB2 and Ki-67 staining. The frequency of metastasis were harder to quantify in control mice since GFP positive cells comprised only a fraction of the tumor burden, making the detection of small mets less accurate.

The highly epithelial and ductal morphological resemblances between primary lung tumors and lung metastasis of mammary origin is a confounding diagnostic problem in the clinic (Yang and Nonaka 2010). The immunohistochemical pattern of expression of thyroid

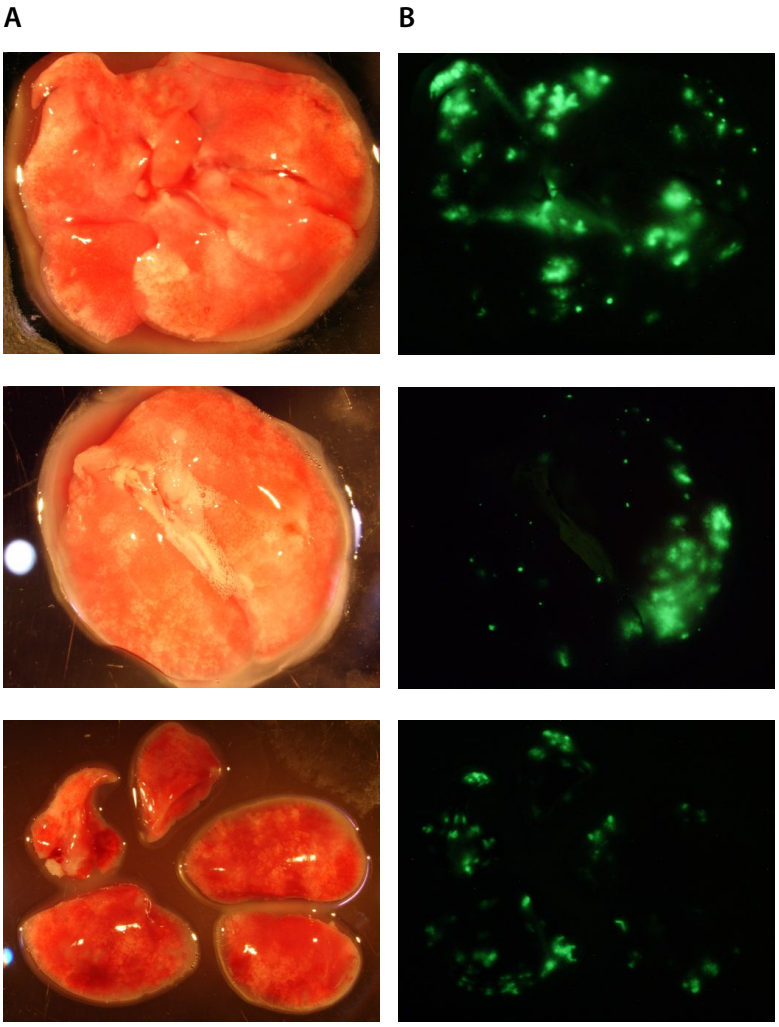

Figure 4.13 GFP/mKate2 positive lung metastasis consistently observed in TG-shPTEN mice. MMTV-Neu;RIK;WAP-Cre;TG-shPTEN parous, on dox mice at terminal disease endpoint. (A) Brightfield and (B) GFP images of lungs; mKate2 was always observed co-expressed (images not shown).

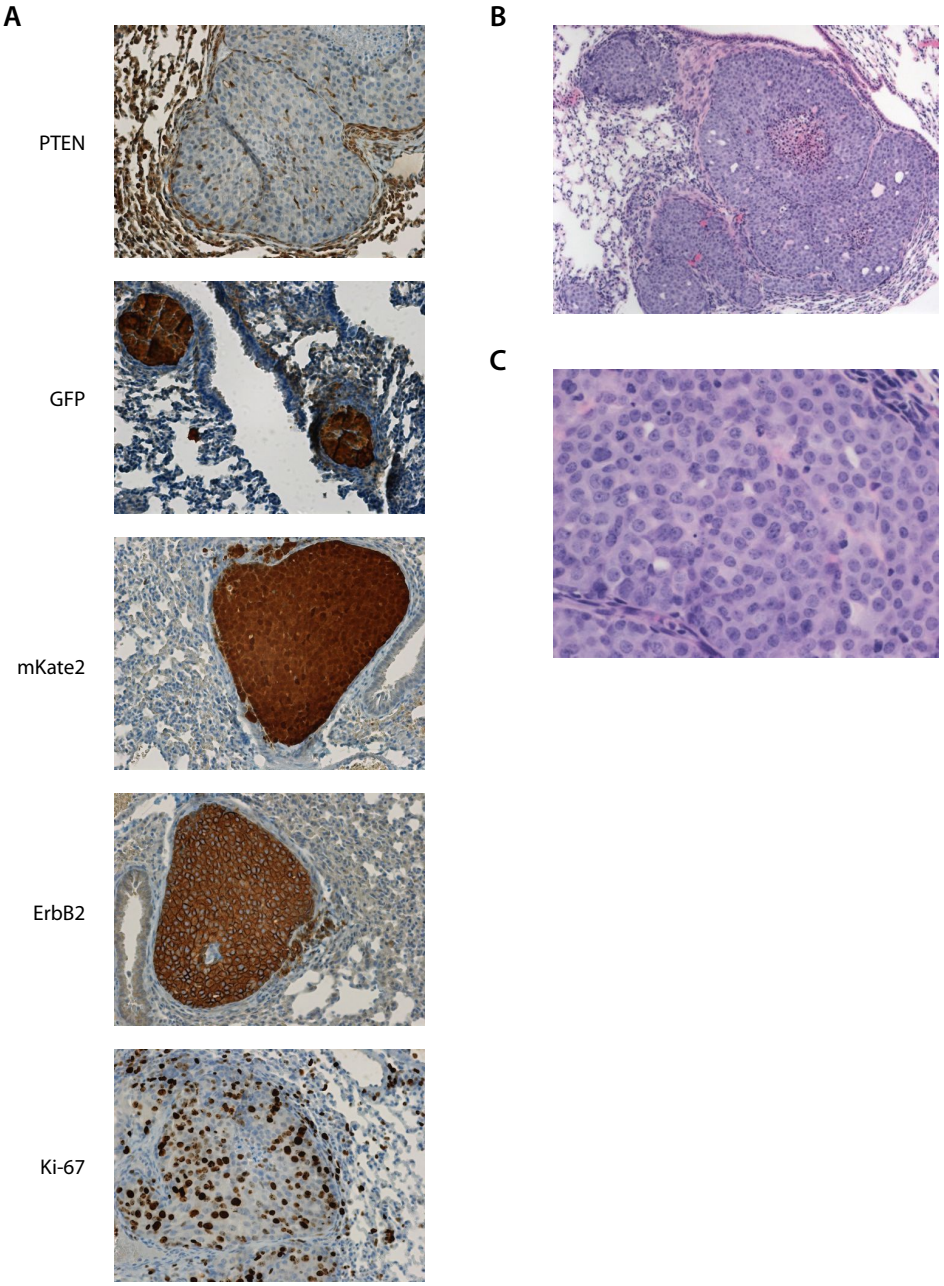

Figure 4.14 Evidence of spontaneous lung metastasis. Lungs of mice suffering from terminal disease burden at primary site. Representative images from an MMTV-NeuNT;RIK;WAP-Cre;TG-shPTEN parous, dox treated mouse. (A) Analysis by immunohistochimistry for key features of primary disease; all images at 20x. (B) H&E staining of lung tissue with metastatic lesions, 20x image; (C) 40x image.

transcription factor 1 (TTF1) is an established clinical marker used to aid in accurate diagnostic distinction between primary and metastatic pulmonary adenocarcinomas, although some controversy over specificity and clinical effectiveness still remains (Reis-Filho et al. 2000; Moldvay et al. 2004; Zhu and Michael 2007; Maeshima et al. 2008). Staining of lung lesions with TTF1 is ongoing. Additionally, we have begun probing the lung sections with luminal and myoepithelial markers for cross-comparison to their respective primary tumors, and we will also stain for hormone receptors, which are traditionally associated with mammary tumors (Tennis et al. 2010).

Histological assessment of lung mets based on H&E staining indicated cell morphology, high mitotic index and undifferentiated growth patterns that drew a very close resemblance to the primary mammary tumors, providing additional confirmation that the observed phenotype was in fact invasive, spontaneous metastasis originating in the mammary gland [Figure 4.14].

***In vitro* culture of tumor-derived cells and *in vivo* serial transplantation**

We were successful in culturing tumor-derived cells *in vitro* for multiple passages in low serum (1%) and low oxygen (5-7%) conditions on gelatin-coated plates in RPMI media supplemented with hydrocortisone, insulin and prolactin [Figure 4.15a]. The fluorescent markers were used in some cases to enrich for tumor cells by FACS sorting. Cells were maintained on dox *in vitro* at all times unless otherwise noted.

We tested the capacity for transplantation of the spontaneous mammary tumors from primary transgenic animals into secondary recipient mice as a potential platform for future experimentation (Varticovski et al. 2007). The mixed strain background prevents the use of syngeneic animals and consequently we opted for orthotopic transplantation into the

un-cleared mammary fat pads of athymic nude mice on a dox diet. Tumors were harvested from primary transgenics, mechanically and enzymatically dissociated to generate a single-cell digest, and then plated overnight on gelatin-coated plates before transplantation the following day. In preliminary experiments, the tumor-derived cells from two independent TG-shPTEN animals with advanced disease (TG-shPTEN line #9 and #10) were injected and these cells displayed similar latency and growth patterns [Figure 4.15b]. The histological assessment of tumor sections stained in H&E indicated a similarly high mitotic index and a cell morphology resembling the primary transgenic tumors. Additionally, formation of glandular structures at the periphery was noted (data not shown).

Subsequently, serial transplantation was tested. Tumors isolated from nude recipients were dissociated under the same conditions as before and transplanted into secondary recipients on a dox diet. The tumors arising from these injections showed a slight acceleration in growth in the secondary transplant setting compared to their first transplant (TG-shPTEN line #9 and #10) [FIGURE 4.15c]. Additionally, we explored the option of transplanting small $1mm^3$ tumor fragments that were frozen after tumor harvest. This method has the advantage of preserving the stromal architecture of the original primary transgenic tumor, reminiscent of the practice of xenografting patient tumor isolates from the clinic directly into mice (Vargo-Gogola and Rosen 2007). GFP positive tumor fragments from one TG-shRLuc and one TG-shPTEN mouse with advanced disease were thawed and inserted into the fat pads of recipient mice. Although tumors developed from fragments in both cases, a discrepancy was observed in the latency to tumor onset, penetrance, survival of transplanted animals and incidence of lung metastasis between TG-shRLuc and TG-shPTEN [Figure 4.15d-f].

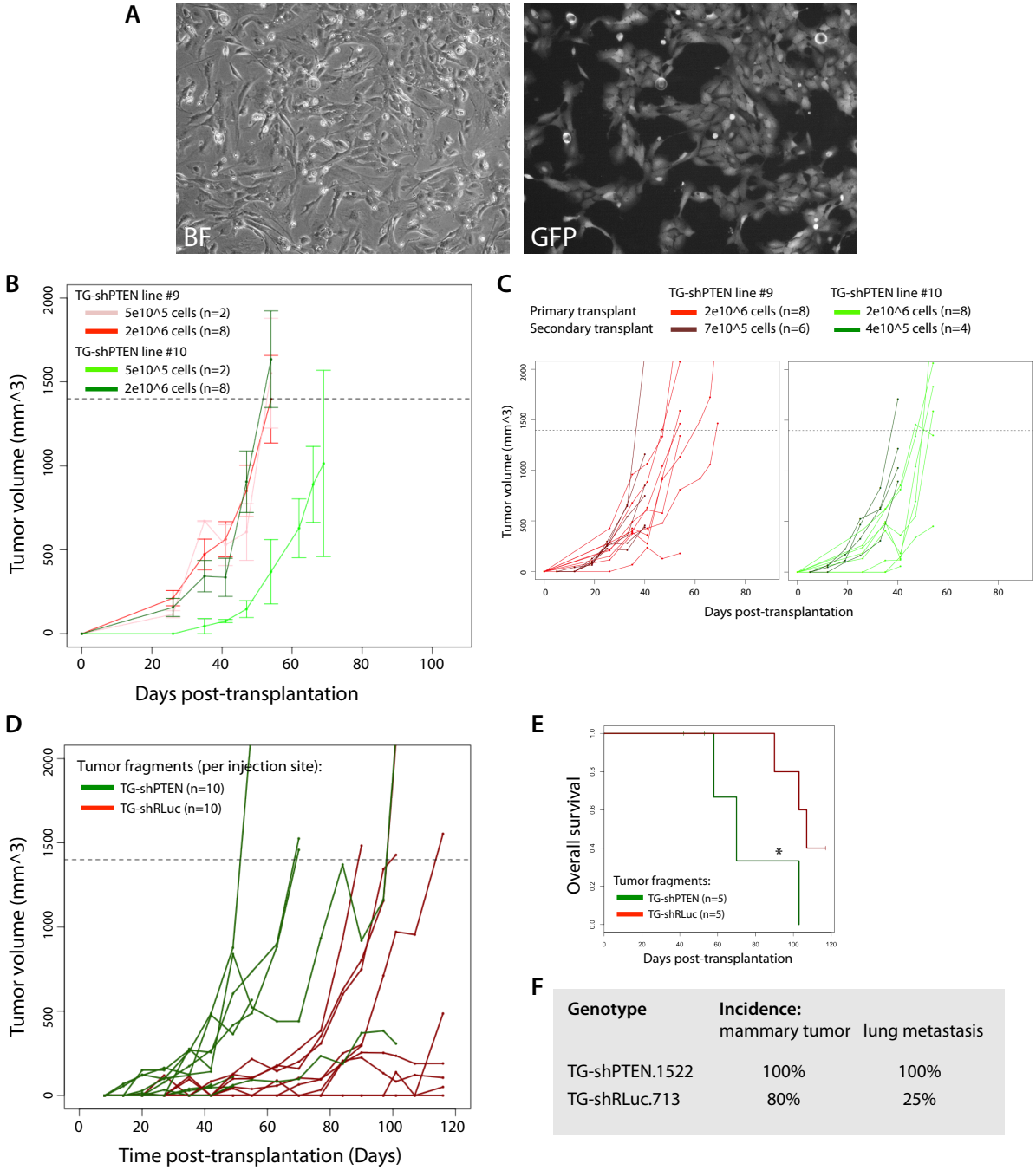

Genotype	Incidence: mammary tumor	lung metastasis
TG-shPTEN.1522	100%	100%
TG-shRLuc.713	80%	25%

Figure 4.15 Primary transgenic tumor-derived cell lines and serial *in vivo* transplantation model. (A) Representative images of MMTV-NeuNT;RIK;WAP-Cre;TG-PTEN.1522 tumor-derived cells in 2D culture during first passage; high yield of GFP positive cells and epithelial morphology. (B) Orthotopic transplantation of dissociated primary tumors after overnight culture into nude mice; average tumor volume per condition; error bars SEM. (C) Orthotopic transplantation into secondary recipient nude mice graphed as compared to tumor volumes in secondary recipients; tumor volume per fat pad injection. (D) Orthotopic transplantation of defrosted tumor fragments cut and frozen immediately after harvest from MMTV-NeuNT;RIK;WAP-Cre;TG-shRNA mice. (E) KM overall survival; p value < 0.05. (F) Pevelance of metastatsis in secondary recients transplanted with tumor fragments.

PTEN knockdown is required for tumor maintenance

The cooperation between PTEN knockdown and NeuNT overexpression was very robust, demonstrating an undeniable advantage in tumor initiation, progression, and metastasis. We next took advantage of the reversible nature of the RNAi technology to examine the effects of restoring PTEN protein levels in the growing tumors to ask the question if PTEN loss is required for tumor maintenance.

In a pilot experiment, we monitored a parous MMTV-NeuNT ; RIK ; WAP-Cre ; TG-shPTEN.1522 mouse that began dox treatment 21 days after giving birth to her litter, simultaneous with weaning of her pups. After approximately two and a half months, the animal presented tumors in all four quadrants. The largest tumor was surgically removed from the left abdominal fat pad region and dox was removed from the diet. Over the course of a month, the GFP signal disappeared and tumor regression was observed [Figure 4.16]. The *in vivo* fluorescence imaging showed that the abdominal right region had a tumor that was largely negative in reporter signal when imaged sagittally. The large quantity of bloody fluid in this cyst is the likely explanation for why the tumor did not show any sign of shrinkage.

We subsequently conducted a small study involving five parous MMTV-NeuNT ; RIK ; WAP-Cre ; TG-shPTEN.1522 mice. Dox treatment was administered 4 weeks after litter birth (i.e. one week after the weaning of her pups). After thirteen weeks on dox treatment, three of the five mice were placed on regular chow and all five were monitored through small animal magnetic resonance imaging (MRI) [Figure 4.17]. We complemented this approach with caliper measurements for rapid assessment of changes in tumor burden. While the sum total tumor burden in the mice with PTEN knockdown continued to increase exponentially, with a rapid need for euthanasia, those mice with restored PTEN levels

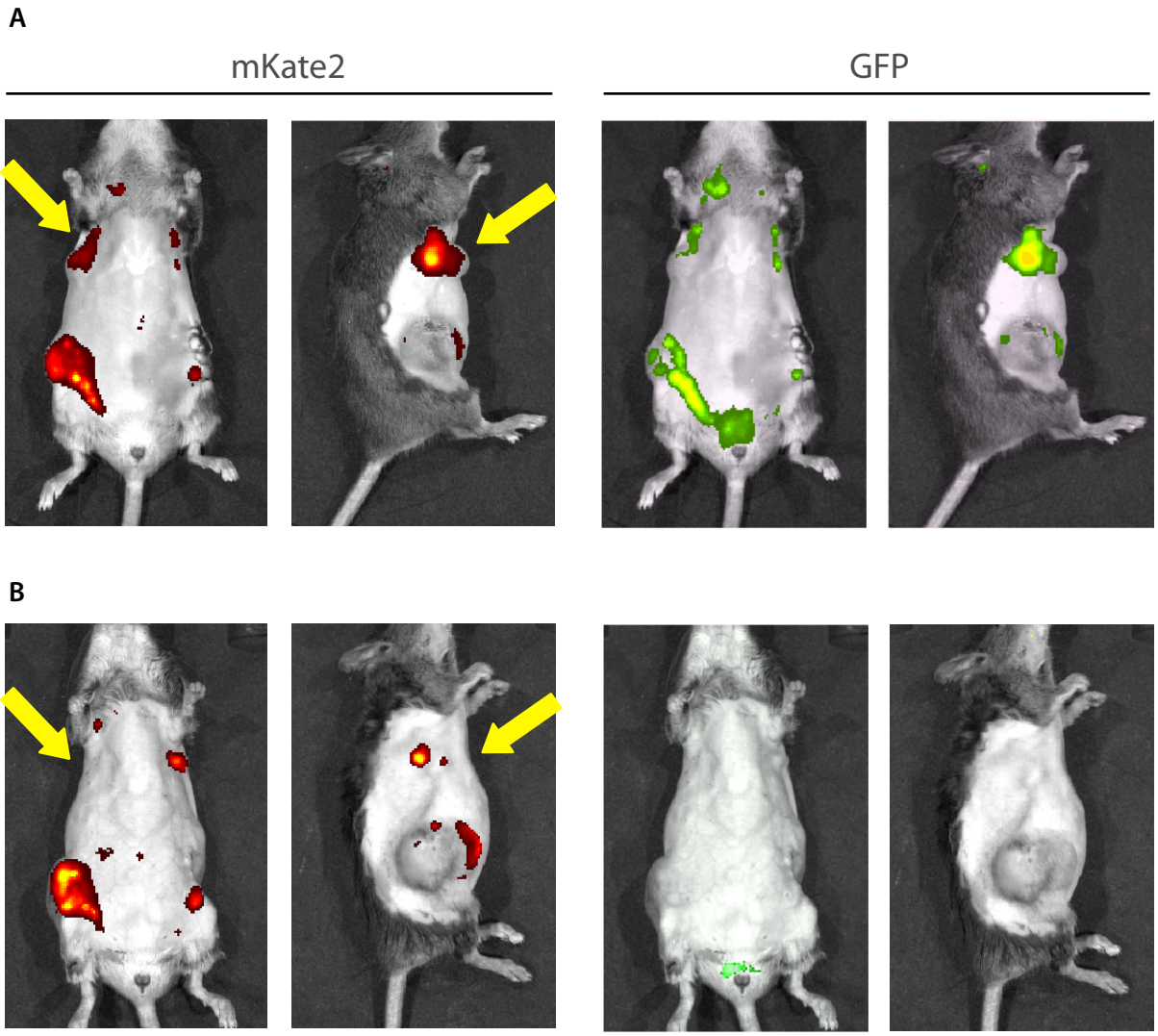

Figure 4.16 Pilot study: TG-shPTEN mouse shows evidence of tumor regression. MMTV-NeuNT;RIK;WAP-Cre;TG-shPTEN parous mouse at (A) dox treated time point immediately prior to dox removal and (B) 30 days after dox removal. Loss of GFP reporter expression and tumor shrinkage (yellow arrows) was observed.

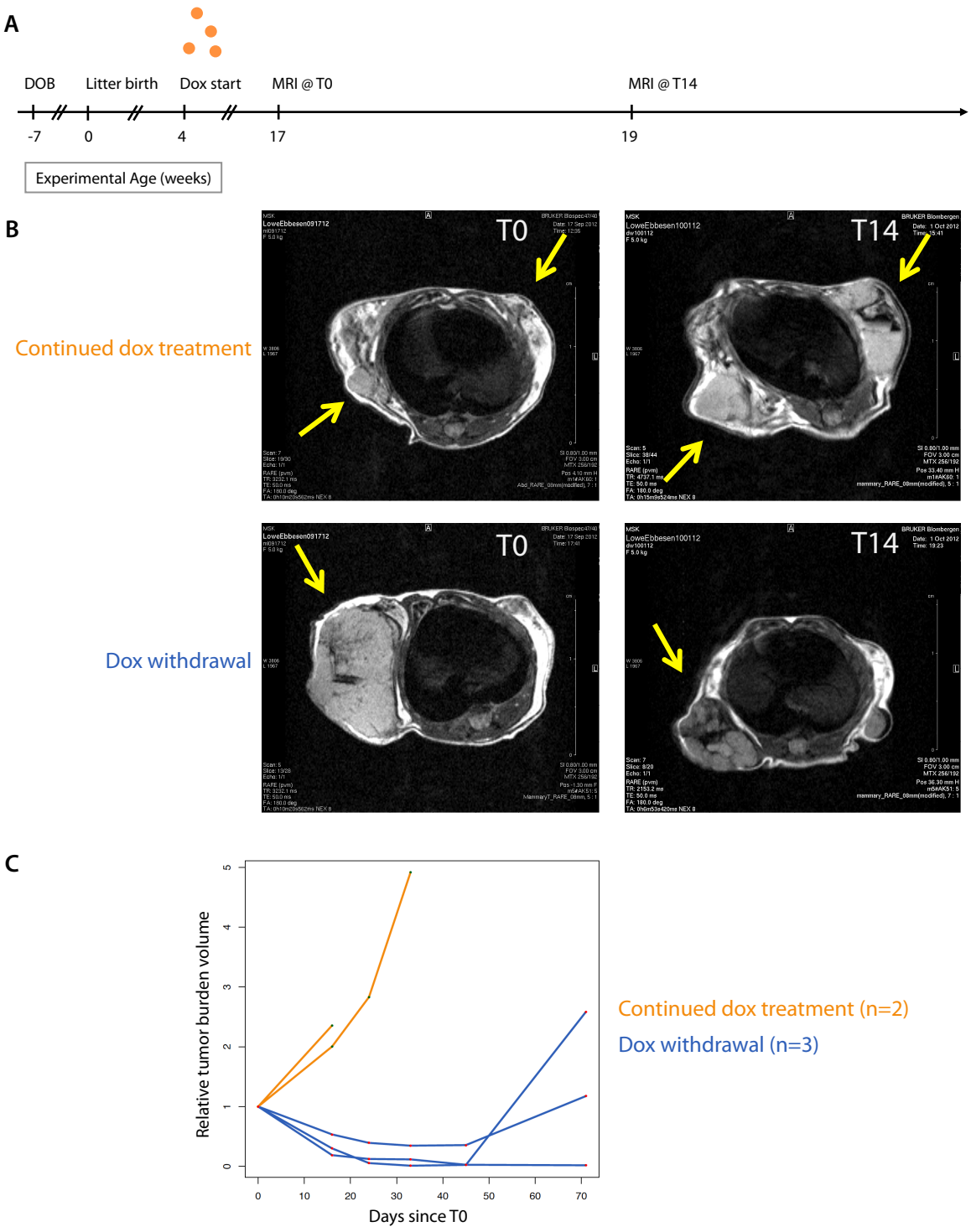

Figure 4.17 MRI imaging documents tumor regression upon dox withrawal in TG-shPTEN mice. MMTV-NeuNT;RIK;WAP-Cre;TG-shPTEN parous, dox treated since 4 weeks after litter birth. (A) Experimental schematic. (B) Representative images of MRI small animal imaging at T=0 days and T=14 days. (C) Relative tumor burden volume per mouse assessed through caliper measurement, normalized to T0.

showed a dramatic reduction in tumor burden during the first three weeks and a greatly increased overall survival. While two of the three off dox animals began to show increases in tumor burden after a month and a half, one mouse failed to develop any substantial tumor burden for over 90 days after removal of dox from the diet.

To test whether our results would be reproducible over a larger cohort of animals, we followed-up with a study involving twelve parous MMTV-NeuNT ; RIK ; WAP-Cre ; TG-shPTEN.1522 mice that began dox treatment the day of litter birth, as described in the standard experimental procedure in Chapter 3. In this iteration, shPTEN.1522 mice were monitored through weekly palpation until the first tumor was observed. Dox treatment was halted two weeks after tumor onset and weekly caliper measurements were used to assess tumor burden. All twelve mice showed some degree of reduction in tumor burden but the intensity of the effect varied [Figure 4.18a]. Despite the wide range of responses, a statistically significant increase in survival benefit was observed, as well as a slowed progression in quadrant progression and penetrance [Figure 4.18b]. Control TG-shRLuc mice were also taken off dox to verify that the change in diet does not contribute to altered patterns of tumor growth [Figure 4.19a]. During these tumor regression studies fur removal was avoided to prevent increased stress and adverse inflammatory responses that could affect experimental outcomes.

Some degree of tumor regression was also observed in transplanted recipients with TG-shPTEN primary tumor-derived cell lines (#9 and #10) after removal of dox [Figure 4.19b]. In this context, the short-lived and moderate response was attributed to the large size of the transplanted tumors as well as their origin in primary mice with aggressive, advanced mammary tumors. In culture, tumor-derived cell lines did not display any significant changes in proliferation upon dox removal, although GFP signal steadily decreased as

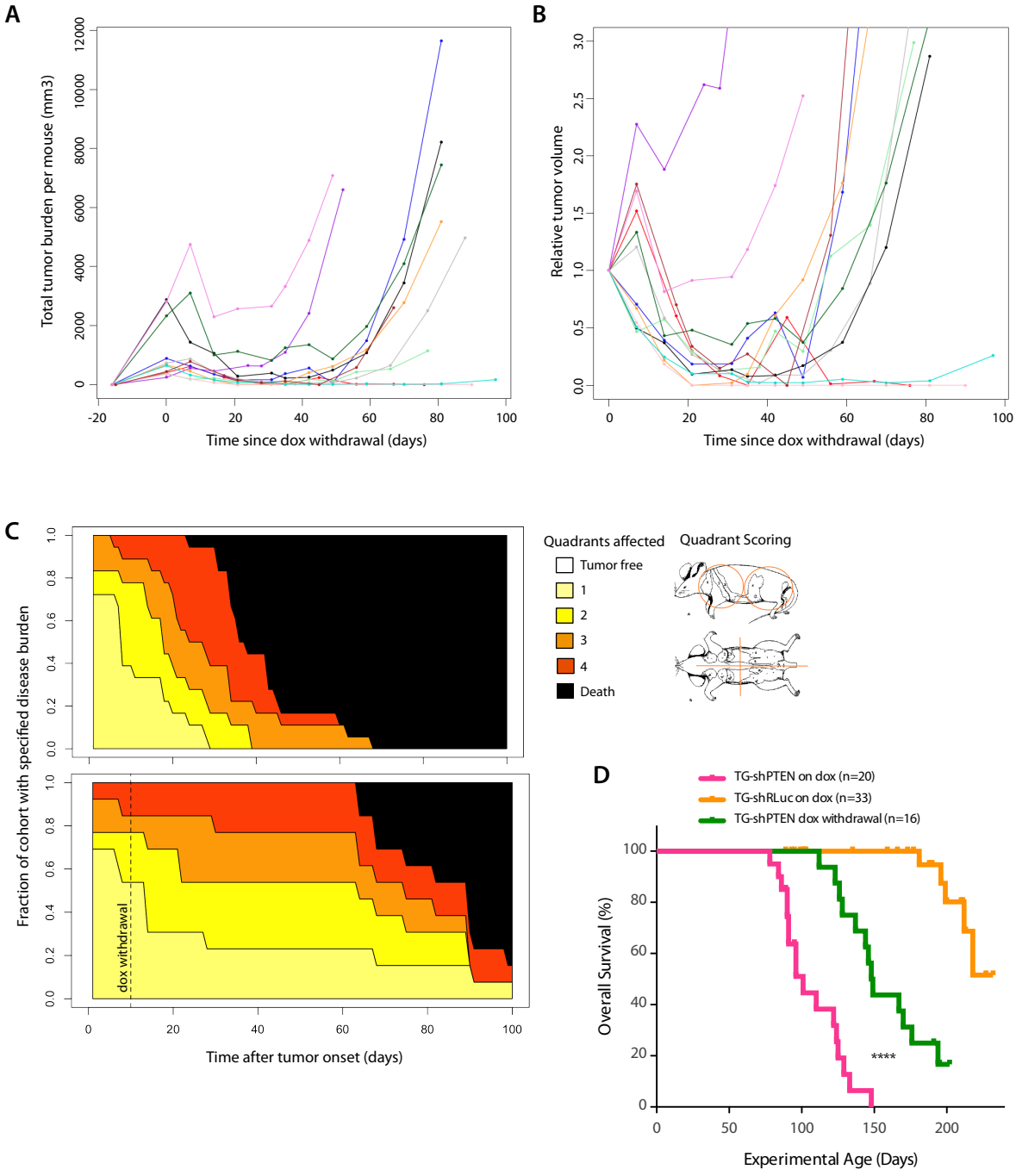

Figure 4.18 PTEN restoration causes tumor regression, incease in overall survival and slowed disease progression. Twelve parous, on dox MMTV-NeuNT;RIK;WAP-Cre;TG-shPTEN animals were taken off dox treatment two weeks after tumor onset was detected during weekly palpations. (A) Total burden per mouse per time point, as quantified by caliper measurements. (B) Data graphed as relative tumor burden normalized to tumor burden on day of dox withdrawal. (C) Disease progression depicted through quadrant penetrance over time. (D) KM survival curve; dox withdrawal causes statistically significant survival benefit; Log-rank (Mantel-Cox) Test $p<0.0001$, HR=0.1203.

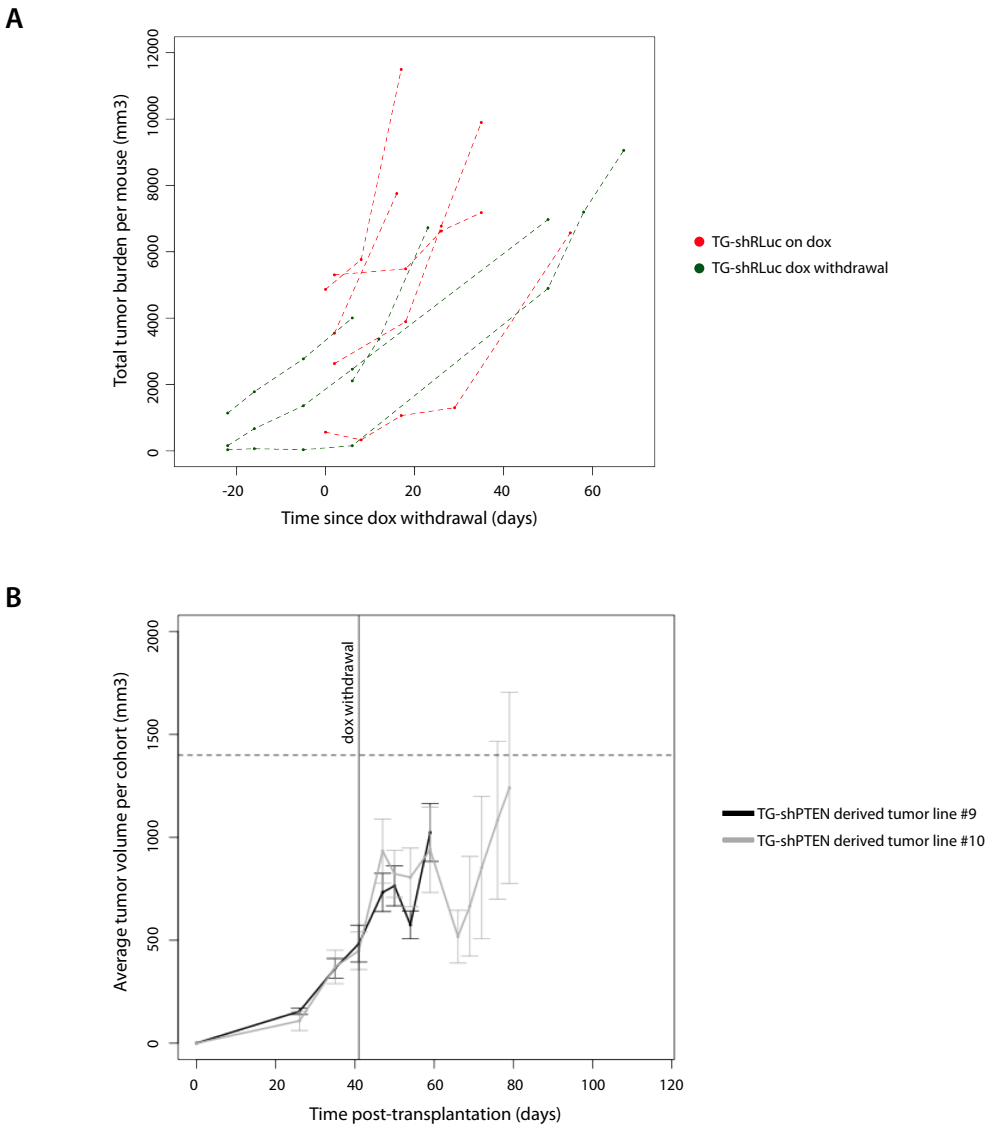

Figure 4.19 Dox withdrawal in TG-shRLuc controls and in transplantation assay. (A) MMTV-NeuNT;RIK;WAP-Cre;TG-shRLuc parous mice; tumor growth was measured by caliper measurements. (B) *in vivo* transplantation assay using TG-shPTEN primary tumor derived cell lines (#9 and #10). Three mice per cohort (n=6 tumors). Dox withdrawal 41 days after transplantation. Mean +/- SEM .

expected over the first 7 days, indicating that the Tet-On system was still intact (data not shown).

Exploring the mechanism of tumor regression and long term resistance upon restoration of PTEN protein

As demonstrated in the experiments described above [Figure 4.17, 4.19], quantifiable and consistent reduction in tumor burden was observed after the withdrawal of dox from the diets of MMTV-NeuNT ; RIK ; WAP-Cre ; TG-shPTEN.1522 mice at early stages of tumorigenesis. This effect appears to diminish in mice bearing a larger tumor burden at the start of the experiment, and this trend persisted in the transplant setting. In early trials involving mice with tumor burdens nearing experimental disease endpoint, the documented effect was at best cytostatic, as no regression could be measured although tumor growth was diminished and overall survival could also be extended in these mice (data not shown).

Elevated levels of necrosis is a common feature in the fast growing transgenic TG-shPTEN tumors under dox treatment, confounding the use of necrotic features in dox withdrawn tumors as an index of heighted cell death. However, transplanted tumors display lowered rates of proliferation in the first two weeks following the removal of dox diet, as evidenced both in reduced staining of the proliferation index Ki-67 and a decreased mitotic index by histological assessment (data not shown).

Complementing the observed slowed rate of tumor cell proliferation, we expect to find evidence of increased cell death in these tumors. Hyperactivation of the AKT pathway is expected to decline upon restored of PTEN phosphatase activity, thus leading to an increase in apoptotic signal. To gain a better understanding of the mechanism underlying

the tumor shrinkage phenotype, efforts to quantify changes in signaling, cell proliferation, and rates of apoptosis (cleaved caspase-3) are currently ongoing.

In this model, MMTV-NeuNT can drive tumorigenesis in cells that do not express the WAP-Cre transgene, a feature that has been confirmed from the high rate of tumors arising in TG-RLuc mice that are negative for GFP/mKate2 fluorescence signal. Consequently, we expect to see the eventual appearance of NeuNT-driven tumor growth in TG-shPTEN animals where substantial tumor regression was initially observed upon dox withdrawal. Interestingly, tumors harvested from TG-shPTEN mice that suffered from 'resistance' to PTEN restoration, a more complex picture emerged. In addition to the expected presentation of fluorescence-negative tumors, we also documented lesions that were mKate2+/GFP- and mKate2+/GFP(+) [Figure 4.20]. This latter category of tumors indicates a breakdown in the tet-regulatable machinery, since the TRE-GFP-miR30 allele is being expressed in the absence of dox, albeit at substantially lowered levels compared to dox treated tumors. The most interesting set of tumors are the mKate2+/GFP- samples, which may be mimicking a therapy resistance phenotype. We are actively investigating these samples in order to identify the escape mechanism underlying the rapid growth of cells that had previously benefitted from the strong knockdown of PTEN. Of note, some mice displayed evidence of all three tumor types at tumor burden endpoint harvest.

DISCUSSION

Using our transgenic RNAi model comprising of the MMTV-NeuNT, WAP-Cre, RIK and TG-shRNA alleles, we were able to demonstrate a highly significant acceleration of mammary tumorigenesis when *Pten* is knocked down. The disease phenotype displayed shortened tumor-free and overall survival, with 100% penetrance. Additionally, there was

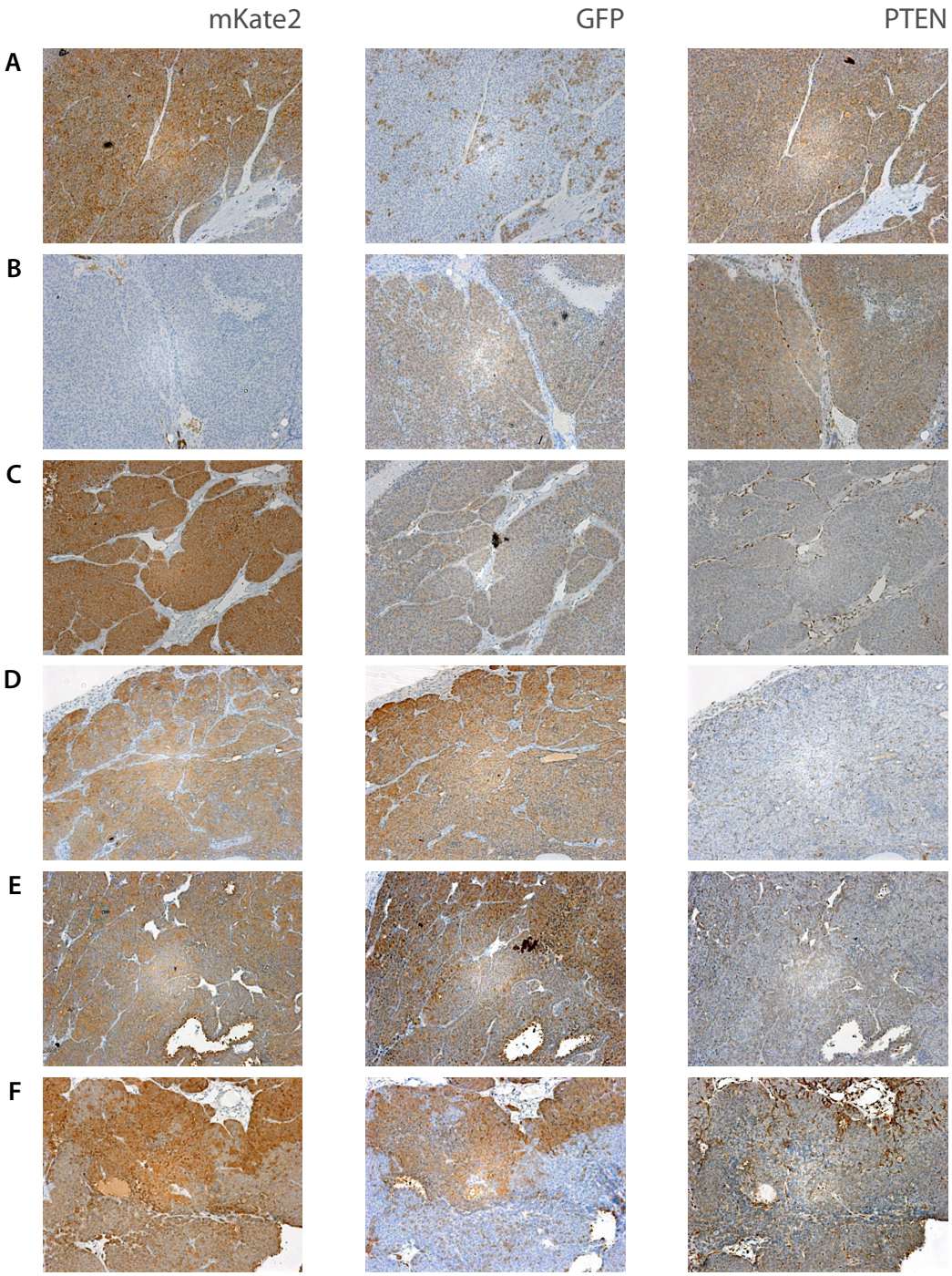

Figure 4.20 Varied patterns of fluorescent markers and PTEN expression in TG-shPTEN tumors in the absence of dox. IHC analysis of recurred tumor sections from MMTV-NeuNT;RIK;WAP-Cre;TG-shPTEN on dox withdrawal treatment. Multiple expression patterns observed in tumors arising within one animal. (A) Expected pattern: strong mKate2, no GFP and restored PTEN. (B) Example of NeuNT-driven tumor that has maintained PTEN expression. (C) mKate2+ tumor that has found alternative means of inactivating PTEN. (D,E) Strong expression of both fluorescent reporters and loss of PTEN, likely rtTA mutations. (F) Example of heterogenous pattern of expression observed within one tumor section.

an increase in the rate and severity of the metastatic phenotype. The shortened latency was so dramatic that almost all of the TG-shPTEN mice had achieved terminal disease endpoint before tumor onset was observed in control TG-shRLuc animals. Although this finding serves to demonstrate the level of impact that PTEN knockdown has on NeuNT oncogene driven tumorigenesis, it complicated experimental analysis since tumors from TG-shPTEN and TG-shRLuc mice could not be harvested at the same time point for meaningful cross-comparative analysis of disease phenotypes.

Two publications from Bill Muller's group had previously made similar observations using a conditional knockout model of *Pten* (Dourdin et al. 2008; Schade et al. 2009). In the first study, ErbB2 overexpression was driven from its endogenous promoter (ErbB2^{KI}) and coupled with an MMTV-Cre that acted on the PTEN conditional knockout allele (Andrechek et al. 2000; Li et al. 2002). Mammary-specific deletion of PTEN resulted in a dramatic acceleration of ErbB2-induced tumor progression and also increased the incidence of metastasis to the lung. In this particular model they report that the PTEN-deficient tumors acquired pathologic characteristics resembling the basal-like subtype of human breast cancers. The study included animals with both heterozygous and homozygous conditional loss of PTEN. Interestingly, tumor progression was associated with LOH at the PTEN locus in over 50% of tumors from PTEN heterozygous null animals.

After examination of upstream and downstream targets of PTEN and ErbB2, Dourdin and colleagues conclude that sustained activation of the PI3K/Akt signaling pathway is not the mechanism responsible for the accelerated mammary tumor formation in their PTEN-deficient/ErbB2^{KI} mouse model. We plan to verify these findings in our own system through comparative analysis of pathway activation status in TG-shPTEN and TG-shRLuc tumors, although potential discrepancies in findings could be explained by

differences in basic tumor biology arising from the molecular and histopathological heterogeneity described in this knockout model and the general homogeneity and luminal phenotype observed in our RNAi model.

In the second study, Schade and colleagues exchanged the ErbB2^{KI} strain for a system that drives transcription of an activated ErbB2/Neu from the strong viral MMTV promoter in a bicistronic configuration with Cre recombinase (MMTV-NIC), which couples the expression of the oncogene and Cre within the same mammary epithelial cells (Siegel et al. 1999; Ursini-Siegel et al. 2008). In line with the previous study, they report a dramatic acceleration of mammary tumor onset, and the development of multifocal and invasive metastasizing disease in mice with homozygous inactivation of PTEN in the presence of NeuNT. In contrast, however, they describe tumors with a homogenous morphology and a loss of basal and myoepithelial markers leading to histopathological and molecular characteristics of the luminal subtype, as well as a hyperactivation of the PI3K/Akt pathway.

The variation in phenotypes conferred by the various mouse models once again emphasizes the importance of the fundamental model design, and how differences in the timing of transgene expression, subtle discrepancies in the expression levels of key elements, or selection of distinct cell populations may all have a profound impact on experimental results.

Although we cannot circumvent the issue of highly discrepant tumor latency, some of the control TG-shRLuc tumors, those expressing GFP and thus resulting from the same luminal cell compartment as the TG-shPTEN tumors, could be used as a strong point of reference when examining the mechanism of cooperation behind the combined oncogenic effect of heightened HER2/neu signaling and PTEN impairment. Thus far the pathological

analysis does not indicate any differences in morphology and once developed, these control tumors also display fast growth and invasive capacity. Nonetheless we plan to look for evidence of PTEN loss and PIK3CA mutations in these tumors, as well as other possible changes in signaling patterns, that might point towards an explanation for the strong cooperation documented in these models of cooperation between PTEN loss and ErbB2/neu hyperactivity.

In this regard, our inducible RNAi model presents some unprecedented opportunities. We have already explored one setting of delayed doxycycline treatment but this could be extended further to, for example, better mimic what is found in the clinic or to generate a series of tumor samples where the cooperating shRNA is introduced at staggered time points. In the knockout models discussed above and in our own current iteration described in this chapter, PTEN deficiency has been incorporated into the initiation of the tumorigenic process and this presents itself as a major caveat in the accurate portrayal of human tumor biology. Additionally, the employment of the mutant *neu* allele undermines our capacity to test targeted therapies against ErbB2 or ErbB3. Although the latency is longer, in future studies it may be preferable to switch to the wild type MMTV-neu strain such that our platform might serve as a better preclinical model for testing novel therapeutic agents. Furthermore, to gain the capacity to effectively study resistance to trastuzumab in the context of a GEMM of mammary adenocarcinoma, the transgenic strain overexpressing human HER2 (huHER2) from the MMTV promoter would need to be employed (Finkle et al. 2004). Genentech has developed and tested the murine form of trastuzumab, mu4D5, in the MMTV-huHER2 model and observed some acquired resistance although the mechanism was not determined.

Our finding that TG-shPTEN driven tumors regress upon restoration of PTEN protein levels suggests that heightened PI3K/Akt signaling is a critical element of these tumor cells' sustained survival and proliferative advantage. However, depending on the size and stage of tumor growth, we observe a varied degree and length of responses to the reversal of PTEN knockdown. We are actively investigating the mechanisms by which these tumors progress through the initial phases of reduction in tumor burden followed by the eventual return of a highly proliferative disease. We are confident that the re-activation of PTEN function can be more than cytostatic and truly cytotoxic since some tumors suffer a substantial and long-term reduction in tumor burden. As our primary experimental animals are immune competent, it would be equally tempting to investigate the possible role of immune clearance or wound healing, as well as the involvement of other components of the microenvironment, that may contribute to this regression phenotype.

Preliminary analysis of the 'relapsed' tumors indicates that in some circumstances the tumor cells have found ways to bypass the tet-regulated machinery. Mutations in rtTA have been previously reported in the literature (Podsypanina et al. 2008), and the presence of faint levels of GFP in some tumors points towards such a breakdown in the system. Confirmation of the rtTA mutational status, and an estimate of its prevalence, is pending. Tumors that display mKate2 signal but no GFP have presumably found alternative mechanisms of restoring the survival and proliferative advantages from which they previously benefitted. A thorough analysis of the downstream signaling profile of these tumors, as well as examination of the mutational status of PIK3CA and PTEN or a possible LOH of 10q23, will help to explain this 'acquired resistance' phenomenon.

Previous examples of restoration of tumor suppressor function include studies in GEMMs of lymphoma, sarcoma and hepatocellular carcinoma, were it was demonstrated

that p53 restoration induced tumor cell apoptosis (lymphoma) or senescence (sarcoma/carcinoma) and resulted in tumor regression and clearance (Martins et al. 2006; Ventura et al. 2007; Xue et al. 2007). In the context of breast cancer, Boxer and colleagues reported a lack of sustained regression of *c-Myc* induced mammary adenocarcinomas following both brief and prolonged inactivation of the oncogene in a doxycycline-inducible system driving rtTA from MMTV-LTR (Gunther et al. 2002; Boxer et al. 2004). In parallel studies, the downregulation of *neu* expression in an MMTV-rtTA driven tet-regulatable NeuNT model resulted in tumor regression. However, mice bearing fully regressed tumors eventually developed spontaneous recurrences in the absence of *neu* expression (Moody et al. 2002), and the transcriptional repressor *Snail* was shown to be spontaneously upregulated and accompanied by EMT in these recurrent tumors *in vivo* (Moody et al. 2005).

Virtually all targeted therapies used in the clinic today were developed on the principle that one oncogenic mutation can be identified and selected for treatment by a specific agent. This paradigm fundamentally ignores the role of cellular signaling crosstalk and the intrinsic plasticity of mechanisms that allow for maintained cellular homeostasis. Many studies have illustrated the dynamic interactions between major signaling networks, all emphasizing the role of feedback activation of pathways as a roadblock in attaining the desired therapeutic benefit of single agent targeted therapies. Inhibition of the mTORC1 complex with rapamycin-like drugs causes activation of PI3K and AKT, thus limiting their clinical efficacy due to the release of a negative regulatory feedback loop that triggers AKT and ERK signaling (O'Reilly et al. 2006; Cloughesy et al. 2008; Tabernero et al. 2008; Baselga et al. 2009). Similarly, inhibition of AKT has been shown to induce the expression and phosphorylation of multiple RTKs (Chandarlapaty et al. 2011). Moreover, inhibition of MEK

in basal-like breast cancer also caused activation of RTKs, precluding a response to single-agent MEK inhibitors *in vivo* (Duncan et al. 2012).

In follow-up studies, we plan to delve further into the metastatic phenotype as much remains to be explored. By taking advantage of the secondary transplantation and *in vitro* culture systems that were established, it would be very interesting to examine how each site of dissemination exerts unique requirements for successful metastasis and how those sites may differ, or not, in their responses to the reactivation of *Pten*. The dual-fluorescent reporter system allows us to easily track the relevant disseminated cells and continue to monitor their activity even after the shRNA has been shut off. This element of our mouse model offers us many new experimental possibilities.

Finally, the novel allelic combination of WAP-Cre and RIK to drive the shRNA transgene has yielded reproducible and clean results, and we believe that we have been able to build a robust model that will be essential in the validation of novel tumor suppressor genes, such as *Nf1*, that will be identified in larger screening efforts in the future.

CHAPTER CONTRIBUTIONS

Cornelius Miething tested and made the TG-shPTEN mouse strains (Fig 4.1). Ted Kastenhuber performed the immunohistochemical stains presented in Chapter 4. All work involving tumor-derived cell lines and serial transplantation was conducted together with Ted Kastenhuber (Fig 4.15, Fig 4.20). Hannah Wen provided the histological analysis. Carl Le and his team at the Small Animal Imagining Core performed MRI imaging (Fig 4.18). Janelle Simon performed the tumor removal surgery (Fig 4.17). Saya Ebbesen performed all other experiments.

V. Conclusions and Future Perspectives

Diversity and complexity are hallmarks of the cancer genome (Hanahan and Weinberg 2000; Hanahan and Weinberg 2011). Even in cancer types where clear driving oncogenes have been identified, a complex web of additional genetic lesions help to facilitate the uncontrolled expansion and eventual metastasis of the tumor. As a consequence, the behavior of individual tumors is heterogeneous and remains difficult to predict. The advent of sophisticated array and sequencing technology has exposed the complexity of the cancer genome; yet functional studies are required to determine the impact of different genetic configurations on cancer progression and to identify the unique vulnerabilities they create.

The vast majority of published studies use cell culture models to examine the effects of specific genes on the processes of disease initiation, progression and maintenance, as well as response to therapy. Undoubtedly, certain aspects of the transformed phenotype can be mimicked in cell culture, but cancer is fundamentally a disease of the whole organism. In addition to the vast complexity of multiple cellular mechanisms, cancerous disease is influenced significantly by the cellular microenvironment, a fact that has been extensively documented in breast cancer (Egeblad et al. 2010; Polyak and Kalluri 2010). Therefore, while *in vitro* approaches can uncover and characterize certain important and novel details, ultimately their relevance must be verified *in vivo*. In addition, *in vivo* models provide a robust means to identify novel mechanisms involved in the malignant progression of cancer, both at the physiological and molecular level, which is critical towards a better understanding of metastasis, the form of disseminated disease that is the main cause of death in human breast cancer patients.

However, such studies, particularly those involving relevant *in vivo* experimentation, have been slow, expensive, and often unable to efficiently model the diversity of human breast cancer subtypes in a way that allows for conclusive and meaningful insights. A major goal of our efforts described in this thesis has been to speed up these analyses through the development and adaptation of innovative research methodology, such as the RNAi technology pioneered by our laboratory, to explore the biology of tumor suppressor genes.

A major goal of the work described in Chapter 2 was the development of an orthotopic transplantation model that would be well adapted for high-throughput screening, and we aimed to be able to search for novel TSGs or oncogenes through *in vivo* positive selection of virally introduced constructs. Our first setback was in the choice of cells for transplantation. Previous efforts in the lab to produce mosaic models of different cancer types had relied on the isolation of tissue progenitor cells, such as hematopoietic stem and progenitor cells or hepatoblasts, that can be readily cultured and re-transplanted into recipients (Zender et al. 2008; Bric et al. 2009; Zuber et al. 2009; Zuber et al. 2011b; Scuoppo et al. 2012). This approach has the advantage of developing physiologically relevant mouse models of cancer without the burden of producing and crossing many germ line mutant strains, complementing the transgenic methods such as those discussed in Chapters 3 and 4. However, while we were able to harvest primary mammary progenitor cells capable of differentiating into a fully branched ductal epithelium, we were unsuccessful in isolating and propagating these cells at sufficient numbers to produce a tractable and affordable mosaic model for large-scale studies. In future iterations of such a screening project, we hope to circumvent these technical difficulties and perhaps adopt the methodology of combining *in vitro* screens utilizing human cell lines with individual hit validation in mouse models. Our identification of *NF1* as a putative novel tumor suppressor, nonetheless,

confirms that the fundamental strategy of mining human patient copy number variation data for deleted chromosomal regions for subsequent filtering through the mouse remains an efficient way of finding relevant driver genes.

When this positive selection screen was first conceived, the concept of molecular profiles of human breast cancer subtypes was only just emerging. If we were to repeat this project again we would undoubtedly segregate the patient tumor samples into the appropriate molecular categories, provided sufficient numbers could be gathered to achieve statistical significance. Combining this refinement of the candidate cancer gene lists with additional knowledge regarding the predicted cells-of-origin and the sensitizing oncogenes most relevant to each subgroup would allow us to conduct screens with more sophistication and an increased likelihood of achieving clinical relevance.

Chapter 3 described the development of a multi-alleleic RNAi mouse model that utilizes a novel combination of both established and newly generated genetically engineered mouse strains. In Chapter 4, this model was then applied to the study of the role of PTEN in HER2 positive breast cancer, and we characterized the aggressive, highly metastatic disease phenotype observed. The cooperation of PTEN knockdown and NeuNT overexpression in the luminal mammary epithelium was almost too efficient, as we observed highly proliferative and multifocal tumor growth, but the model system proved robust and a 100% penetrance of mammary tumor development was documented in TG-shPTEN animals. Since spontaneous metastasis to multiple organ sites is a rare feature in most animal models of cancer, further studies to test the differential requirement for cellular transformation required for efficient homing to and growth in the lung, liver and bone niches may provide important answers. Techniques such as barcoding or single-cell whole genome sequencing could be powerful in furthering our understanding of critical details such as the clonality of

the primary and metastatic tumorigenic processes, the timing of circulating tumor cell shedding and the potential role of self-seeding in tumor evolution, or the relationship between cellular changes that occur in the primary versus distal niches and their contribution to the transformative selection and growth (Kim et al. 2009; Navin et al. 2011).

Finally, to maximize the potential of the multi-allelic mouse model such as the one described here for the assessment of gene function *in vivo*, we hope to expand our methodology to include the re-derivation of ESCs and further apply *ex vivo* manipulation to introduce inducible, reversible alleles (shRNAs, cDNAs, microRNAs) to the *ColA1* locus. The ultimate goal is to make breast cancer mouse modeling a more rapid, flexible, and scalable platform where multiple combinations of cooperating genetic legions can be analyzed in parallel and the effects of tissue-specific transient gene activation or inhibition can be easily assessed at different stages of disease using the inducible, reversible alleles. Such models increase our capacity to physiologically filter through the vast quantities of oncogenomic data being produced, for which the biological impact remains largely uncharacterized. While xenograft models are an effective means of propagating human cancers and capturing their unique complexity, well-defined and sophisticated GEMMs present a genetically tractable arena in which sporadic and *de novo* tumorigenesis can be studied in an immunologically competent organism.

VI. Materials and Methods

ROMA breast cancer data set

Representational Oligonucleotide Microarray Analysis (ROMA) was conducted as previously described (Lucito et al. 2003; Hicks et al. 2006). Pinning analysis was conducted on ROMA data from 247 frozen breast tissue samples: 139 from the Karolinska Institute in Stockholm, Sweden, and 118 from the Radium Hospital in Oslo, Norway. The deletion size/frequency analysis was performed on those 247 samples plus ROMA data from 43 human breast cancer cell lines.

shRNA library production

BIOPREDsi was used to design shRNA sequences (Huesken et al. 2005). 125-bp oligonucleotides encompassing the whole stem-loop miR-30 shRNA precursor, flanked by EcoRI and XhoI cloning sites were ordered from Agilent (Santa Clara, CA), and amplified with a library-specific reverse primer (for main library: TTCTGCAAGGCCTCCAGGTTGG, for priority set: TTCACGATCTGCTGCAGAATGTGTCT) and a common forward primer (miRXhoF: TACAATACTCGAGAAGGTATATTGCTGTTGACAGTGAGCG). Pooled cloning was conducted as described (Zuber et al. 2011a; Scuoppo et al. 2012). To avoid the introduction of oligonucleotides with synthesis errors, such as mutations introduced during PCR amplification steps or concatemerization of inserts during vector ligation, each unique shRNA vector was verified by sequencing before inclusion in the resulting library. Clones were miniprepped and sequenced in 96-well format.

Viral constructs

shRNA vectors – MLS and MLP (LMP) miR-30 based shRNA vectors were cloned as previously described (Dickins et al. 2005). For MLR, the GFP cDNA was replaced with

dsRed cDNA. shRNAs were designed using the BIOPREDsi algorithm (www.biopredsi.org, discontinued) (Huesken et al. 2005), PCR amplified from oligos, and cloned into the miR-30 backbone as described using XhoI/EcoRI restriction sites (Zuber et al. 2011a).

Oncogene vectors – MultiSite Gateway® Cloning Technology (Invitrogen Technologies) was use to make all lentriviral plasmid vectors, including UbC-NeuNT, CMV-NeuNT and all other oncogene cDNA overexpression vectors employed. These vectors contained a blasticidin resistance marker.

Cell lines

Comma-D cells were obtained from Senthil Muthuswamy. NMuMG cells were purchased from ATCC (Catalog # CRL-1636).

Cell culture

Retroviral transfections/infections – For calcium phosphate transfection, $6x10^6$ phoenix cells were plated in 10cm plates 6 to 12 hours prior to transfection with 15μg shRNA construct and 5 μg ecotropic helper plasmid (McCurrach and Lowe 2001). Fresh media was added 12 hours after transfection and viral supernatant was collected twice at 36 and 48 hours post-transfection. Viral supernatant was filtered through a .45μm filter, then diluted 1:2 with fresh media and supplemented with polybrene (4μg/mL final conc.) for a single infection of target cells. Target cells (NMuMG, Comma-D) were split 1:3 from confluent plates 12~24 hours prior to second virus collection. Infection rates were determined using GUAVA flow cytometers (Millipore, Billerica, MA).

Lentiviral transfections/infections – Similarly, for lentiviral calcium phosphate transfections, 293FT cells were plated for transfection density $8x10^6$ cells per 10cm plate. 10μg plasmid DNA was combined with 3.5μg VSVG, 2.5μg REV and 6.5μg MDL helper

constructs during transfection. After collection of the viral supernatant, it was centrifuged prior to filtration in order to remove the large quantity of cell debris.

ESC targeting and culture

ColA1-targeting constructs were cloned as described (Premsrirut et al. 2011; Dow et al. 2012). TREtight promoter modified version was previously described (McJunkin et al. 2011). KH2 ESCs were targeted by electroporation of 50μg of targeting construct with 25μg pCAGGs-Flpe as described (Premsrirut et al. 2011; Dow et al. 2012). ESCs were cultured on irradiated DR4 fibroblast feeder layers on gelatinized plates in M15 media containing LIF as described (Beard et al. 2006).

Primary mammary gland harvest and isolation of MaSCs

Isolation of primary murine mammary stem/progenitor cells was conducted as previously described (Shackleton et al. 2006). Briefly, 8 to 14 week old mice were euthanized by CO_2 inhalation, followed by cervical dislocation. A midline incision of the skin was performed and the mammary fad pads were exposed. The mammary glands were excised and placed into mammary gland digestion medium. Crude epithelial organoids were obtained by incubating the mammary glands in digestion medium for 6 to 8 hours at 37 °C with hourly pipetet-mixing and vortexing. A single cell suspension of mammary epithelial cells was obtained by sequentially digesting the organoids with Trypsin/EDTA, dispase and DNAse and trituration using fire-polished glass pasteur pipettes. The resulting cell suspension was filtered through a 40um cells strainer and cells were plated into growth medium on ultra-low attachment tissue culture plates.

in vivo animal studies

The Institutional Animal Care and Use Committees of Cold Spring Harbor Laboratory and Memorial Sloan-Kettering Cancer Center approved all mouse experiments conducted in their respective animal facilities.

Orthotopic transplantation into mammary fat pads

Orthotopic transplantations were conducted as follows: the mouse was anesthetized with isoflurane (1-4%) administered with a precision vaporizer. Depth of anesthesia was monitored at least every 10 minutes throughout the procedure by observing that there was no change in respiratory rate associated with surgical manipulation. Following confirmation that a suitable anesthetic plane (no response to stimulation) has been attained, the fur covering the lower abdominal area was removed (unless conducting surgery on a nude mouse) with an electric clipper with a #40 blade exposing an area of skin approximately 150% larger than the area of the incision and sterile eye lubricant was applied to both eyes to prevent corneal drying during surgery. Loose fur was removed with a moist gauze pad. A small volume (0.1-0.2cc) of local anesthetic agent, such as bupivacaine (Marcaine 0.25-0.5%), was infiltrated into the tissue adjacent to the intended incision line. The mouse was placed on a circulating water heating pad and covered with a drape. The area was then prepped for surgery using three rounds of alternating scrubs of 10% povidone-iodine and 70% ethanol soaked gauze sponges. The skin was then painted with a 10% povidone-iodine. All surgical instruments and equipment were sterilized by steam sterilization prior to surgery and sterilized between individuals using a glass bead sterilizer. The animal, which was positioned in the supine position, was covered with sterile surgical crepe paper. A 3.0 cm x 3.0 cm square hole that has been cut into the drape was located over the intended incision site. Sterilized surgical scissors were used to make an incision in the abdominal region that

penetrates the skin but not into the peritoneal cavity. The opening was be enlarged vertically and horizontally in order to expose the abdominal mammary fat pads of the mouse. To avoid drying of the exposed tissue, each flank of the animal was manipulated in sequential order. In some cases the fat pad was cleared, removing all of the tissue before the lymph node. The fat pad was then injected with cells (primary or cell line), tumor (fragment or digested) or virus (Adeno) using a syringe. The volume ranged from 10 to 20μL. After both abdominal fat pads were manipulated, the skin was be brought together and closed using sterile 4-0 or 5-0 vicryl sutures or surgical glue or both. After surgery, animals were observed until they could maintain sternal recumbency. Before being returned to the housing area, they were administered 1 mg/kg buprenorphine, SQ. They were evaluated at least one additional time the day of surgery and at least daily for the next 48 hours. Tumor progression was monitored by *in vivo* fluorescence imaging, palpation and/or caliper measurements depending on the assay.

Immunohistochemistry

Immunostaining was conducted on a Discovery Ultra automated device (Ventana) with the following antibodies and concentrations: GFP (Cell Signalling 2956,1:200), tRFP (for mKate2; Evrogen AB233, 1:5000), ErbB2 (for Neu; Abcam ab2428, 1:500), PTEN (Cell Signaling 9559, 1:100), Ki-67 (Abcam 16667,1:100), CK5 (Covance PRB-160P, 1:10000), CK14 (Covance PRB-155P, 1:1000), CK19 (Abcam ab15463, 1:100), TTF1(Novus Biologicals,1:100). Primary antibodies were applied at room temperature for 3 hours and secondary antibody from goat source (Vector Laboratories) was applied at 1:300 at 37°C for 20 minutes. Streptavidin-biotin peroxidase-based DAB Map Detection Kit (Ventana 760-124) was used and slides were counterstained with Hematoxylin (Ventana, 760-2021) and Bluing Reagent (Ventana, 760-2037).

Doxycycline treatment

Cell culture – All dox-containing media was prepared at a dose of 1μg/ml doxycycline (Sigma-Aldrich, St. Louis, MO).

Animal studies – Mice were treated with doxycycline hyclate at a dose of 625mg/kg in alfalfa-free rodent diet with 18.2% protein, 48% carbohydrate and 5.8% fat content (Harlan Laboratories, Madison, WI). The diet is designed to deliver a daily dose of 2-3mg of doxycycline based on consumption of 4-5g/day by a mouse; doxycycline hyclate contains approximately 87% doxycycline. Since the chlorophyll from the alfalfa found in standard mouse food has been found to fluoresce in the near infrared part of the spectrum; we used alfalfa-free dox chow in our experimentation (Troy et al. 2004; Inoue et al. 2008).

Adenoviral Cre

Adeno-Cre virus was purchased commercially from the Gene Transfer Vector Core of the University of Iowa. A 10μL volume was injected into the fat pad at a dose of 10^9pfu.

Table 6.1 shRNA sequences

shRNA (Prediction algorithm)	**Sequence**
Renilla-Luciferase.713 (BIOPREDsi)	CTCGAGAAGGTATATTGCTGTTGACAGTGAGCGCAGGAAT TATAATGCTTATCTATAGTGAAGCCACAGATGTATAGATA AGCATTATAATTCCTATGCCTACTGCCTCGGAATTC
Luciferase.1309 (Codex)	CTCGAGAAGGTATATTGCTGTTGACAGTGAGCGCCCGCCT GAAGTCTCTGATTAATAGTGAAGCCACAGATGTATTAATC AGAGACTTCAGGCGGTTGCCTACTGCCTCGGAATTC
Pten.1522 (BIOPREDsi)	CTCGAGAAGGTATATTGCTGTTGACAGTGAGCGACCAGCT AAAGGTGAAGATATATAGTGAAGCCACAGATGTATATATC TTCACCTTTAGCTGGCTGCCTACTGCCTCGGAATTC
Pten.2049 (BIOPREDsi)	CTCGAGAAGGTATATTGCTGTTGACAGTGAGCGAAAGATC AGCATTCACAAATTATAGTGAAGCCACAGATGTATAATTT GTGAATGCTGATCTTCTGCCTACTGCCTCGGAATTC
Nf1.6074 (BIOPREDsi)	CTCGAGAAGGTATATTGCTGTTGACAGTGAGCGACAGATG TATCCTTCTATTCAATAGTGAAGCCACAGATGTATTGAATA GAAGGATACATCTGCTGCCTACTGCCTCGGAATTC
Nf1.8594 (Codex)	CTCGAGAAGGTATATTGCTGTTGACAGTGAGCGAGCTGGC AGTTTCAAACGTAATTAGATGAAGCACAGATGTAATTACG TTTGAAACTGCCAGCGTGCCTACTGCCTCGGAATTC
Nf1.9930 (BIOPREDsi)	CTCGAGAAGGTATATTGCTGTTGACAGTGAGCGCCTCAGTT AAGATTGAACTATATAGTGAAGCCACAGATGTATATAGTT CAATCTTAACTGAGATGCCTACTGCCTCGGAATTC

**shRNA sequences are listed as full length 116nt XhoI/EcoRI fragments for miR-30 cloning.*

Table 6.2 Genotyping PCR primer sequences

Transgenic allele	Primers
Renilla-Luciferase.713 (shRNA specific)	5' GTATAGATAAGCATTATAATTCCTA 5' GAAAGAACAATCAAGGGTCC
Pten.1522 (shRNA specific)	5' CAGATGTATATATCTTCACCTTT 5' CACCCTGAAAACTTTGCCCC
Nf1.6074 (shRNA specific)	5' GCCACAGATGTATTGAATAGAA 5' GAAAGAACAATCAAGGGTCC
Nf1.8594 (shRNA specific)	5' CCACAGATGTAATTACGTTTGA 5' CACCCTGAAAACTTTGCCCC
ColA1 locus Targeted/wild type	5′ AATCATCCCAGGTGCACAGCATTGCGG 5′ CTTTGAGGGCTCATGAACCTCCCAGG 5′ ATCAAGGAAACCCTGGACTACTGCG
ColA1 locus Targeted/empty CHC	5' AATCATCCCAGGTGCACAGCATTGCGG 5' GGATGTGGAATGTGTGCGAG 5' CTTTGAGGGCTCATGAACCTCCCAGG
Rosa26 locus (for RIK or R26-rtTA2)	5′ AAAGTCGCTCTGAGTTGTTAT 5′ GCGAAGAGTTTGTCCTCAACC 5′ GGAGCGGGAGGAATGGATATG
WAP-Cre Presence/absence	5' CTAGGCCACAGAATTGAAAGATCT 5' GTAGGTGGAAATTCTAGCATCATCC 5' GCGGTCTGGCAGTAAAAACTATC 5' GTGAAACAGCATTGCTGTCACTT
MMTV-NeuNT Presence/absence	5' CCCCGGGAGTATGTGAGTGA 5' TGAGCTGTT TTGAGGCTGCA
CAGs-rtTA3 ("4288")	5′ TGCCTATCATGTTGTCAAA 5′ CGAAACTCTGGTTGACATG 5′ CTGCTGTCCATTCCTTATTC

Table 6.3 Transgenic mouse strains

Strain	Reference
Renilla-Luciferase.713	TRE promoter: Premsrirut et al. 2011 TREtight promoter: *unpublished*
Pten.1522	Miething, et al., In preparation
Pten.2049	Miething, et al., In preparation
Nf1.6074	*Unpublished*
Nf1.8594	*Unpublished*
Rosa26-rtTA-M2	Hochedlinger et al. 2005
MMTV-tTA	Hennighausen et al. 1995
RIK	*Unpublished*
WAP-Cre	Wagner et al. 1997
MMTV-NeuNT	Muller et al. 1988
CAGs-rtTA3 "4288"	Premsrirut et al. 2011

VII. References

Ahlquist T, Bottillo I, Danielsen SA, Meling GI, Rognum TO, Lind GE, Dallapiccola B, Lothe RA. 2008. RAS signaling in colorectal carcinomas through alteration of RAS, RAF, NF1, and/or RASSF1A. *Neoplasia* **10**: 680-686, 682 p following 686.

Al-Hajj M, Becker MW, Wicha M, Weissman I, Clarke MF. 2004. Therapeutic implications of cancer stem cells. *Curr Opin Genet Dev* **14**: 43-47.

Alimonti A, Carracedo A, Clohessy JG, Trotman LC, Nardella C, Egia A, Salmena L, Sampieri K, Haveman WJ, Brogi E et al. 2010. Subtle variations in Pten dose determine cancer susceptibility. *Nat Genet* **42**: 454-458.

American Cancer Society. 2012. Cancer facts and figures 2012. *American Cancer Society*.

Anders K, Buschow C, Charo J, Blankenstein T. 2012. Depot formation of doxycycline impairs Tet-regulated gene expression in vivo. *Transgenic Res* **21**: 1099-1107.

Andrechek ER, Hardy WR, Siegel PM, Rudnicki MA, Cardiff RD, Muller WJ. 2000. Amplification of the neu/erbB-2 oncogene in a mouse model of mammary tumorigenesis. *Proc Natl Acad Sci U S A* **97**: 3444-3449.

Andrulis IL, Bull SB, Blackstein ME, Sutherland D, Mak C, Sidlofsky S, Pritzker KP, Hartwick RW, Hanna W, Lickley L et al. 1998. neu/erbB-2 amplification identifies a poor-prognosis group of women with node-negative breast cancer. Toronto Breast Cancer Study Group. *J Clin Oncol* **16**: 1340-1349.

Arteaga CL, Sliwkowski MX, Osborne CK, Perez EA, Puglisi F, Gianni L. 2012. Treatment of HER2-positive breast cancer: current status and future perspectives. *Nat Rev Clin Oncol* **9**: 16-32.

Backman CM, Zhang Y, Hoffer BJ, Tomac AC. 2004. Tetracycline-inducible expression systems for the generation of transgenic animals: a comparison of various inducible systems carried in a single vector. *J Neurosci Methods* **139**: 257-262.

Balkwill F, Charles KA, Mantovani A. 2005. Smoldering and polarized inflammation in the initiation and promotion of malignant disease. *Cancer Cell* **7**: 211-217.

Barcellos-Hoff MH, Ravani SA. 2000. Irradiated mammary gland stroma promotes the expression of tumorigenic potential by unirradiated epithelial cells. *Cancer Res* **60**: 1254-1260.

Baselga J. 2001. Clinical trials of Herceptin(trastuzumab). *Eur J Cancer* **37 Suppl 1**: S18-24.

-. 2011. Targeting the phosphoinositide-3 (PI3) kinase pathway in breast cancer. *Oncologist* **16 Suppl 1**: 12-19.

Baselga J, Norton L, Albanell J, Kim YM, Mendelsohn J. 1998. Recombinant humanized anti-HER2 antibody (Herceptin) enhances the antitumor activity of paclitaxel and doxorubicin against HER2/neu overexpressing human breast cancer xenografts. *Cancer Res* **58**: 2825-2831.

Baselga J, Semiglazov V, van Dam P, Manikhas A, Bellet M, Mayordomo J, Campone M, Kubista E, Greil R, Bianchi G et al. 2009. Phase II randomized study of neoadjuvant everolimus plus letrozole compared with placebo plus letrozole in patients with estrogen receptor-positive breast cancer. *J Clin Oncol* **27**: 2630-2637.

Baselga J, Tripathy D, Mendelsohn J, Baughman S, Benz CC, Dantis L, Sklarin NT, Seidman AD, Hudis CA, Moore J et al. 1996. Phase II study of weekly intravenous recombinant humanized anti-p185HER2 monoclonal antibody in patients with HER2/neu-overexpressing metastatic breast cancer. *J Clin Oncol* **14**: 737-744.

Beard C, Hochedlinger K, Plath K, Wutz A, Jaenisch R. 2006. Efficient method to generate single-copy transgenic mice by site-specific integration in embryonic stem cells. *Genesis* **44**: 23-28.

Beatson GT. 1896. On the treatment of inoperable cases of carcinoma of the mamma: Suggestions for a new method of treatment, with illustrated cases. *Lancet* **2**: 104-107 and 162-165.

Behbod F, Kittrell FS, LaMarca H, Edwards D, Kerbawy S, Heestand JC, Young E, Mukhopadhyay P, Yeh HW, Allred DC et al. 2009. An intraductal human-in-mouse transplantation model mimics the subtypes of ductal carcinoma in situ. *Breast Cancer Res* **11**: R66.

Berger AH, Pandolfi PP. 2011. Haplo-insufficiency: a driving force in cancer. *J Pathol* **223**: 137-146.

Bernards R. 2012. A missing link in genotype-directed cancer therapy. *Cell* **151**: 465-468.

Berns K, Horlings HM, Hennessy BT, Madiredjo M, Hijmans EM, Beelen K, Linn SC, Gonzalez-Angulo AM, Stemke-Hale K, Hauptmann M et al. 2007. A functional genetic approach identifies the PI3K pathway as a major determinant of trastuzumab resistance in breast cancer. *Cancer Cell* **12**: 395-402.

Berry DA, Cronin KA, Plevritis SK, Fryback DG, Clarke L, Zelen M, Mandelblatt JS, Yakovlev AY, Habbema JD, Feuer EJ. 2005. Effect of screening and adjuvant therapy on mortality from breast cancer. *N Engl J Med* **353**: 1784-1792.

Berry DA, Inoue L, Shen Y, Venier J, Cohen D, Bondy M, Theriault R, Munsell MF. 2006. Modeling the impact of treatment and screening on U.S. breast cancer mortality: a Bayesian approach. *J Natl Cancer Inst Monogr*: 30-36.

Bignell GR, Greenman CD, Davies H, Butler AP, Edkins S, Andrews JM, Buck G, Chen L, Beare D, Latimer C et al. 2010. Signatures of mutation and selection in the cancer genome. *Nature* **463**: 893-898.

Bloom HJ, Richardson WW. 1957. Histological grading and prognosis in breast cancer; a study of 1409 cases of which 359 have been followed for 15 years. *Br J Cancer* **11**: 359-377.

Bollag G, Clapp DW, Shih S, Adler F, Zhang YY, Thompson P, Lange BJ, Freedman MH, McCormick F, Jacks T et al. 1996. Loss of NF1 results in activation of the Ras signaling pathway and leads to aberrant growth in haematopoietic cells. *Nat Genet* **12**: 144-148.

Bose S, Wang SI, Terry MB, Hibshoosh H, Parsons R. 1998. Allelic loss of chromosome 10q23 is associated with tumor progression in breast carcinomas. *Oncogene* **17**: 123-127.

Bouchard L, Lamarre L, Tremblay PJ, Jolicoeur P. 1989. Stochastic appearance of mammary tumors in transgenic mice carrying the MMTV/c-neu oncogene. *Cell* **57**: 931-936.

Boxer RB, Jang JW, Sintasath L, Chodosh LA. 2004. Lack of sustained regression of c-MYC-induced mammary adenocarcinomas following brief or prolonged MYC inactivation. *Cancer Cell* **6**: 577-586.

Brannan CI, Perkins AS, Vogel KS, Ratner N, Nordlund ML, Reid SW, Buchberg AM, Jenkins NA, Parada LF, Copeland NG. 1994. Targeted disruption of the neurofibromatosis type-1 gene leads to developmental abnormalities in heart and various neural crest-derived tissues. *Genes Dev* **8**: 1019-1029.

Brems H, Beert E, de Ravel T, Legius E. 2009. Mechanisms in the pathogenesis of malignant tumours in neurofibromatosis type 1. *Lancet Oncol* **10**: 508-515.

Bric A, Miething C, Bialucha CU, Scuoppo C, Zender L, Krasnitz A, Xuan Z, Zuber J, Wigler M, Hicks J et al. 2009. Functional identification of tumor-suppressor genes through an in vivo RNA interference screen in a mouse lymphoma model. *Cancer Cell* **16**: 324-335.

Brierley J. 2006. The evolving TNM cancer staging system: an essential component of cancer care. *CMAJ* **174**: 155-156.

Brummelkamp TR, Bernards R, Agami R. 2002. A system for stable expression of short interfering RNAs in mammalian cells. *Science* **296**: 550-553.

Buzdar AU, Hortobagyi G. 1998. Update on endocrine therapy for breast cancer. *Clin Cancer Res* **4**: 527-534.

Cacev T, Radosevic S, Spaventi R, Pavelic K, Kapitanovic S. 2005. NF1 gene loss of heterozygosity and expression analysis in sporadic colon cancer. *Gut* **54**: 1129-1135.

Cancer Genome Atlas Network. 2012. Comprehensive molecular portraits of human breast tumours. *Nature* **490**: 61-70.

Cantley LC. 2002. The phosphoinositide 3-kinase pathway. *Science* **296**: 1655-1657.

Cantley LC, Neel BG. 1999. New insights into tumor suppression: PTEN suppresses tumor formation by restraining the phosphoinositide 3-kinase/AKT pathway. *Proc Natl Acad Sci U S A* **96**: 4240-4245.

Cardiff RD, Moghanaki D, Jensen RA. 2000. Genetically engineered mouse models of mammary intraepithelial neoplasia. *J Mammary Gland Biol Neoplasia* **5**: 421-437.

Cardiff RD, Wellings SR. 1999. The comparative pathology of human and mouse mammary glands. *J Mammary Gland Biol Neoplasia* **4**: 105-122.

Carey LA, Dees EC, Sawyer L, Gatti L, Moore DT, Collichio F, Ollila DW, Sartor CI, Graham ML, Perou CM. 2007. The triple negative paradox: primary tumor chemosensitivity of breast cancer subtypes. *Clin Cancer Res* **13**: 2329-2334.

Cavenee WK, Dryja TP, Phillips RA, Benedict WF, Godbout R, Gallie BL, Murphree AL, Strong LC, White RL. 1983. Expression of recessive alleles by chromosomal mechanisms in retinoblastoma. *Nature* **305**: 779-784.

Chandarlapaty S, Sawai A, Scaltriti M, Rodrik-Outmezguine V, Grbovic-Huezo O, Serra V, Majumder PK, Baselga J, Rosen N. 2011. AKT inhibition relieves feedback suppression of receptor tyrosine kinase expression and activity. *Cancer Cell* **19**: 58-71.

Chang K, Elledge SJ, Hannon GJ. 2006. Lessons from Nature: microRNA-based shRNA libraries. *Nat Methods* **3**: 707-714.

Chao RC, Pyzel U, Fridlyand J, Kuo YM, Teel L, Haaga J, Borowsky A, Horvai A, Kogan SC, Bonifas J et al. 2005. Therapy-induced malignant neoplasms in Nf1 mutant mice. *Cancer Cell* **8**: 337-348.

Chin L, Gray JW. 2008. Translating insights from the cancer genome into clinical practice. *Nature* **452**: 553-563.

Clontech. 2003. Gene Expression Systems. *Clontechniques* **XVIII**: 1.

Cloughesy TF, Yoshimoto K, Nghiemphu P, Brown K, Dang J, Zhu S, Hsueh T, Chen Y, Wang W, Youngkin D et al. 2008. Antitumor activity of rapamycin in a Phase I trial for patients with recurrent PTEN-deficient glioblastoma. *PLoS Med* **5**: e8.

Clynes RA, Towers TL, Presta LG, Ravetch JV. 2000. Inhibitory Fc receptors modulate in vivo cytotoxicity against tumor targets. *Nat Med* **6**: 443-446.

Cobleigh MA, Vogel CL, Tripathy D, Robert NJ, Scholl S, Fehrenbacher L, Wolter JM, Paton V, Shak S, Lieberman G et al. 1999. Multinational study of the efficacy and safety of humanized anti-HER2 monoclonal antibody in women who have HER2-overexpressing metastatic breast cancer that has progressed after chemotherapy for metastatic disease. *J Clin Oncol* **17**: 2639-2648.

Collado M, Blasco MA, Serrano M. 2007. Cellular senescence in cancer and aging. *Cell* **130**: 223-233.

Courtney KD, Corcoran RB, Engelman JA. 2010. The PI3K pathway as drug target in human cancer. *J Clin Oncol* **28**: 1075-1083.

David G, Van der Schueren B, Bernfield M. 1981. Basal lamina formation by normal and transformed mouse mammary epithelial cells duplicated in vitro. *J Natl Cancer Inst* **67**: 719-728.

De Raedt T, Walton Z, Yecies JL, Li D, Chen Y, Malone CF, Maertens O, Jeong SM, Bronson RT, Lebleu V et al. 2011. Exploiting cancer cell vulnerabilities to develop a combination therapy for ras-driven tumors. *Cancer Cell* **20**: 400-413.

Deckers M, van Dinther M, Buijs J, Que I, Lowik C, van der Pluijm G, ten Dijke P. 2006. The tumor suppressor Smad4 is required for transforming growth factor beta-induced epithelial to mesenchymal transition and bone metastasis of breast cancer cells. *Cancer Res* **66**: 2202-2209.

Di Cristofano A, Kotsi P, Peng YF, Cordon-Cardo C, Elkon KB, Pandolfi PP. 1999. Impaired Fas response and autoimmunity in Pten+/- mice. *Science* **285**: 2122-2125.

Dickins RA, Hemann MT, Zilfou JT, Simpson DR, Ibarra I, Hannon GJ, Lowe SW. 2005. Probing tumor phenotypes using stable and regulated synthetic microRNA precursors. *Nat Genet* **37**: 1289-1295.

Ding L, Getz G, Wheeler DA, Mardis ER, McLellan MD, Cibulskis K, Sougnez C, Greulich H, Muzny DM, Morgan MB et al. 2008. Somatic mutations affect key pathways in lung adenocarcinoma. *Nature* **455**: 1069-1075.

Dinh P, Sotiriou C, Piccart MJ. 2007. The evolution of treatment strategies: aiming at the target. *Breast* **16 Suppl 2**: S10-16.

Dourdin N, Schade B, Lesurf R, Hallett M, Munn RJ, Cardiff RD, Muller WJ. 2008. Phosphatase and tensin homologue deleted on chromosome 10 deficiency accelerates tumor induction in a mouse model of ErbB-2 mammary tumorigenesis. *Cancer Res* **68**: 2122-2131.

Dow LE, Premsrirut PK, Zuber J, Fellmann C, McJunkin K, Miething C, Park Y, Dickins RA, Hannon GJ, Lowe SW. 2012. A pipeline for the generation of shRNA transgenic mice. *Nat Protoc* **7**: 374-393.

Duncan JS, Whittle MC, Nakamura K, Abell AN, Midland AA, Zawistowski JS, Johnson NL, Granger DA, Jordan NV, Darr DB et al. 2012. Dynamic reprogramming of the kinome in response to targeted MEK inhibition in triple-negative breast cancer. *Cell* **149**: 307-321.

Egeblad M, Ewald AJ, Askautrud HA, Truitt ML, Welm BE, Bainbridge E, Peeters G, Krummel MF, Werb Z. 2008. Visualizing stromal cell dynamics in different tumor microenvironments by spinning disk confocal microscopy. *Dis Model Mech* **1**: 155-167; discussion 165.

Egeblad M, Rasch MG, Weaver VM. 2010. Dynamic interplay between the collagen scaffold and tumor evolution. *Curr Opin Cell Biol* **22**: 697-706.

Eggan K, Akutsu H, Loring J, Jackson-Grusby L, Klemm M, Rideout WM, 3rd, Yanagimachi R, Jaenisch R. 2001. Hybrid vigor, fetal overgrowth, and viability of mice derived by nuclear cloning and tetraploid embryo complementation. *Proc Natl Acad Sci U S A* **98**: 6209-6214.

Elbashir SM, Harborth J, Lendeckel W, Yalcin A, Weber K, Tuschl T. 2001. Duplexes of 21-nucleotide RNAs mediate RNA interference in cultured mammalian cells. *Nature* **411**: 494-498.

Esteva FJ, Valero V, Booser D, Guerra LT, Murray JL, Pusztai L, Cristofanilli M, Arun B, Esmaeli B, Fritsche HA et al. 2002. Phase II study of weekly docetaxel and trastuzumab for patients with HER-2-overexpressing metastatic breast cancer. *J Clin Oncol* **20**: 1800-1808.

Feilotter HE, Coulon V, McVeigh JL, Boag AH, Dorion-Bonnet F, Duboue B, Latham WC, Eng C, Mulligan LM, Longy M. 1999. Analysis of the 10q23 chromosomal region and the PTEN gene in human sporadic breast carcinoma. *Br J Cancer* **79**: 718-723.

Fellmann C, Zuber J, McJunkin K, Chang K, Malone CD, Dickins RA, Xu Q, Hengartner MO, Elledge SJ, Hannon GJ et al. 2011. Functional identification of optimized RNAi triggers using a massively parallel sensor assay. *Mol Cell* **41**: 733-746.

Fendly BM, Kotts C, Vetterlein D, Lewis GD, Winget M, Carver ME, Watson SR, Sarup J, Saks S, Ullrich A et al. 1990. The extracellular domain of HER2/neu is a potential immunogen for active specific immunotherapy of breast cancer. *J Biol Response Mod* **9**: 449-455.

Finkle D, Quan ZR, Asghari V, Kloss J, Ghaboosi N, Mai E, Wong WL, Hollingshead P, Schwall R, Koeppen H et al. 2004. HER2-targeted therapy reduces incidence and progression of midlife mammary tumors in female murine mammary tumor virus huHER2-transgenic mice. *Clin Cancer Res* **10**: 2499-2511.

Fire A, Xu S, Montgomery MK, Kostas SA, Driver SE, Mello CC. 1998. Potent and specific genetic interference by double-stranded RNA in Caenorhabditis elegans. *Nature* **391**: 806-811.

Forbes SA, Bindal N, Bamford S, Cole C, Kok CY, Beare D, Jia M, Shepherd R, Leung K, Menzies A et al. 2011. COSMIC: mining complete cancer genomes in the Catalogue of Somatic Mutations in Cancer. *Nucleic Acids Res* **39**: D945-950.

Fujita T, Doihara H, Kawasaki K, Takabatake D, Takahashi H, Washio K, Tsukuda K, Ogasawara Y, Shimizu N. 2006. PTEN activity could be a predictive marker of trastuzumab efficacy in the treatment of ErbB2-overexpressing breast cancer. *Br J Cancer* **94**: 247-252.

Futreal PA, Kasprzyk A, Birney E, Mullikin JC, Wooster R, Stratton MR. 2001. Cancer and genomics. *Nature* **409**: 850-852.

Gallardo A, Lerma E, Escuin D, Tibau A, Munoz J, Ojeda B, Barnadas A, Adrover E, Sanchez-Tejada L, Giner D et al. 2012. Increased signalling of EGFR and IGF1R, and deregulation of PTEN/PI3K/Akt pathway are related with trastuzumab resistance in HER2 breast carcinomas. *Br J Cancer* **106**: 1367-1373.

Garcia JM, Silva JM, Dominguez G, Gonzalez R, Navarro A, Carretero L, Provencio M, Espana P, Bonilla F. 1999. Allelic loss of the PTEN region (10q23) in breast carcinomas of poor pathophenotype. *Breast Cancer Res Treat* **57**: 237-243.

Gelber RD, Bonetti M, Castiglione-Gertsch M, Coates AS, Goldhirsch A. 2003. Tailoring adjuvant treatments for the individual breast cancer patient. *Breast* **12**: 558-568.

Gossen M, Bujard H. 1992. Tight control of gene expression in mammalian cells by tetracycline-responsive promoters. *Proc Natl Acad Sci U S A* **89**: 5547-5551.

Gossen M, Freundlieb S, Bender G, Muller G, Hillen W, Bujard H. 1995. Transcriptional activation by tetracyclines in mammalian cells. *Science* **268**: 1766-1769.

Goswami S, Sahai E, Wyckoff JB, Cammer M, Cox D, Pixley FJ, Stanley ER, Segall JE, Condeelis JS. 2005. Macrophages promote the invasion of breast carcinoma cells via a colony-stimulating factor-1/epidermal growth factor paracrine loop. *Cancer Res* **65**: 5278-5283.

Greenman C, Stephens P, Smith R, Dalgliesh GL, Hunter C, Bignell G, Davies H, Teague J, Butler A, Stevens C et al. 2007. Patterns of somatic mutation in human cancer genomes. *Nature* **446**: 153-158.

Gunther EJ, Belka GK, Wertheim GB, Wang J, Hartman JL, Boxer RB, Chodosh LA. 2002. A novel doxycycline-inducible system for the transgenic analysis of mammary gland biology. *FASEB J* **16**: 283-292.

Guran S, Safali M. 2005. A case of neurofibromatosis and breast cancer: loss of heterozygosity of NF1 in breast cancer. *Cancer Genet Cytogenet* **156**: 86-88.

Guy CT, Cardiff RD, Muller WJ. 1992a. Induction of mammary tumors by expression of polyomavirus middle T oncogene: a transgenic mouse model for metastatic disease. *Mol Cell Biol* **12**: 954-961.

Guy CT, Webster MA, Schaller M, Parsons TJ, Cardiff RD, Muller WJ. 1992b. Expression of the neu protooncogene in the mammary epithelium of transgenic mice induces metastatic disease. *Proc Natl Acad Sci U S A* **89**: 10578-10582.

Haider S, Ballester B, Smedley D, Zhang J, Rice P, Kasprzyk A. 2009. BioMart Central Portal--unified access to biological data. *Nucleic Acids Res* **37**: W23-27.

Hall HG, Farson DA, Bissell MJ. 1982. Lumen formation by epithelial cell lines in response to collagen overlay: a morphogenetic model in culture. *Proc Natl Acad Sci U S A* **79**: 4672-4676.

Hanahan D, Weinberg RA. 2000. The hallmarks of cancer. *Cell* **100**: 57-70.

-. 2011. Hallmarks of cancer: the next generation. *Cell* **144**: 646-674.

Hannon GJ. 2002. RNA interference. *Nature* **418**: 244-251.

Harvey HA. 1996. Aromatase inhibitors in clinical practice: current status and a look to the future. *Semin Oncol* **23**: 33-38.

Haverty PM, Fridlyand J, Li L, Getz G, Beroukhim R, Lohr S, Wu TD, Cavet G, Zhang Z, Chant J. 2008. High-resolution genomic and expression analyses of copy number alterations in breast tumors. *Genes Chromosomes Cancer* **47**: 530-542.

Haybittle JL, Blamey RW, Elston CW, Johnson J, Doyle PJ, Campbell FC, Nicholson RI, Griffiths K. 1982. A prognostic index in primary breast cancer. *Br J Cancer* **45**: 361-366.

Hennighausen L, Wall RJ, Tillmann U, Li M, Furth PA. 1995. Conditional gene expression in secretory tissues and skin of transgenic mice using the MMTV-LTR and the tetracycline responsive system. *J Cell Biochem* **59**: 463-472.

Henrard D, Ross SR. 1988. Endogenous mouse mammary tumor virus is expressed in several organs in addition to the lactating mammary gland. *J Virol* **62**: 3046-3049.

Herschkowitz JI, Simin K, Weigman VJ, Mikaelian I, Usary J, Hu Z, Rasmussen KE, Jones LP, Assefnia S, Chandrasekharan S et al. 2007. Identification of conserved gene expression features between murine mammary carcinoma models and human breast tumors. *Genome Biol* **8**: R76.

Hicks J, Krasnitz A, Lakshmi B, Navin NE, Riggs M, Leibu E, Esposito D, Alexander J, Troge J, Grubor V et al. 2006. Novel patterns of genome rearrangement and their association with survival in breast cancer. *Genome Res* **16**: 1465-1479.

Hochedlinger K, Yamada Y, Beard C, Jaenisch R. 2005. Ectopic expression of Oct-4 blocks progenitor-cell differentiation and causes dysplasia in epithelial tissues. *Cell* **121**: 465-477.

Hudziak RM, Lewis GD, Winget M, Fendly BM, Shepard HM, Ullrich A. 1989. p185HER2 monoclonal antibody has antiproliferative effects in vitro and sensitizes human breast tumor cells to tumor necrosis factor. *Mol Cell Biol* **9**: 1165-1172.

Huesken D, Lange J, Mickanin C, Weiler J, Asselbergs F, Warner J, Meloon B, Engel S, Rosenberg A, Cohen D et al. 2005. Design of a genome-wide siRNA library using an artificial neural network. *Nat Biotechnol* **23**: 995-1001.

Huijbers IJ, Krimpenfort P, Berns A, Jonkers J. 2011. Rapid validation of cancer genes in chimeras derived from established genetically engineered mouse models. *Bioessays* **33**: 701-710.

Ingberg E, Theodorsson A, Theodorsson E, Strom JO. 2012. Methods for long-term 17beta-estradiol administration to mice. *Gen Comp Endocrinol* **175**: 188-193.

Inoue Y, Izawa K, Kiryu S, Tojo A, Ohtomo K. 2008. Diet and abdominal autofluorescence detected by in vivo fluorescence imaging of living mice. *Mol Imaging* **7**: 21-27.

Jelovac D, Wolff AC. 2012. The adjuvant treatment of HER2-positive breast cancer. *Curr Treat Options Oncol* **13**: 230-239.

Jerry DJ, Medina D, Butel JS. 1994. p53 mutations in COMMA-D cells. *In Vitro Cell Dev Biol Anim* **30A**: 87-89.

Jones N, Bonnet F, Sfar S, Lafitte M, Lafon D, Sierankowski G, Brouste V, Banneau G, Tunon de Lara C, Debled M et al. 2013. Comprehensive analysis of PTEN status in breast carcinomas. *Int J Cancer*.

Jonkers J, Meuwissen R, van der Gulden H, Peterse H, van der Valk M, Berns A. 2001. Synergistic tumor suppressor activity of BRCA2 and p53 in a conditional mouse model for breast cancer. *Nat Genet* **29**: 418-425.

Jordan VC, Dowse LJ. 1976. Tamoxifen as an anti-tumour agent: effect on oestrogen binding. *J Endocrinol* **68**: 297-303.

Kalra R, Paderanga DC, Olson K, Shannon KM. 1994. Genetic analysis is consistent with the hypothesis that NF1 limits myeloid cell growth through p21ras. *Blood* **84**: 3435-3439.

Kim MY, Oskarsson T, Acharyya S, Nguyen DX, Zhang XH, Norton L, Massague J. 2009. Tumor self-seeding by circulating cancer cells. *Cell* **139**: 1315-1326.

King CR, Kraus MH, Aaronson SA. 1985. Amplification of a novel v-erbB-related gene in a human mammary carcinoma. *Science* **229**: 974-976.

Klarenbeek S, van Miltenburg MH, Jonkers J. 2013. Genetically engineered mouse models of PI3K signaling in breast cancer. *Mol Oncol*.

Kluger HM, Chelouche Lev D, Kluger Y, McCarthy MM, Kiriakova G, Camp RL, Rimm DL, Price JE. 2005. Using a xenograft model of human breast cancer metastasis to find genes associated with clinically aggressive disease. *Cancer Res* **65**: 5578-5587.

Knudson AG. 2001. Two genetic hits (more or less) to cancer. *Nat Rev Cancer* **1**: 157-162.

Knudson AG, Jr. 1971. Mutation and cancer: statistical study of retinoblastoma. *Proc Natl Acad Sci U S A* **68**: 820-823.

Lacroix M, Leclercq G. 2004. Relevance of breast cancer cell lines as models for breast tumours: an update. *Breast Cancer Res Treat* **83**: 249-289.

Lee J, Wang J, Torbenson M, Lu Y, Liu QZ, Li S. 2010. Loss of SDHB and NF1 genes in a malignant phyllodes tumor of the breast as detected by oligo-array comparative genomic hybridization. *Cancer Genet Cytogenet* **196**: 179-183.

Lee RC, Feinbaum RL, Ambros V. 1993. The C. elegans heterochronic gene lin-4 encodes small RNAs with antisense complementarity to lin-14. *Cell* **75**: 843-854.

Leong AS, Zhuang Z. 2011. The changing role of pathology in breast cancer diagnosis and treatment. *Pathobiology* **78**: 99-114.

Ley TJ, Mardis ER, Ding L, Fulton B, McLellan MD, Chen K, Dooling D, Dunford-Shore BH, McGrath S, Hickenbotham M et al. 2008. DNA sequencing of a cytogenetically normal acute myeloid leukaemia genome. *Nature* **456**: 66-72.

Li DM, Sun H. 1997. TEP1, encoded by a candidate tumor suppressor locus, is a novel protein tyrosine phosphatase regulated by transforming growth factor beta. *Cancer Res* **57**: 2124-2129.

Li G, Robinson GW, Lesche R, Martinez-Diaz H, Jiang Z, Rozengurt N, Wagner KU, Wu DC, Lane TF, Liu X et al. 2002. Conditional loss of PTEN leads to precocious development and neoplasia in the mammary gland. *Development* **129**: 4159-4170.

Li J, Yen C, Liaw D, Podsypanina K, Bose S, Wang SI, Puc J, Miliaresis C, Rodgers L, McCombie R et al. 1997. PTEN, a putative protein tyrosine phosphatase gene mutated in human brain, breast, and prostate cancer. *Science* **275**: 1943-1947.

Liaw D, Marsh DJ, Li J, Dahia PL, Wang SI, Zheng Z, Bose S, Call KM, Tsou HC, Peacocke M et al. 1997. Germline mutations of the PTEN gene in Cowden disease, an inherited breast and thyroid cancer syndrome. *Nat Genet* **16**: 64-67.

Lin SC, Lee KF, Nikitin AY, Hilsenbeck SG, Cardiff RD, Li A, Kang KW, Frank SA, Lee WH, Lee EY. 2004. Somatic mutation of p53 leads to estrogen receptor alpha-positive and -negative mouse mammary tumors with high frequency of metastasis. *Cancer Res* **64**: 3525-3532.

Lin TP. 1966. Microinjection of mouse eggs. *Science* **151**: 333-337.

Linder CC. 2006. Genetic variables that influence phenotype. *ILAR J* **47**: 132-140.

Litton JK, Arun BK, Brown PH, Hortobagyi GN. 2012. Aromatase inhibitors and breast cancer prevention. *Expert Opin Pharmacother* **13**: 325-331.

Lucito R, Healy J, Alexander J, Reiner A, Esposito D, Chi M, Rodgers L, Brady A, Sebat J, Troge J et al. 2003. Representational oligonucleotide microarray analysis: a high-resolution method to detect genome copy number variation. *Genome Res* **13**: 2291-2305.

MacDonald IC, Chambers AF. 2006. Breast cancer metastasis progression as revealed by intravital videomicroscopy. *Expert Rev Anticancer Ther* **6**: 1271-1279.

Maehama T, Dixon JE. 1998. The tumor suppressor, PTEN/MMAC1, dephosphorylates the lipid second messenger, phosphatidylinositol 3,4,5-trisphosphate. *J Biol Chem* **273**: 13375-13378.

Maeshima AM, Omatsu M, Tsuta K, Asamura H, Matsuno Y. 2008. Immunohistochemical expression of TTF-1 in various cytological subtypes of primary lung adenocarcinoma, with special reference to intratumoral heterogeneity. *Pathol Int* **58**: 31-37.

Mardis ER. 2008. The impact of next-generation sequencing technology on genetics. *Trends Genet* **24**: 133-141.

Martins CP, Brown-Swigart L, Evan GI. 2006. Modeling the therapeutic efficacy of p53 restoration in tumors. *Cell* **127**: 1323-1334.

McCurrach ME, Lowe SW. 2001. Methods for studying pro- and antiapoptotic genes in nonimmortal cells. *Methods Cell Biol* **66**: 197-227.

McJunkin K, Mazurek A, Premsrirut PK, Zuber J, Dow LE, Simon J, Stillman B, Lowe SW. 2011. Reversible suppression of an essential gene in adult mice using transgenic RNA interference. *Proc Natl Acad Sci U S A* **108**: 7113-7118.

McLendon R, Friedman A, Bigner D, Van Meir EG, Brat DJ, Mastrogianakis GM, Olson JJ, Mikkelsen T, Lehman N, Aldape K Y et al. 2008. Comprehensive genomic characterization defines human glioblastoma genes and core pathways. *Nature* **455**: 1061-1068.

Medina D, Oborn CJ, Kittrell FS, Ullrich RL. 1986. Properties of mouse mammary epithelial cell lines characterized by in vivo transplantation and in vitro immunocytochemical methods. *J Natl Cancer Inst* **76**: 1143-1156.

Minn AJ, Gupta GP, Siegel PM, Bos PD, Shu W, Giri DD, Viale A, Olshen AB, Gerald WL, Massague J. 2005. Genes that mediate breast cancer metastasis to lung. *Nature* **436**: 518-524.

Miron A, Varadi M, Carrasco D, Li H, Luongo L, Kim HJ, Park SY, Cho EY, Lewis G, Kehoe S et al. 2010. PIK3CA mutations in in situ and invasive breast carcinomas. *Cancer Res* **70**: 5674-5678.

Moasser MM. 2007. The oncogene HER2: its signaling and transforming functions and its role in human cancer pathogenesis. *Oncogene* **26**: 6469-6487.

Moldvay J, Jackel M, Bogos K, Soltesz I, Agocs L, Kovacs G, Schaff Z. 2004. The role of TTF-1 in differentiating primary and metastatic lung adenocarcinomas. *Pathol Oncol Res* **10**: 85-88.

Molina MA, Codony-Servat J, Albanell J, Rojo F, Arribas J, Baselga J. 2001. Trastuzumab (herceptin), a humanized anti-Her2 receptor monoclonal antibody, inhibits basal and activated Her2 ectodomain cleavage in breast cancer cells. *Cancer Res* **61**: 4744-4749.

Montel V, Huang TY, Mose E, Pestonjamasp K, Tarin D. 2005. Expression profiling of primary tumors and matched lymphatic and lung metastases in a xenogeneic breast cancer model. *Am J Pathol* **166**: 1565-1579.

Montemurro F, Rossi V, Geuna E, Valabrega G, Martinello R, Milani A, Aglietta M. 2012. Current status and future perspectives in the endocrine treatment of postmenopausal, hormone receptor-positive metastatic breast cancer. *Expert Opin Pharmacother* **13**: 2143-2156.

Moody SE, Perez D, Pan TC, Sarkisian CJ, Portocarrero CP, Sterner CJ, Notorfrancesco KL, Cardiff RD, Chodosh LA. 2005. The transcriptional repressor Snail promotes mammary tumor recurrence. *Cancer Cell* **8**: 197-209.

Moody SE, Sarkisian CJ, Hahn KT, Gunther EJ, Pickup S, Dugan KD, Innocent N, Cardiff RD, Schnall MD, Chodosh LA. 2002. Conditional activation of Neu in the mammary epithelium of transgenic mice results in reversible pulmonary metastasis. *Cancer Cell* **2**: 451-461.

Moser AR, Pitot HC, Dove WF. 1990. A dominant mutation that predisposes to multiple intestinal neoplasia in the mouse. *Science* **247**: 322-324.

Mullally A, Ebert BL. 2010. NF1 inactivation revs up Ras in adult acute myelogenous leukemia. *Clin Cancer Res* **16**: 4074-4076.

Muller WJ, Sinn E, Pattengale PK, Wallace R, Leder P. 1988. Single-step induction of mammary adenocarcinoma in transgenic mice bearing the activated c-neu oncogene. *Cell* **54**: 105-115.

Nagata Y, Lan KH, Zhou X, Tan M, Esteva FJ, Sahin AA, Klos KS, Li P, Monia BP, Nguyen NT et al. 2004. PTEN activation contributes to tumor inhibition by trastuzumab, and loss of PTEN predicts trastuzumab resistance in patients. *Cancer Cell* **6**: 117-127.

Navin N, Kendall J, Troge J, Andrews P, Rodgers L, McIndoo J, Cook K, Stepansky A, Levy D, Esposito D et al. 2011. Tumour evolution inferred by single-cell sequencing. *Nature* **472**: 90-94.

Navin N, Krasnitz A, Rodgers L, Cook K, Meth J, Kendall J, Riggs M, Eberling Y, Troge J, Grubor V et al. 2010. Inferring tumor progression from genomic heterogeneity. *Genome Res* **20**: 68-80.

Neve RM, Chin K, Fridlyand J, Yeh J, Baehner FL, Fevr T, Clark L, Bayani N, Coppe JP, Tong F et al. 2006. A collection of breast cancer cell lines for the study of functionally distinct cancer subtypes. *Cancer Cell* **10**: 515-527.

O'Reilly KE, Rojo F, She QB, Solit D, Mills GB, Smith D, Lane H, Hofmann F, Hicklin DJ, Ludwig DL et al. 2006. mTOR inhibition induces upstream receptor tyrosine kinase signaling and activates Akt. *Cancer Res* **66**: 1500-1508.

Ogata H, Sato H, Takatsuka J, De Luca LM. 2001. Human breast cancer MDA-MB-231 cells fail to express the neurofibromin protein, lack its type I mRNA isoform and show accumulation of P-MAPK and activated Ras. *Cancer Lett* **172**: 159-164.

Orimo A, Gupta PB, Sgroi DC, Arenzana-Seisdedos F, Delaunay T, Naeem R, Carey VJ, Richardson AL, Weinberg RA. 2005. Stromal fibroblasts present in invasive human breast carcinomas promote tumor growth and angiogenesis through elevated SDF-1/CXCL12 secretion. *Cell* **121**: 335-348.

Owens RB. 1974. Glandular epithelial cells from mice: a method for selective cultivation. *J Natl Cancer Inst* **52**: 1375-1378.

Oxnard GR. 2012. Strategies for overcoming acquired resistance to epidermal growth factor receptor: targeted therapies in lung cancer. *Arch Pathol Lab Med* **136**: 1205-1209.

Paddison PJ, Caudy AA, Bernstein E, Hannon GJ, Conklin DS. 2002. Short hairpin RNAs (shRNAs) induce sequence-specific silencing in mammalian cells. *Genes Dev* **16**: 948-958.

Pauletti G, Godolphin W, Press MF, Slamon DJ. 1996. Detection and quantitation of HER-2/neu gene amplification in human breast cancer archival material using fluorescence in situ hybridization. *Oncogene* **13**: 63-72.

Perez EA, Spano JP. 2012. Current and emerging targeted therapies for metastatic breast cancer. *Cancer* **118**: 3014-3025.

Perou CM, Sorlie T, Eisen MB, van de Rijn M, Jeffrey SS, Rees CA, Pollack JR, Ross DT, Johnsen H, Akslen LA et al. 2000. Molecular portraits of human breast tumours. *Nature* **406**: 747-752.

Perren A, Weng LP, Boag AH, Ziebold U, Thakore K, Dahia PL, Komminoth P, Lees JA, Mulligan LM, Mutter GL et al. 1999. Immunohistochemical evidence of loss of PTEN expression in primary ductal adenocarcinomas of the breast. *Am J Pathol* **155**: 1253-1260.

Petit AM, Rak J, Hung MC, Rockwell P, Goldstein N, Fendly B, Kerbel RS. 1997. Neutralizing antibodies against epidermal growth factor and ErbB-2/neu receptor tyrosine kinases down-regulate vascular endothelial growth factor production by tumor cells in vitro and in vivo: angiogenic implications for signal transduction therapy of solid tumors. *Am J Pathol* **151**: 1523-1530.

Piek E, Moustakas A, Kurisaki A, Heldin CH, ten Dijke P. 1999. TGF-(beta) type I receptor/ALK-5 and Smad proteins mediate epithelial to mesenchymal transdifferentiation in NMuMG breast epithelial cells. *J Cell Sci* **112 (Pt 24)**: 4557-4568.

Podsypanina K, Politi K, Beverly LJ, Varmus HE. 2008. Oncogene cooperation in tumor maintenance and tumor recurrence in mouse mammary tumors induced by Myc and mutant Kras. *Proc Natl Acad Sci U S A* **105**: 5242-5247.

Polyak K, Kalluri R. 2010. The role of the microenvironment in mammary gland development and cancer. *Cold Spring Harb Perspect Biol* **2**: a003244.

Premsrirut PK, Dow LE, Kim SY, Camiolo M, Malone CD, Miething C, Scuoppo C, Zuber J, Dickins RA, Kogan SC et al. 2011. A rapid and scalable system for studying gene function in mice using conditional RNA interference. *Cell* **145**: 145-158.

Proia DA, Kuperwasser C. 2006. Reconstruction of human mammary tissues in a mouse model. *Nat Protoc* **1**: 206-214.

Pylayeva-Gupta Y, Grabocka E, Bar-Sagi D. 2011. RAS oncogenes: weaving a tumorigenic web. *Nat Rev Cancer* **11**: 761-774.

Reis-Filho JS, Carrilho C, Valenti C, Leitao D, Ribeiro CA, Ribeiro SG, Schmitt FC. 2000. Is TTF1 a good immunohistochemical marker to distinguish primary from metastatic lung adenocarcinomas? *Pathol Res Pract* **196**: 835-840.

Richert MM, Schwertfeger KL, Ryder JW, Anderson SM. 2000. An atlas of mouse mammary gland development. *J Mammary Gland Biol Neoplasia* **5**: 227-241.

Riond JL, Riviere JE. 1988. Pharmacology and toxicology of doxycycline. *Vet Hum Toxicol* **30**: 431-443.

Ripperger T, Gadzicki D, Meindl A, Schlegelberger B. 2009. Breast cancer susceptibility: current knowledge and implications for genetic counselling. *Eur J Hum Genet* **17**: 722-731.

Robertson D. 1998. Genentech's anticancer Mab expected by November. *Nat Biotechnol* **16**: 615.

Ross JS, Slodkowska EA, Symmans WF, Pusztai L, Ravdin PM, Hortobagyi GN. 2009. The HER-2 receptor and breast cancer: ten years of targeted anti-HER-2 therapy and personalized medicine. *Oncologist* **14**: 320-368.

Saal LH, Holm K, Maurer M, Memeo L, Su T, Wang X, Yu JS, Malmstrom PO, Mansukhani M, Enoksson J et al. 2005. PIK3CA mutations correlate with hormone receptors, node metastasis, and ERBB2, and are mutually exclusive with PTEN loss in human breast carcinoma. *Cancer Res* **65**: 2554-2559.

Sakamoto K, Schmidt JW, Wagner KU. 2012. Generation of a novel MMTV-tTA transgenic mouse strain for the targeted expression of genes in the embryonic and postnatal mammary gland. *PLoS One* **7**: e43778.

Salemis NS, Nakos G, Sambaziotis D, Gourgiotis S. 2010. Breast cancer associated with type 1 neurofibromatosis. *Breast Cancer* **17**: 306-309.

Sangha N, Wu R, Kuick R, Powers S, Mu D, Fiander D, Yuen K, Katabuchi H, Tashiro H, Fearon ER et al. 2008. Neurofibromin 1 (NF1) defects are common in human ovarian serous carcinomas and co-occur with TP53 mutations. *Neoplasia* **10**: 1362-1372, following 1372.

Sawey ET, Chanrion M, Cai C, Wu G, Zhang J, Zender L, Zhao A, Busuttil RW, Yee H, Stein L et al. 2011. Identification of a therapeutic strategy targeting amplified FGF19 in liver cancer by Oncogenomic screening. *Cancer Cell* **19**: 347-358.

Sawicki JA, Morris RJ, Monks B, Sakai K, Miyazaki J. 1998. A composite CMV-IE enhancer/beta-actin promoter is ubiquitously expressed in mouse cutaneous epithelium. *Exp Cell Res* **244**: 367-369.

Schade B, Rao T, Dourdin N, Lesurf R, Hallett M, Cardiff RD, Muller WJ. 2009. PTEN deficiency in a luminal ErbB-2 mouse model results in dramatic acceleration of mammary tumorigenesis and metastasis. *J Biol Chem* **284**: 19018-19026.

Schechter AL, Stern DF, Vaidyanathan L, Decker SJ, Drebin JA, Greene MI, Weinberg RA. 1984. The neu oncogene: an erb-B-related gene encoding a 185,000-Mr tumour antigen. *Nature* **312**: 513-516.

Schwertfeger KL, Rosen JM, Cohen DA. 2006. Mammary gland macrophages: pleiotropic functions in mammary development. *J Mammary Gland Biol Neoplasia* **11**: 229-238.

Scuoppo C, Miething C, Lindqvist L, Reyes J, Ruse C, Appelmann I, Yoon S, Krasnitz A, Teruya-Feldstein J, Pappin D et al. 2012. A tumour suppressor network relying on the polyamine-hypusine axis. *Nature* **487**: 244-248.

See WL, Tan IL, Mukherjee J, Nicolaides T, Pieper RO. 2012. Sensitivity of glioblastomas to clinically available MEK inhibitors is defined by neurofibromin 1 deficiency. *Cancer Res* **72**: 3350-3359.

Seidman AD, Fornier MN, Esteva FJ, Tan L, Kaptain S, Bach A, Panageas KS, Arroyo C, Valero V, Currie V et al. 2001. Weekly trastuzumab and paclitaxel therapy for metastatic breast cancer with analysis of efficacy by HER2 immunophenotype and gene amplification. *J Clin Oncol* **19**: 2587-2595.

Selbert S, Bentley DJ, Melton DW, Rannie D, Lourenco P, Watson CJ, Clarke AR. 1998. Efficient BLG-Cre mediated gene deletion in the mammary gland. *Transgenic Res* **7**: 387-396.

Serpi R, Klein-Rodewald T, Calzada-Wack J, Neff F, Schuster T, Gailus-Durner V, Fuchs H, Poutanen M, Hrabre de Angelis M, Esposito I. 2013. Inbred wild type mouse strains have distinct spontaneous morphological phenotypes. *Histol Histopathol* **28**: 79-88.

Shackleton M, Vaillant F, Simpson KJ, Stingl J, Smyth GK, Asselin-Labat ML, Wu L, Lindeman GJ, Visvader JE. 2006. Generation of a functional mammary gland from a single stem cell. *Nature* **439**: 84-88.

Shah SP, Morin RD, Khattra J, Prentice L, Pugh T, Burleigh A, Delaney A, Gelmon K, Guliany R, Senz J et al. 2009. Mutational evolution in a lobular breast tumour profiled at single nucleotide resolution. *Nature* **461**: 809-813.

Sharif S, Moran A, Huson SM, Iddenden R, Shenton A, Howard E, Evans DG. 2007. Women with neurofibromatosis 1 are at a moderately increased risk of developing breast cancer and should be considered for early screening. *J Med Genet* **44**: 481-484.

Shcherbo D, Murphy CS, Ermakova GV, Solovieva EA, Chepurnykh TV, Shcheglov AS, Verkhusha VV, Pletnev VZ, Hazelwood KL, Roche PM et al. 2009. Far-red fluorescent tags for protein imaging in living tissues. *Biochem J* **418**: 567-574.

Shree T, Olson OC, Elie BT, Kester JC, Garfall AL, Simpson K, Bell-McGuinn KM, Zabor EC, Brogi E, Joyce JA. 2011. Macrophages and cathepsin proteases blunt chemotherapeutic response in breast cancer. *Genes Dev* **25**: 2465-2479.

Siegel PM, Dankort DL, Hardy WR, Muller WJ. 1994. Novel activating mutations in the neu proto-oncogene involved in induction of mammary tumors. *Mol Cell Biol* **14**: 7068-7077.

Siegel PM, Ryan ED, Cardiff RD, Muller WJ. 1999. Elevated expression of activated forms of Neu/ErbB-2 and ErbB-3 are involved in the induction of mammary tumors in transgenic mice: implications for human breast cancer. *EMBO J* **18**: 2149-2164.

Silva JM, Li MZ, Chang K, Ge W, Golding MC, Rickles RJ, Siolas D, Hu G, Paddison PJ, Schlabach MR et al. 2005. Second-generation shRNA libraries covering the mouse and human genomes. *Nat Genet* **37**: 1281-1288.

Singh B, Ittmann MM, Krolewski JJ. 1998. Sporadic breast cancers exhibit loss of heterozygosity on chromosome segment 10q23 close to the Cowden disease locus. *Genes Chromosomes Cancer* **21**: 166-171.

Sinn E, Muller W, Pattengale P, Tepler I, Wallace R, Leder P. 1987. Coexpression of MMTV/v-Ha-ras and MMTV/c-myc genes in transgenic mice: synergistic action of oncogenes in vivo. *Cell* **49**: 465-475.

Slamon DJ, Clark GM, Wong SG, Levin WJ, Ullrich A, McGuire WL. 1987. Human breast cancer: correlation of relapse and survival with amplification of the HER-2/neu oncogene. *Science* **235**: 177-182.

Slamon DJ, Godolphin W, Jones LA, Holt JA, Wong SG, Keith DE, Levin WJ, Stuart SG, Udove J, Ullrich A et al. 1989. Studies of the HER-2/neu proto-oncogene in human breast and ovarian cancer. *Science* **244**: 707-712.

Slamon DJ, Leyland-Jones B, Shak S, Fuchs H, Paton V, Bajamonde A, Fleming T, Eiermann W, Wolter J, Pegram M et al. 2001. Use of chemotherapy plus a monoclonal antibody against HER2 for metastatic breast cancer that overexpresses HER2. *N Engl J Med* **344**: 783-792.

Sliwkowski MX, Lofgren JA, Lewis GD, Hotaling TE, Fendly BM, Fox JA. 1999. Nonclinical studies addressing the mechanism of action of trastuzumab (Herceptin). *Semin Oncol* **26**: 60-70.

Song MS, Salmena L, Pandolfi PP. 2012. The functions and regulation of the PTEN tumour suppressor. *Nat Rev Mol Cell Biol* **13**: 283-296.

Sorlie T, Perou CM, Tibshirani R, Aas T, Geisler S, Johnsen H, Hastie T, Eisen MB, van de Rijn M, Jeffrey SS et al. 2001. Gene expression patterns of breast carcinomas distinguish tumor subclasses with clinical implications. *Proc Natl Acad Sci U S A* **98**: 10869-10874.

Stambolic V, Suzuki A, de la Pompa JL, Brothers GM, Mirtsos C, Sasaki T, Ruland J, Penninger JM, Siderovski DP, Mak TW. 1998. Negative regulation of PKB/Akt-dependent cell survival by the tumor suppressor PTEN. *Cell* **95**: 29-39.

Steck PA, Pershouse MA, Jasser SA, Yung WK, Lin H, Ligon AH, Langford LA, Baumgard ML, Hattier T, Davis T et al. 1997. Identification of a candidate tumour suppressor gene, MMAC1, at chromosome 10q23.3 that is mutated in multiple advanced cancers. *Nat Genet* **15**: 356-362.

Stegmeier F, Hu G, Rickles RJ, Hannon GJ, Elledge SJ. 2005. A lentiviral microRNA-based system for single-copy polymerase II-regulated RNA interference in mammalian cells. *Proc Natl Acad Sci U S A* **102**: 13212-13217.

Stemke-Hale K, Gonzalez-Angulo AM, Lluch A, Neve RM, Kuo WL, Davies M, Carey M, Hu Z, Guan Y, Sahin A et al. 2008. An integrative genomic and proteomic analysis of PIK3CA, PTEN, and AKT mutations in breast cancer. *Cancer Res* **68**: 6084-6091.

Stewart TA, Pattengale PK, Leder P. 1984. Spontaneous mammary adenocarcinomas in transgenic mice that carry and express MTV/myc fusion genes. *Cell* **38**: 627-637.

Stingl J, Eirew P, Ricketson I, Shackleton M, Vaillant F, Choi D, Li HI, Eaves CJ. 2006. Purification and unique properties of mammary epithelial stem cells. *Nature* **439**: 993-997.

Stratton MR, Campbell PJ, Futreal PA. 2009. The cancer genome. *Nature* **458**: 719-724.

Tabernero J, Rojo F, Calvo E, Burris H, Judson I, Hazell K, Martinelli E, Ramon y Cajal S, Jones S, Vidal L et al. 2008. Dose- and schedule-dependent inhibition of the mammalian target of rapamycin pathway with everolimus: a phase I tumor pharmacodynamic study in patients with advanced solid tumors. *J Clin Oncol* **26**: 1603-1610.

Tanic N, Milovanovic Z, Dzodic R, Juranic Z, Susnjar S, Plesinac-Karapandzic V, Tatic S, Dramicanin T, Davidovic R, Dimitrijevic B. 2012. The impact of PTEN tumor suppressor gene on acquiring resistance to tamoxifen treatment in breast cancer patients. *Cancer Biol Ther* **13**: 1165-1174.

Tennis M, Singh B, Hjerpe A, Prochazka M, Czene K, Hall P, Shields PG. 2010. Pathological confirmation of primary lung cancer following breast cancer. *Lung Cancer* **69**: 40-45.

Troy T, Jekic-McMullen D, Sambucetti L, Rice B. 2004. Quantitative comparison of the sensitivity of detection of fluorescent and bioluminescent reporters in animal models. *Mol Imaging* **3**: 9-23.

Tsang RY, Finn RS. 2012. Beyond trastuzumab: novel therapeutic strategies in HER2-positive metastatic breast cancer. *Br J Cancer* **106**: 6-13.

Ursini-Siegel J, Hardy WR, Zuo D, Lam SH, Sanguin-Gendreau V, Cardiff RD, Pawson T, Muller WJ. 2008. ShcA signalling is essential for tumour progression in mouse models of human breast cancer. *EMBO J* **27**: 910-920.

Vargo-Gogola T, Rosen JM. 2007. Modelling breast cancer: one size does not fit all. *Nat Rev Cancer* **7**: 659-672.

Varticovski L, Hollingshead MG, Robles AI, Wu X, Cherry J, Munroe DJ, Lukes L, Anver MR, Carter JP, Borgel SD et al. 2007. Accelerated preclinical testing using transplanted tumors from genetically engineered mouse breast cancer models. *Clin Cancer Res* **13**: 2168-2177.

Velculescu VE. 2008. Defining the blueprint of the cancer genome. *Carcinogenesis* **29**: 1087-1091.

Ventura A, Kirsch DG, McLaughlin ME, Tuveson DA, Grimm J, Lintault L, Newman J, Reczek EE, Weissleder R, Jacks T. 2007. Restoration of p53 function leads to tumour regression in vivo. *Nature* **445**: 661-665.

Vogel CL, Cobleigh MA, Tripathy D, Gutheil JC, Harris LN, Fehrenbacher L, Slamon DJ, Murphy M, Novotny WF, Burchmore M et al. 2002. Efficacy and safety of trastuzumab as a single agent in first-line treatment of HER2-overexpressing metastatic breast cancer. *J Clin Oncol* **20**: 719-726.

Vonderhaar BK, Ginsburg E. 2000. Intramammary delivery of hormones, growth factors, and cytokines. in *Methods in Mammary Gland Biology and Breast Cancer Research* (eds. MIP Margot, BB Asch), pp. 97-99. Kluwer Academic/Plenum Publishers, Buffalo.

Voskoglou-Nomikos T, Pater JL, Seymour L. 2003. Clinical predictive value of the in vitro cell line, human xenograft, and mouse allograft preclinical cancer models. *Clin Cancer Res* **9**: 4227-4239.

Wagner KU, McAllister K, Ward T, Davis B, Wiseman R, Hennighausen L. 2001. Spatial and temporal expression of the Cre gene under the control of the MMTV-LTR in different lines of transgenic mice. *Transgenic Res* **10**: 545-553.

Wagner KU, Wall RJ, St-Onge L, Gruss P, Wynshaw-Boris A, Garrett L, Li M, Furth PA, Hennighausen L. 1997. Cre-mediated gene deletion in the mammary gland. *Nucleic Acids Res* **25**: 4323-4330.

Wallace JA, Li F, Leone G, Ostrowski MC. 2011. Pten in the breast tumor microenvironment: modeling tumor-stroma coevolution. *Cancer Res* **71**: 1203-1207.

Wallace MD, Pfefferle AD, Shen L, McNairn AJ, Cerami EG, Fallon BL, Rinaldi VD, Southard TL, Perou CM, Schimenti JC. 2012. Comparative oncogenomics implicates the neurofibromin 1 gene (NF1) as a breast cancer driver. *Genetics* **192**: 385-396.

Watring WG, Byfield JE, Lagasse LD, Lee YD, Juillard G, Jacobs M, Smith ML. 1974. Combination Adriamycin and radiation therapy in gynecologic cancers. *Gynecol Oncol* **2**: 518-526.

Whittaker SR, Theurillat JP, Van Allen E, Wagle N, Hsiao J, Cowley GS, Schadendorf D, Root DE, Garraway LA. 2013. A genome-scale RNA interference screen implicates NF1 loss in resistance to RAF inhibition. *Cancer Discov*.

Wightman B, Ha I, Ruvkun G. 1993. Posttranscriptional regulation of the heterochronic gene lin-14 by lin-4 mediates temporal pattern formation in C. elegans. *Cell* **75**: 855-862.

Wood LD, Parsons DW, Jones S, Lin J, Sjoblom T, Leary RJ, Shen D, Boca SM, Barber T, Ptak J et al. 2007. The genomic landscapes of human breast and colorectal cancers. *Science* **318**: 1108-1113.

Wyckoff JB, Wang Y, Lin EY, Li JF, Goswami S, Stanley ER, Segall JE, Pollard JW, Condeelis J. 2007. Direct visualization of macrophage-assisted tumor cell intravasation in mammary tumors. *Cancer Res* **67**: 2649-2656.

Xue W, Zender L, Miething C, Dickins RA, Hernando E, Krizhanovsky V, Cordon-Cardo C, Lowe SW. 2007. Senescence and tumour clearance is triggered by p53 restoration in murine liver carcinomas. *Nature* **445**: 656-660.

Yakes FM, Chinratanalab W, Ritter CA, King W, Seelig S, Arteaga CL. 2002. Herceptin-induced inhibition of phosphatidylinositol-3 kinase and Akt Is required for antibody-mediated effects on p27, cyclin D1, and antitumor action. *Cancer Res* **62**: 4132-4141.

Yang M, Nonaka D. 2010. A study of immunohistochemical differential expression in pulmonary and mammary carcinomas. *Mod Pathol* **23**: 654-661.

Yarden Y. 2001. Biology of HER2 and its importance in breast cancer. *Oncology* **61 Suppl 2**: 1-13.

Yarden Y, Sliwkowski MX. 2001. Untangling the ErbB signalling network. *Nat Rev Mol Cell Biol* **2**: 127-137.

Yin Y, Shen WH. 2008. PTEN: a new guardian of the genome. *Oncogene* **27**: 5443-5453.

Yu D, Hung MC. 2000. Overexpression of ErbB2 in cancer and ErbB2-targeting strategies. *Oncogene* **19**: 6115-6121.

Zender L, Xue W, Zuber J, Semighini CP, Krasnitz A, Ma B, Zender P, Kubicka S, Luk JM, Schirmacher P et al. 2008. An oncogenomics-based in vivo RNAi screen identifies tumor suppressors in liver cancer. *Cell* **135**: 852-864.

Zhang XH, Wang Q, Gerald W, Hudis CA, Norton L, Smid M, Foekens JA, Massague J. 2009. Latent bone metastasis in breast cancer tied to Src-dependent survival signals. *Cancer Cell* **16**: 67-78.

Zhao H, Langerod A, Ji Y, Nowels KW, Nesland JM, Tibshirani R, Bukholm IK, Karesen R, Botstein D, Borresen-Dale AL et al. 2004. Different gene expression patterns in invasive lobular and ductal carcinomas of the breast. *Mol Biol Cell* **15**: 2523-2536.

Zhu W, Michael CW. 2007. WT1, monoclonal CEA, TTF1, and CA125 antibodies in the differential diagnosis of lung, breast, and ovarian adenocarcinomas in serous effusions. *Diagn Cytopathol* **35**: 370-375.

Zuber J, McJunkin K, Fellmann C, Dow LE, Taylor MJ, Hannon GJ, Lowe SW. 2011a. Toolkit for evaluating genes required for proliferation and survival using tetracycline-regulated RNAi. *Nat Biotechnol* **29**: 79-83.

Zuber J, Radtke I, Pardee TS, Zhao Z, Rappaport AR, Luo W, McCurrach ME, Yang MM, Dolan ME, Kogan SC et al. 2009. Mouse models of human AML accurately predict chemotherapy response. *Genes Dev* **23**: 877-889.

Zuber J, Shi J, Wang E, Rappaport AR, Herrmann H, Sison EA, Magoon D, Qi J, Blatt K, Wunderlich M et al. 2011b. RNAi screen identifies Brd4 as a therapeutic target in acute myeloid leukaemia. *Nature* **478**: 524-528.

Appendix. Differential expression of TRE and TREtight promoters

In order to assess differences in the promoter expression patterns and levels between TRE and TREtight, a number of age-matched mice were treated with doxycycline and harvested side-by-side. GFP reporter expression as observed by gross examination using fluorescence microscopy. The spleen, kidney, liver, small intestine, colon, skin, pancreas, stomach, lung, heart and thymus were examined and GFP expression levels were documented. Brightfield and GFP images are shown for each organ type in the Appendix figures.

The first cohort of mice was designed to compare single vs. double copy of the Rosa26-rtTA2 allele using TREtight-GFP-shRLuc.713 and TREtight-GFP-shNF1.8594 littermate female mice. Dox treatment was started at 4 weeks of age for 18 days. An age-matched wild type control mouse was included (no dox treatment).

The second cohort sought to compare both single-copy R26-rtTA2 with CAGs-rtTA3 ("4288"), as well as TRE-GFP-miR30 vs. TREtight-GFP-miR30. The following mice were dox treated starting at 6 weeks of age for 16 days:

- CAGs-rtTA3 ; TtG-shRLuc (2 mice) and TtG-shRLuc only (1 mouse) littermates
- R26-rtTA2$^{+/-}$; TtG-shNF1.6074 (2 mice) and TtG-shNF1.6074 only (1 mouse) littermates
- CAGs-rtTA3 ; TG-shAPC.9365 (1 mouse)

The following mice were dox treated starting at 11 weeks of age for 2.5 months:

- R26-rtTA2 ; R26-Luciferase ; TG-shLuci.1309 on dox (two mice)
- R26-rtTA2 ; R26-Luciferase ; TG-shLuci.1309 off dox control (one mouse)

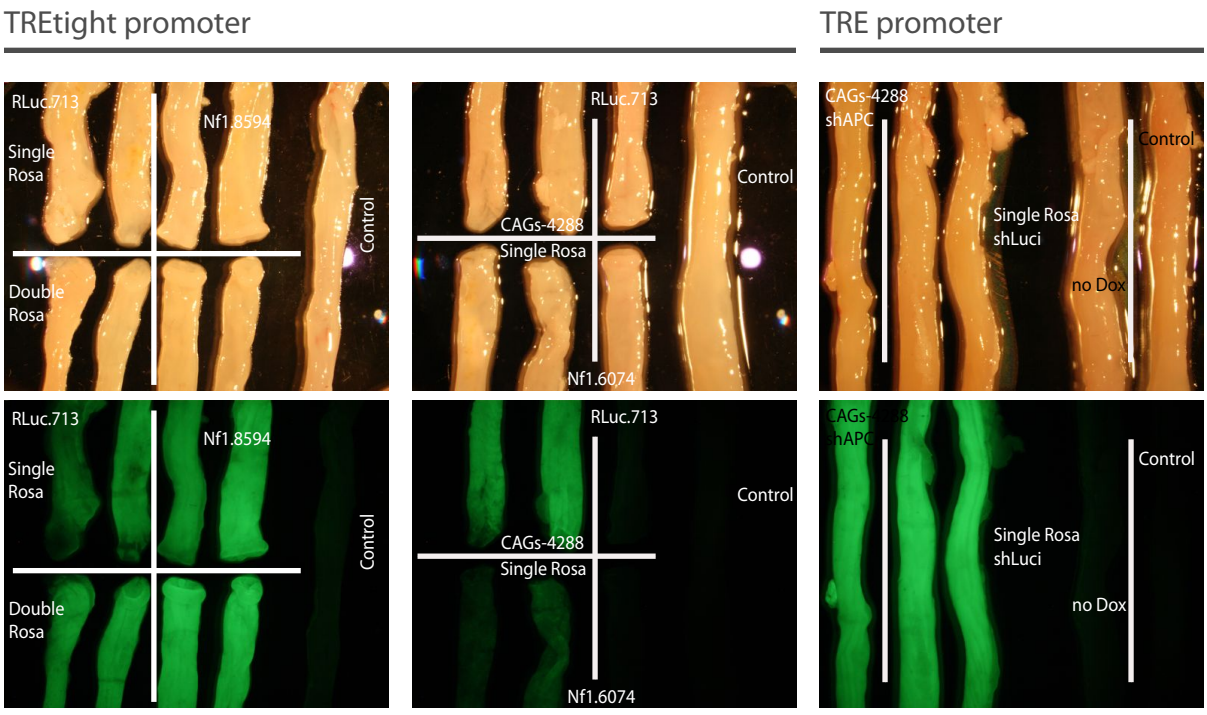

Appendix: Colon

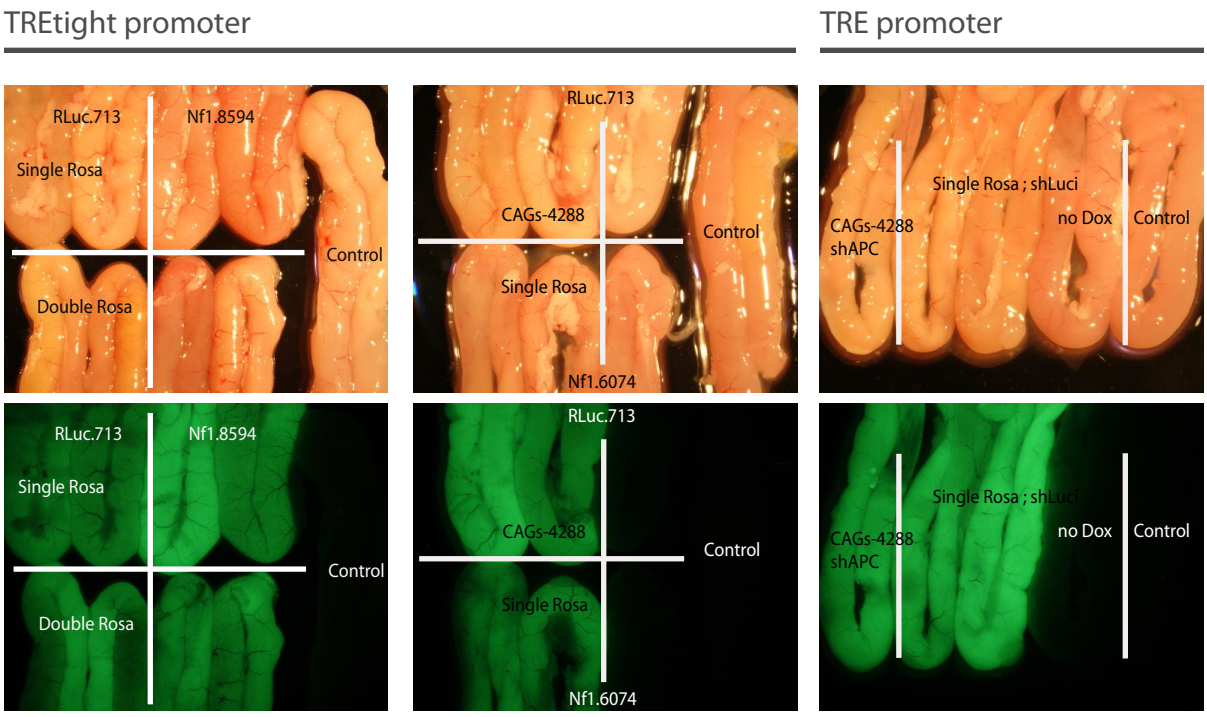

Appendix: Small intestine

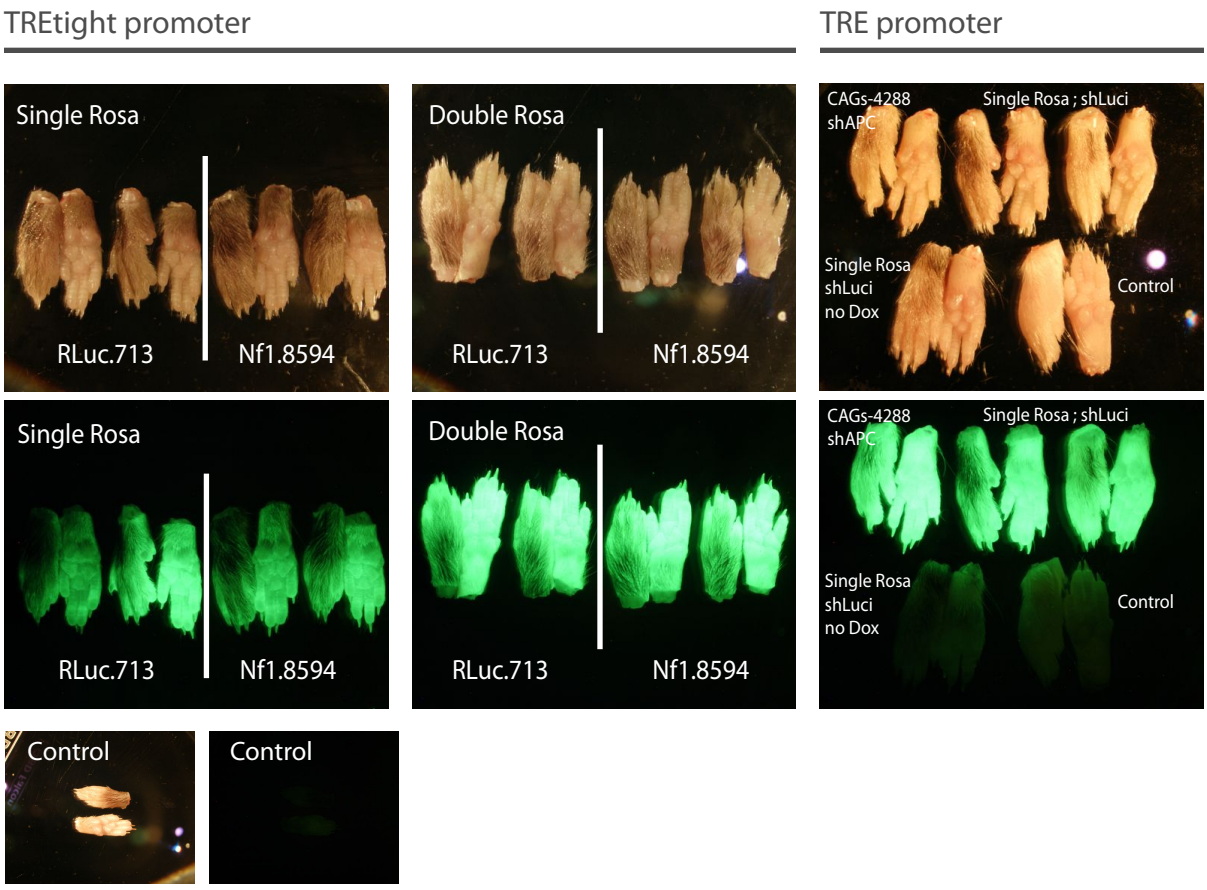

Appendix: Skin

TREtight promoter

TRE promoter

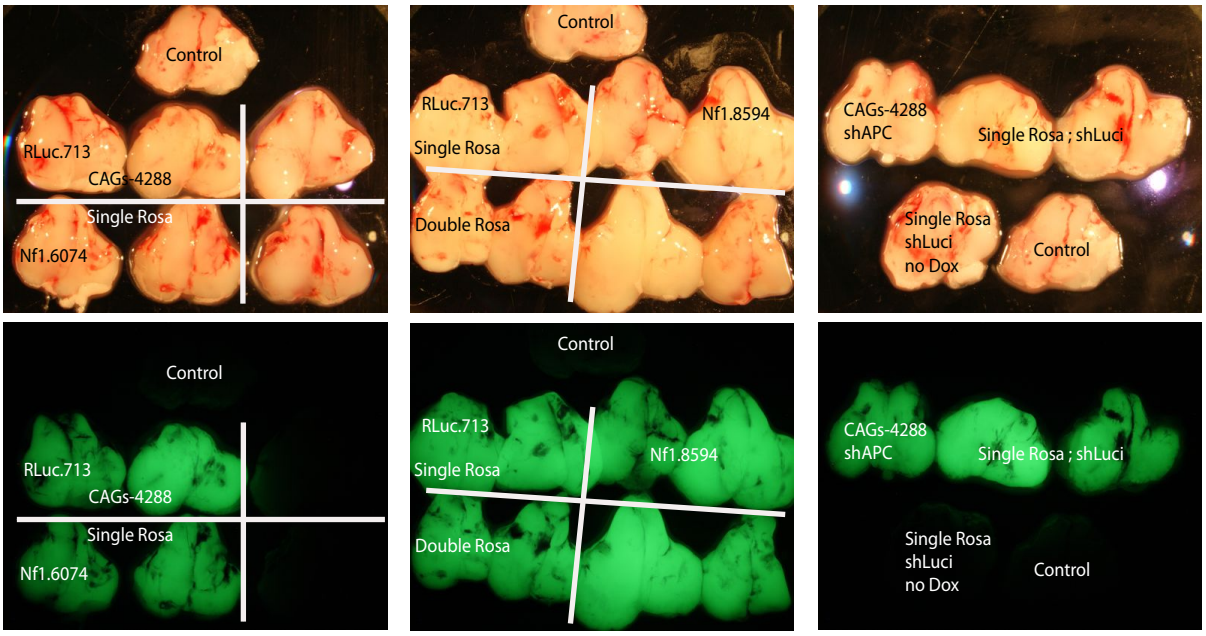

Appendix: Thymus

TREtight promoter

TRE promoter

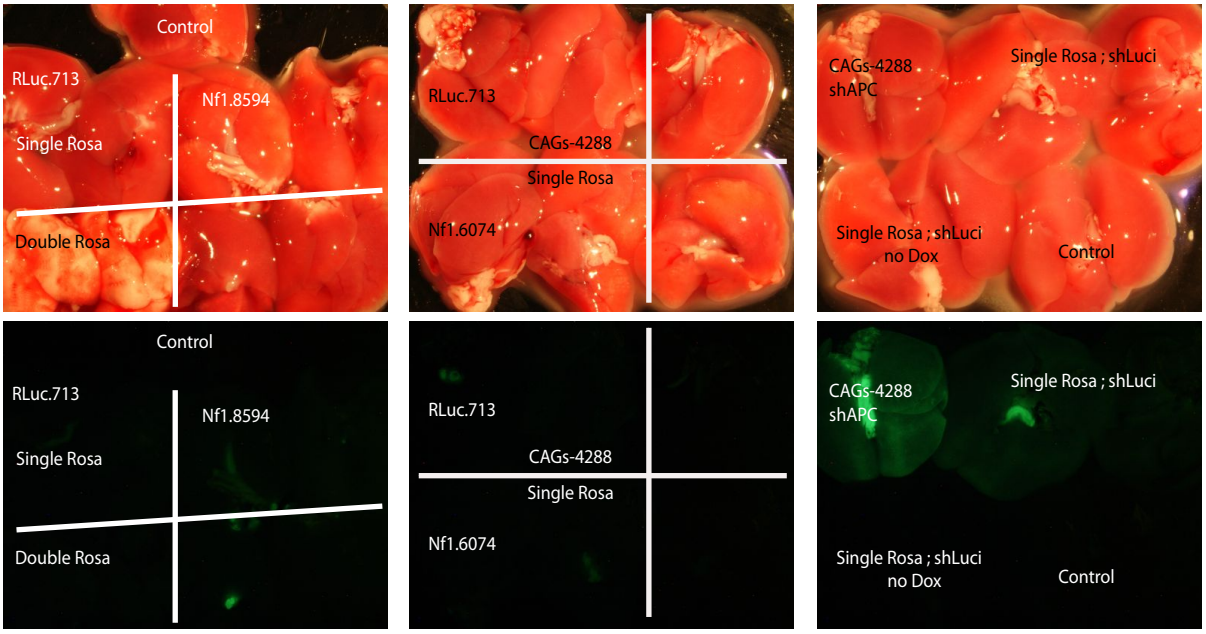

Appendix: Lung

TREtight promoter

TRE promoter

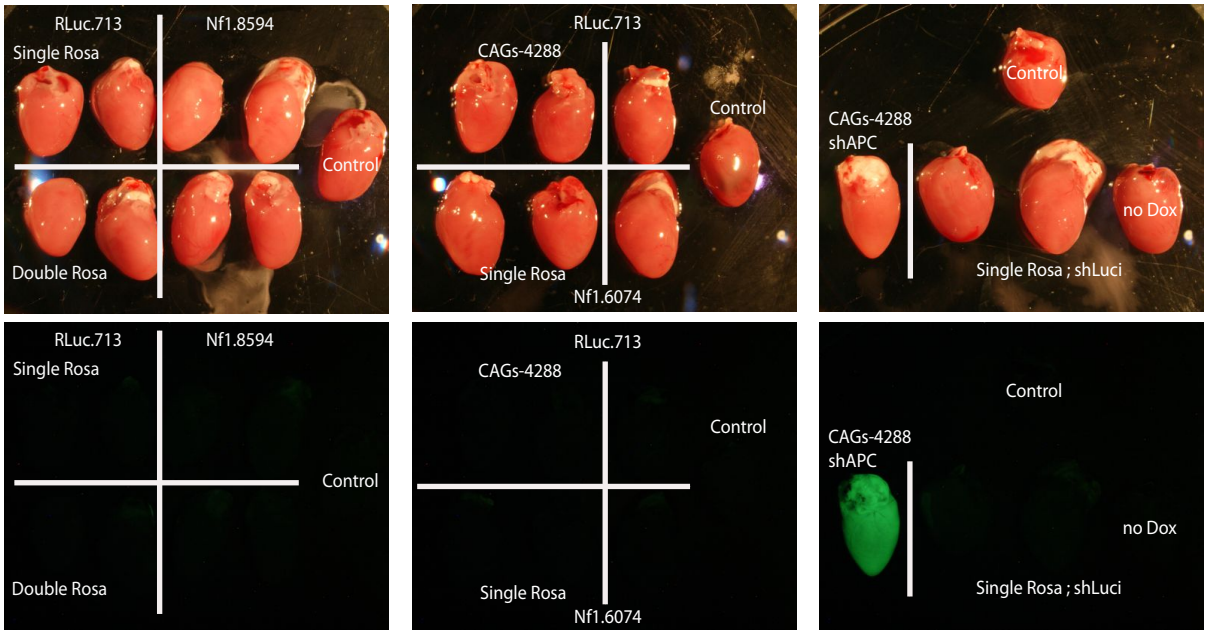

Appendix: Heart

TREtight promoter

TRE promoter

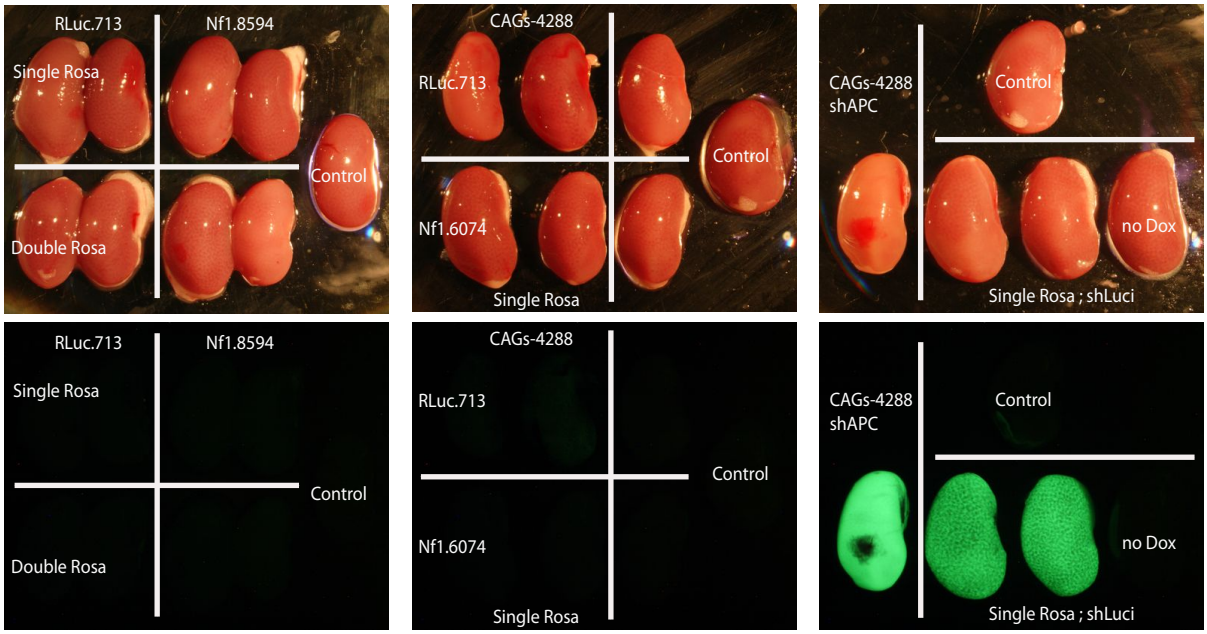

Appendix: Kidney

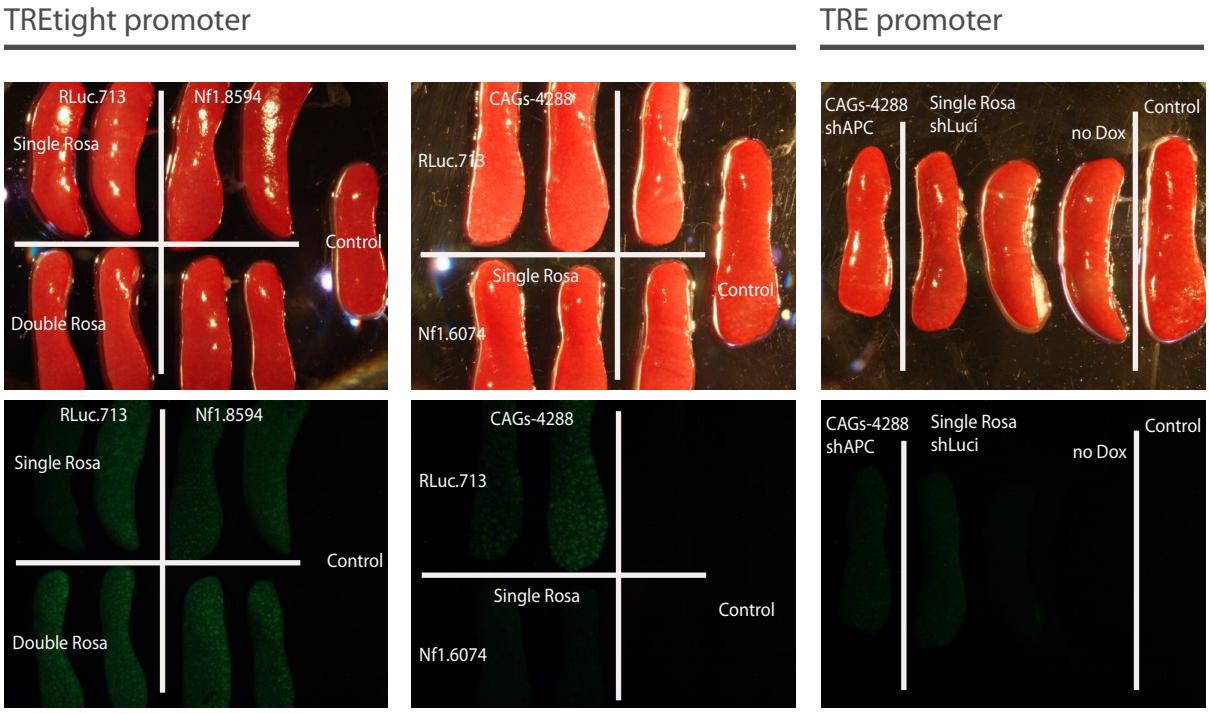

Appendix: Spleen

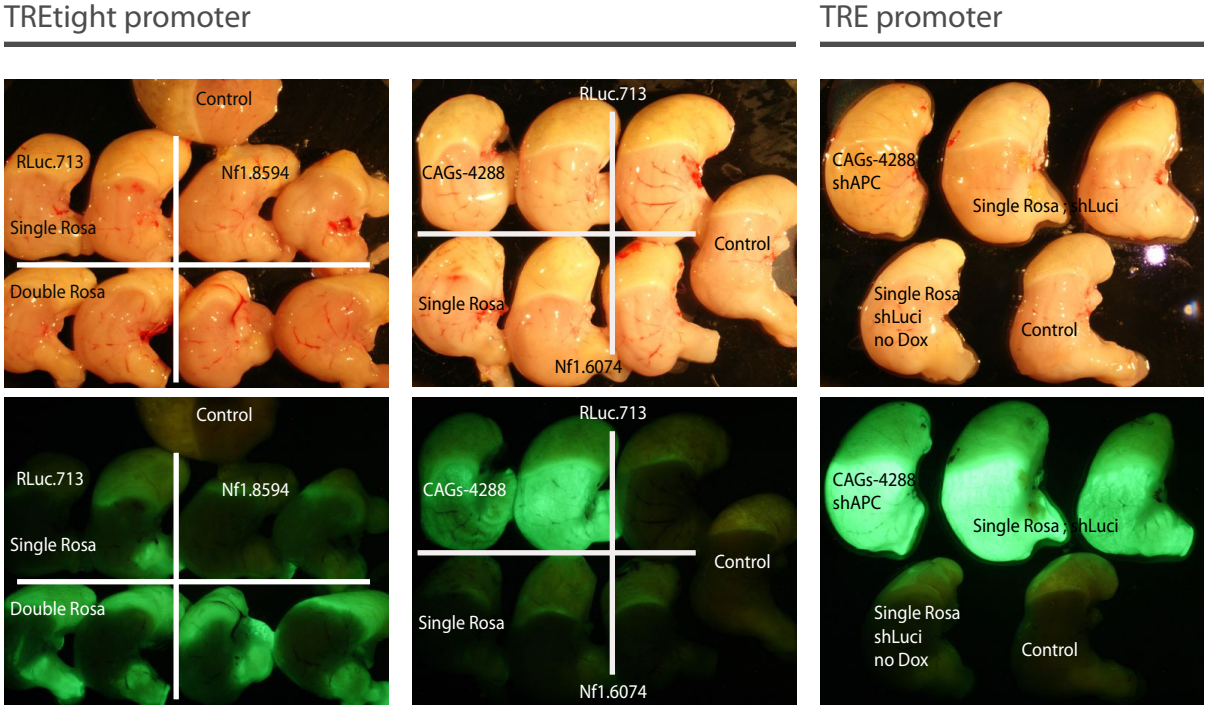

Appendix: Stomach

TREtight promoter

TRE promoter

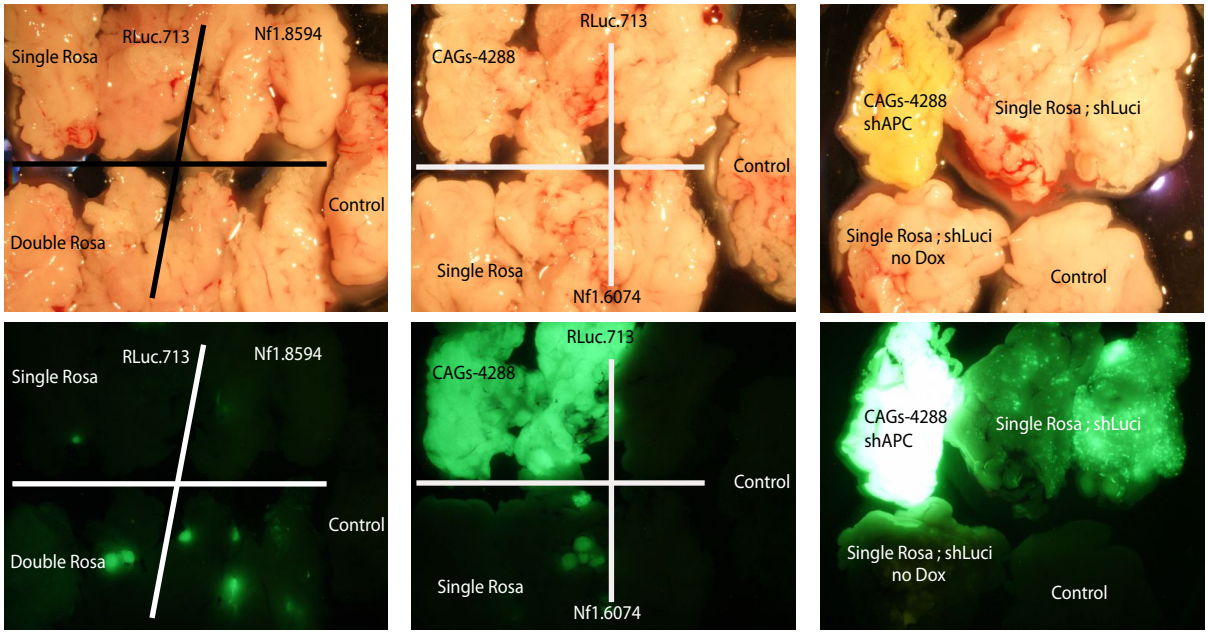

Appendix: Pancreas